Calcium zirconate materials for refractory applications

Von der Fakultät für Maschinenbau, Verfahrens- und Energietechnik

der Technischen Universität Bergakademie Freiberg

genehmigte

DISSERTATION

zur Erlangung des akademischen Grades

Doktor-Ingenieur

Dr.-Ing.

vorgelegt

von Dipl.-Ing. Constantin Jahn

geboren am 13.04.1990 in Karl-Marx-Stadt, jetzt Chemnitz

Gutachter: Prof. Dr.-Ing. habil. Christos G. Aneziris, TU Bergakademie Freiberg

Prof. Dr.-Ing. habil. Helge Jansen, Refratechnik Steel GmbH, Düsseldorf

Tag der Verleihung: 07.05.2020

Declaration

I hereby declare that I completed this work without any improper help from a third party and without using any aids other than those cited. All ideas derived directly or indirectly from other sources are identified as such. No other people did contribute to the writing of this thesis. I did not seek the help of a professional doctorate-consultant. Only those people identified as having done so received any financial payment from me for any work done for me.

This thesis has not previously been published in the same or a similar form in Germany or abroad. In compliance with the "Regulations of the Faculties for the Award of Doctorates" at the Technische Universität Bergakademie Freiberg, part of the following results were recently promulgated in a publication. [JAHN 18]

Freiberg, 09th December 2019 .....

Abstract

In order to contribute to the omnipresent demand for improving refractory materials for more efficient or new metallurgical processes, this dissertation deals with the new refractory material calcium zirconate. Earlier studies investigated this material because of its perovskite structure for technical ceramic rather than for its refractoriness. Due to the almost absence of natural calcium zirconate in nature, different approaches to the synthesis have been proposed by various authors in recent years. None of them produced single phase calcium zirconate in large grain sections for refractory applications, which is intended for this work. Therefore, the aim of this study was to investigate the synthesis of pure calcium zirconate in grain sizes up to 3 mm and to produce first refractory materials based on the hereby gained fractions with the task to always have single phase material. The potential for scaling up to industrial production was also always kept in mind.

To fulfil this task, solid state reaction was chosen as processing route. Therefore, different raw materials as calcium oxide precursor were examined, while monoclinic zirconium dioxide was presumed as the best zirconia source. Calcium carbonate brought the best results and provided the safest handling. Through the decomposition reaction, calcia is formed during the thermal treatment of the synthesis. This reacts with the zirconia to calcium zirconate. The temperature for a complete formation was determined with 1200 °C. The variation of the mole ratio of the reactants resulted in the following observations: While a surplus on zirconia led to an additional cubic, calcia stabilised zirconia phase, an excess of calcia led to free lime. The latter rehydrated during the storage in air, forming calcium hydroxide and destroying the samples due to the accompanying volume expansion. Only the equimolar mixture of the components resulted in single phase calcium zirconate. An increasing sintering temperature decreased the porosity formed earlier by decomposition. A sintering temperature of 1600 °C and above is necessary to have an open porosity of less than 10 %. Another factor is the mixing effort necessary to obtain a homogenous batch. A high mechanical mixing energy through milling ball addition

or the usage of an intensive mixer were found to bring the best results for even larger quantities of up to 6 kg. The fine particles of the raw materials need to be deagglomerated and it is presumed that the softer calcium carbonate particles rub against the harder zirconium dioxide ones. Additionally, compacting the raw material batch is beneficial for handling and shorts the reaction or diffusion paths.

The first refractories based on single phase calcium zirconate were formed using a uniaxial press. The grains, pre-synthesised at 1400 °C, shrunk at the second firing at 1650 °C vigorously, leading to a total porosity of about 5 %. An intended in situ formation of calcium zirconate during the sintering through addition of an equimolar mixture of the raw materials brought further densification. The used grain size of up to 3 mm for standard test specimen showed positive influence on the thermal shock behaviour. After five times of thermal quenching from 950 °C to room temperature, 5 MPa residual strength remained. Another interesting finding was the observable degradation of samples made of inhomogeneous mixed calcium zirconate over time. Residual calcia hydrated slowly during storage leading to a certain facing of powdery touch. Yet, the samples were not destroyed. Also, the colour of the final product varied occasionally. Impurities altering the crystal structure or a potential oxygen deficiency were suspected to cause the colour change but could not be verified within this doctoral thesis. The corrosion tests in laboratory scale showed promising results which should be confirmed in future industrial scale experiments.

Another part of this work handled the production of single phase castables based on $CaZrO_3$. Therefore, a recently developed castable batch based on nonstoichiometric calcium zirconate with cement binder was transferred. Important was the renunciation of extrinsic phase binders to achieve pure phase material. The investigations led to a castable batch which was successfully manufactured into different shapes. The physical and thermomechanical properties were very promising, which presents a starting point for the usage of castables based on calcium zirconate in wide field of possible applications.

Acknowledgement

The present dissertation was accomplished at the Institute of Ceramic, Glass and Construction Materials (IKGB) of the Technische Universität Bergakademie Freiberg beginning with the project “Calcium Zirconate materials for the application in steel and gasification industry”, which has thankfully been financially supported by the Alexander Tutsek-Stiftung.

First, I want to express my gratitude to my doctoral supervisor Prof. Dr.-Ing. habil. Christos G. Aneziris for giving me the opportunity to realize the present work and his helpful and professional support.

I owe my thanks to my second assessor Prof. Dr.-Ing. habil. Helge Jansen from Refratechnik Steel GmbH and Dr.-Ing. Volker Stein representative for all employees of Refratechnik for the excellent cooperation, professional support and helpful discussions throughout the whole time.

For the arrangement of the early project I want to thank Dr.-Ing. Patrick Gehre as well as Dipl.-Ing. Christian Ode for the harmonious cooperation within both of our projects. Moreover, I acknowledge the support of Dr.-Ing. Stefan Schafföner throughout my whole work.

I would like to thank all my former colleagues at the IKGB for their additional support. Thereby, Ms. Ursula Querner, Dipl.-Ing. Marc Neumann, Dipl.-Ing. Piotr Malczyk, and Mr. Uwe Pälchen should be emphasized.

Furthermore, I would like to thank the German Research Foundation (DFG) for funding part of my research under the grant number AN 322/32-1.

Finally, many thanks to my family and my friends for their support, encouragement, and never-ending belief in me. Without them I would not have accomplished this work.

Table of content

List of symbols and acronyms

Symbol	Unit	Description
BSE		back scattered electron
CAC		calcium aluminate cement
CCS	MPa	cold crushing strength
CIP		cold isostatic pressing
CMOR	MPa	cold modulus of rupture
CSZ		calcia stabilised zirconia
HIP		hot isostatic pressing
HMOR	MPa	hot modulus of rupture
ICP-OES		inductively coupled plasma optical emission spectrometry
IET		impulse excitation technique
LTE	10^{-6} K^{-1}	linear thermal expansion
MAH		microwave-assisted hydrothermal method
MOSFET		metal–oxide–semiconductor field-effect transistor
MSS		molten salt synthesis
PLC	cm/m	permanent length change
RUL	°C	refractoriness under load
SCS		solution combustion synthesis
SE		secondary electron
SEM		scanning electron microscope
TS		thermal shock
VIM		vacuum induction melting
WDXRF		wavelength dispersive X-Ray fluorescence
XRD		X-Ray (powder) diffraction

Symbol	Unit	Description
Δd	mm	difference in thickness
Δl	mm	difference in length, here: shift
ΔT	K	temperature difference
A	mm^2	area, section
Bi	-	Biot number
d	mm	diameter, here: characteristic thickness
d_0	mm	original thickness
E	GPa	Young' s Modulus, modulus of elasticity
E_0	GPa	Young's modulus either at 0 K, 0 % porosity or without cracks
F	N	force
G	GPa	modulus of rigidity, modulus of elasticity in shear
G_f	$J \cdot m^{-2}$	specific fracture energy
h	$W \cdot m^{-2} \cdot K^{-1}$	heat transfer coefficient
K	GPa	bulk modulus
l	mm	length
l_0	mm	original length
L_c	m	characteristic length
M	Nm	torque, moment of force
p	Pa	pressure
R	K	thermal shock resistance parameter
R'	$W \cdot m^{-1}$	thermal shock resistance parameter
R""	m	thermal shock damage parameter
R_{ST}	K	thermal shock damage parameter
T	°C	temperature
α	$10^{-6}\ K^{-1}$	thermal expansion coefficient (here linear)
γ	-	shear strain
ε	-	strain
ε_q	-	strain, across tension
λ	$W \cdot m^{-1} \cdot K^{-1}$	thermal conductivity
μ	-	Poisson's ratio

Symbol	Unit	Description
σ	MPa	tensile stress or materials strength, stress
σ_c	MPa	critical stress
τ	MPa	shear stress

Al_2O_3	aluminium oxide, alumina
Al_2O_3-C	carbon bonded alumina, alumina carbon
BaO	barium oxide
$BaZrO_3$	barium zirconate
C	carbon
$Ca_{0.15}Zr_{0.85}O_{1.5}$	cubic calcia stabilised zirconia
$CaCO_3$	calcium carbonate
CaO	calcium oxide, calcia, lime
$CaZrO_3$	calcium zirconate
Cl	chlorine
CO_2	carbon dioxide
Cr_2O_3	chromium(III) oxide, chromia
Fe_2O_3	iron(III) oxide, hematite, ferric oxide
K_2O	potassium oxide, potash
MgO	magnesium oxide, magnesia
Na_2O	sodium oxide
P_2O_5	phosphorus pentoxide
SiC	silicon carbide
SiO_2	silicon dioxide, silica
SO_3	sulphur trioxide
TiO_2	titanium oxide, titania
ZrO_2	zirconium dioxide, zirconia
$ZrSiO_4$	zirconium(IV) silicate, zircon

List of figures

List of tables

1 Motivation

The assertion of humankind on our planet Earth is due to quite different reasons. One is definitely the ability to interact with a changing environment. The discovery and usage of tools for instance helped while evolving to *homo sapiens*. With the Neolithic revolution, while human cultures started settlement all over the world independently from each other, a cultural transformation took place. With the domestication of plants and animals the need to move on faded. People started to build dwellings and gather knowledge which was then transferred to descendants and other cultures as well. The desire for possession aroused and so different materials were processed to become tools on the one hand and valuables on the other. For thousands of years human learned more and more about the different substances they were surrounded by. First ceramics were fabricated, and finally metals were discovered – or rather, their processing evolved.

From the beginning, the processing of metals or their raw materials is connected to the development of ceramics. To produce enough constant thermal energy, furnaces where built to smelt ores, some casting moulds where made of ceramic or stone. Up to now, neither the linkage between metallurgy and ceramics with a certain heat resistance, so called refractories, nor technological development itself ended. Every step in the modern world we know is built on metals, produced in all kinds of vessels made of refractory materials. This merges again in a constant demand on new refractory materials to increase efficiency or make new technologies possible.

Regarding the suitability of ceramics as refractory material, four limiting factors are considered first: the pyrometric cone equivalent according to Seger of 1500 °C or higher, the interaction with the hot matter, tribological effects through movements of all forms, and the behaviour towards thermal induced tensions. [ROUTSCHKA 97] The latter is restricting the service life of a refractory application. Because of the temperature fluctuations in the processes of such applications, for example in a converter for steel making, the thermal tensions also change. Additionally, the therefore necessary start up procedure is accompanied by a one-time thermal shock. Yet, the type of handled hot material is primarily decisive for the choice

of a suiting ceramic. Consequently, only a large variety of refractories can provide economic and ecologic satisfying state of the art as well as future industrial processes. Thus, the research on innovative materials and/or new applications for already existing ones never stops.

Recent studies showed the potential of calcium zirconate as refractory material for titanium alloy melts. [SCHAFFÖNER 13, SCHAFFÖNER 15c] Kim et al. evaluated calcium zirconate as mould material in contact with magnesium alloys which showed high thermal stability. [KIM 01a] There are already investigations on the application as nozzle material for continuous casting of steel concerning clogging behaviour. [OGURI 93, TUTTLE 05, TUTTLE 07] They were also examined as carbon containing multi-phase materials. [SAHU 97]

Natural calcium zirconate is very rare in nature and was unknown until recently. [GALUSKIN 08] Consequently, it must be synthesised from raw materials for technical applications. There are many investigations on the formation of calcium zirconate. [NADLER 55, BROWN 86, GONENLI 99, DURRANI 06, YE 07, KALINKIN 12, KALINKIN 13, LI 13, SCHAFFÖNER 13, FAZLI 14, KALINKIN 14, LIU 14, ŚNIEŻEK 15] But either only fine particles were prepared or nonstoichiometric calcium zirconate was obtained. The aim of the present study is, therefore, to investigate the solid state synthesis of single phase calcium zirconate in form of coarse and fine particles. The yield of calcium zirconate as a function of the mole ratio and sintering temperatures shall be determined as well as the resulting microstructure. Various factors for later industrial applications within sample preparation are also considered along with the comparison of calcium carbonate and calcium hydroxide as different calcia precursors. Subsequently, calcium zirconate refractories are developed and characterised to evaluate this material for different applications. The changes in thermal and corrosion behaviour in relation to the maximum grain size and processing route are investigated.

2 Theoretical background

This chapter shall provide additional information and knowledge, which are helpful to understand certain basic yet uncommon fundamentals or approaches. The main topics of the present work considered here are: a historical as well as a state of the art overview of the investigated material, the background of possible industrial applications, and the demanded properties of refractories and their determination including processing, methods of corrosion tests for ceramics, the characteristics of the modulus of elasticity, followed by the thermal shock parameters.

2.1 Calcium zirconate

2.1.1 General information

Early investigations on compounds of the system $CaO\text{-}ZrO_2$ date back to the beginning of the 20th century. Ruff and his colleagues investigated the high temperature behaviour of certain oxides and their refractoriness. [RUFF 13, RUFF 14a , RUFF 14b , RUFF 16] For zirconium dioxide they found that the thermomechanical behaviour improved with addition of some other oxides. [RUFF 32] Short before, the change of its crystal modification at higher temperatures, causing the poor thermal behaviour, was radiographical documented. [GOLDSCHMIDT 26, RUFF 29b] Consequently, different binary and tertiary phase systems were investigated. [RUFF 29a, RUFF 32, WARTENBERG 32, EBERT 33, WARTENBERG 37] Over time and with improved preparation and analysing methods, the phase system $CaO\text{-}ZrO_2$ was better understood. Kwon and Jung [KWON 17] published the latest version giving also an overview of previous work, see Figure 2-1. The only stable compound in this phase diagram is the equimolar calcium zirconate $CaZrO_3$. The existence or stability of $CaZr_4O_9$ and $Ca_6Zr_{19}O_{44}$ is controversial discussed and in general not yet agreed. [PIZZINI 72, HELLMANN 82, DU 92, KWON 17]

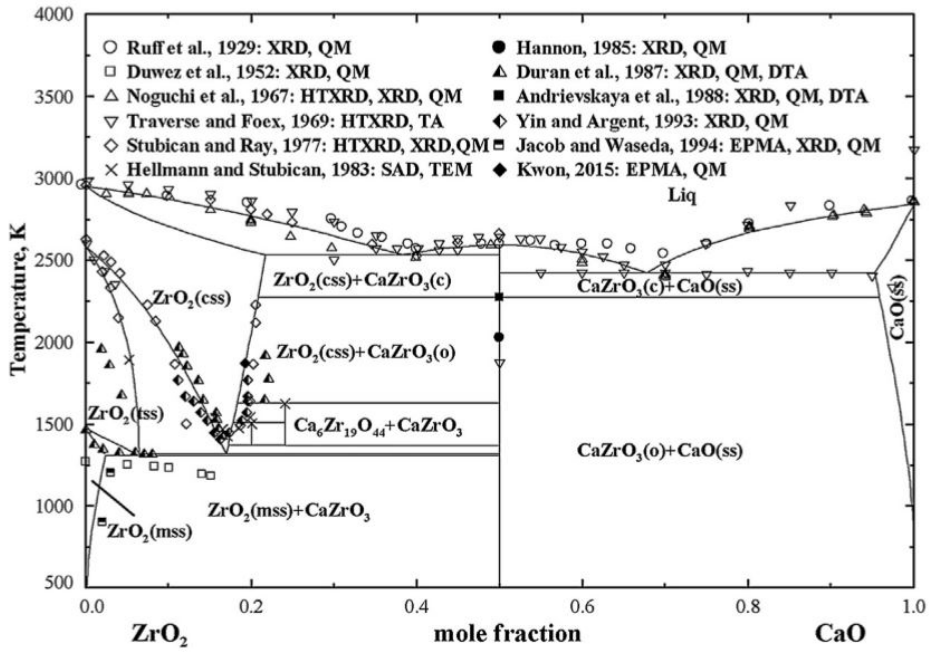

Figure 2-1: Calculated phase diagram of the CaO-ZrO_2 system along with experimental data. [KWON 17]

Calcium zirconate with his formula ABX_3 is a perovskite with an orthorhombic structure up to 1959 °C, above phase modification to cubic structure was observed. [DU 92] According to Moure and Peña [MOURE 15] perovskites in general are structures with large cations for A with mono, di or trivalent character, B can be a di, tri, tetra, penta, or hexavalent cation, and X is preferentially oxygen. With this, large numbers of combinations and substitutions are possible. The common applications are due to their electrical and magnetic properties. From the large number of perovskites, only few exist in nature. [MOURE 15] The natural analogue of calcium zirconate, Lakargiite, was found and approved as new mineral not before the year 2007. [GALUSKIN 08] The rarity was explained by the authors with the high crystallisation temperature and the high activity of prevalent silicon. The already mentioned substitutability leads easily to mixed phase compounds. For these reasons, pure phase calcium zirconate has to be synthesised. In the following section 2.1.2, different possibilities for that are shown and discussed. CaO has a cubic crystal structure (like salt) and ZrO_2 is monoclinic or tetragonal at temperatures above 1170 °C. In the perovskite structure both ions have their own sites so that the occurrence of interchanges or vacancies are not favourable under thermodynamic consideration. [STØLEN 04, p.104–105]

2.1.2 Synthesis routes of $CaZrO_3$

Mainly for its applications due to the perovskite structure, some investigations on the synthesis of calcium zirconate were made. Lately, investigations for refractory applications were focused, too. Yet, most of the studied methods from the literature are not suitable for the aimed production of single-phase, large grained material with attention to the necessary efforts and costs. For this work the solid state reaction method was chosen because the batch preparation is simple, the procurement of the raw materials is easy and comparably cheaper, and the handling of small quantities with only few grams as well as larger quantities of several kilogram is done without bigger expenses. Other suitable methods were recently investigated in other studies and thus not examined in this dissertation. The then following sections show the other processes published in the literature which give an impression on the possible approaches and required efforts and raw materials to obtain calcium zirconate based ceramics.

Solid-state reaction method

The solid-state reaction method is commonly used to produce ceramic materials due to its simplicity and suitability for the cost-efficient mass-production. For the here considered $CaZrO_3$, the procedure consists of annealing a mixture of ZrO_2 and CaO or other oxidic calcium compounds at elevated temperature for several hours. Care has to be taken if the results are compared to other studies objecting solid state synthesis because it is essential to distinguish between aimed stoichiometry and the use of other molar ratios.

Nadler and Fitzsimmons [NADLER 55] were one of the first investigating the preparation of calcium zirconate. They used commercial pure ZrO_2 and CaO, $CaCO_3$, and $Ca(OH)_2$. The latter was obtained from slaking calcia in water. For mixing the respective two components, thin slurries were produced. Water was used for these compounds and carbon tetrachloride (CCl_4) for the pure calcia. After drying, milling, and pressing, whereby hydration of the mixture ZrO_2-CaO was carefully prevented, the samples were first burnt at 1450 °C for 24 h. After crushing, grinding finer than 325 mesh, and once again pressing, the samples were subsequently burnt at 1750 °C, 1850 °C, or 2000 °C for 1 h, respectively. They obtained stable $CaZrO_3$ already after the initial firing at 1450 °C. Yet they observed a pinkish colour, which Fischer et al. [FISCHER 76] noticed for calcia rich samples sintered at 1800 °C. After the second firing at temperatures above 1700 °C, the dye disappeared here. An influence of the kind of calcia source was not remarked. They assigned it to the defect structure due to the absence of transition elements. Additionally, CaO X-ray patterns were detected in all samples but showed no reaction in their test with boiling water which means that

the amount was smaller than 1 %. Parallel, samples made of 51 % CaO balanced to ZrO_2 showed a disintegration after this test. [NADLER 55]

Brown and Bennington [BROWN 86] used calcium carbonate and zirconium dioxide finer than 200 mesh. The stoichiometric amounts were blended and compacted in a platinum dish. At first, the batch was slowly heated to 500 °C and subsequently to 930 °C over a period of 36 h. After grinding to finer 200 mesh, the material was again reheated to 930 °C for 118 h. Followed by two more heating steps with prepended grinding processes at 1200 °C for 18 h and 16 h, respectively. X-ray diffraction showed matching patterns to $CaZrO_3$.

A comparable method used Jacob and Waseda [JACOB 94]. Also blended in platinum dish, the finer than 270 mesh raw materials were slowly heating to 527 °C and then 977 °C for 33.3 h. Afterwards, they ground the material and compacted it again before firing at 1227 °C for 83.3 h three times. The XRD analysis showed only $CaZrO_3$ without traces of the starting materials.

Another method was described by Jonas et al. [JONAS 98] They used wet milling of the equimolar mixture of chemical pure $CaCO_3$ and ZrO_2 in isopropyl alcohol for 8 h. Subsequently, the dried and pelletised batch was fired at 1200 °C. Thereafter, the pellets were pulverised and pressed again before firing at 1300 °C. The dwell times were thereby not reported. In the XRD patterns they observed $CaZrO_3$ peaks which were slightly shifted but nothing else.

Hwang and Choi [HWANG 08] used $CaCO_3$ and ZrO_2 of high purity (99.9%) and ball milled them for 24 h. Whether they used ethanol for their milling, like reported by them in another study was not clarified. [HWANG 05] The calcination took place at 1350 °C for 4 h. They aimed at $Ca_{1-x}ZrO_{3-\delta}$ ($0 \leq x \leq 0.1$). For $x \leq 0.02$ compositions, only $CaZrO_3$ peaks were found in the XRD analysis. Specimen were isostatically pressed from the calcined material and sintered at 1700 °C for 4 h in air. After the second sintering, free CaO, which was not detected in the initial material, was found in SEM micrographs, see Figure 2-2. During storage, the stoichiometric specimen decayed into powder due to hydration of this free lime. In contrast, the zirconia rich phase for $x > 0.02$ was detected in the XRD of the calcined material but was not found in the micrographs of the sintered samples.

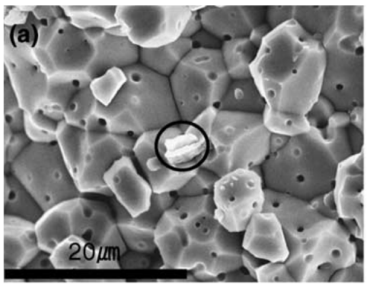

Figure 2-2: SEM micrographs of fractured surface of $Ca_{1-x}ZrO_{3-\delta}$ specimen sintered at 1700 ◦C for 4 h (x=0). Marked in the circle: CaO. [HWANG 05]

Schafföner et al. [SCHAFFÖNER 13] compared his fused material (cf. next chapter) with solid state reacted one. In this study, monoclinic ZrO_2 and $Ca(OH)_2$ were mixed in a tumbling mixer with ZrO_2 balls. With addition of 1 wt.-% cellulose binder and 2 wt.-% distilled water, the batch was die pressed at 60 MPa and, after drying, fired at 1650 °C for 6 h with an additional dwell time of 2 h at 900 °C and a heating rate of 2 $K \cdot min^{-1}$. The phase analysis showed only peaks matching the $CaZrO_3$ pattern.

Another recent study investigated slip casted material for processing to refractories. Li et al. [LI 13] prepared a suspension of water, a dispersing agent based on polymeric acryl, ZrO_2, and $CaCO_3$ powder. The used mole ratio of CaO/ZrO_2 was 1:1.5. The mixing took place in a plastic container with addition of ZrO_2 balls. Bars were casted in plaster moulds. After demoulding and drying at 100 °C, the samples were fired at 1200 °C to 1500 °C with a dwell time of 3 h and a heating rate of 2 $K \cdot min^{-1}$. XRD analysis showed three phases at lower sintering temperature and two phases at sintering temperature of 1400 °C and above. Due to the nonstoichiometric composition, the main phase $CaZrO_3$ was accompanied by cubic calcia stabilised zirconium dioxide (CSZ, $Ca_{0.15}Zr_{0.85}O_{1.85}$). The third phase, found at lower temperatures, was zirconium dioxide. Because of the little amounts and the difficulty of differentiation, the crystal structure was not further determined. [SRINIVASAN 91] Increasing the sintering temperature led also to increasing density due to crystal growth, see Figure 2-3. Thereby, the porosity decreased from about 70 % to 12 %.

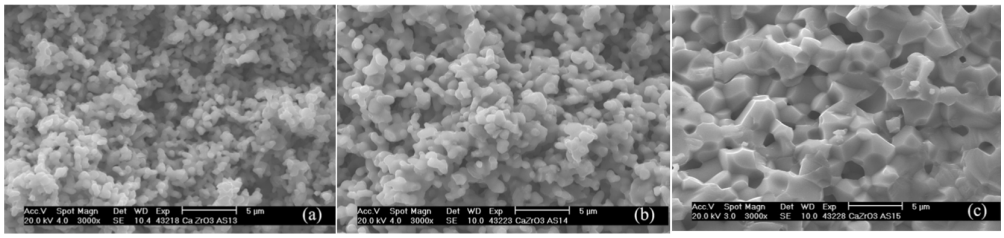

Figure 2-3: Representative micrographs of the slip casted material, sintered at 1300 °C (a), 1400 °C (b), and 1500 °C (c). [LI 13]

Low temperature solid state formation of calcium zirconate using milling assisted mechanical activation was also investigated recently. [KALINKIN 13, KALINKIN 14] A mixture of equimolar proportions of chemically pure m-ZrO_2 and $CaCO_3$ were ball milled in a planetary ball mill using steel balls for 10 min. An annealing at 950 °C for 3 h was enough for single phase $CaZrO_3$, determined by XRD analysis. They obtained nanoscale crystals, growing with increasing annealing temperature. One reason they propose, beside the decreasing particle size, was the smearing of the comparably soft calcium carbonate on the harder zirconium dioxide particles increasing the interface area. An influence of the determined iron contamination of up to 1.87 wt.-% due to the grinding vessel and balls on the synthesis reaction or resulting properties was not reported.

Considering the already performed studies, it was dominantly done a two stage synthesis to ensure homogeneous and fully reacted material even if it was not necessary. Additionally, long dwell periods at the high sintering temperatures were set. Most commonly calcium carbonate was used as calcia precursor. Therefore, in this dissertation these parameters were investigated in detail to differentiate.

Electric arc melting method

This method uses the high electric current between up to three electrodes dipped into the powder or later melt of the here used raw materials. Due to their dielectric behaviour the heat is induced by their resistance in contrast to the processing of metal scraps in an electric arc furnace which is conductive. Another possibility is the usage of a conducting crucible to which the electric current flows from the electrode through the starting material. The most recent studies used this preparation route to obtain dense material. [STOCH 12] Furthermore, the gained materials were often fine grained and not processed into larger grain size classes, which are beneficial for refractory applications. [SCHAFFÖNER 13]

First investigations used $CaCO_3$ in equimolar proportion with ZrO_2 mixed and pressed to small pellets and subsequent melting in an arc furnace within argon atmosphere. They obtained stoichiometric material with density close to the theoretical. [STOCH 12]

Later, Schafföner et al. [SCHAFFÖNER 15c] investigated arc melted mixtures of CaO and ZrO_2. The material was obtained in a Higgins furnace from where only the fused material was further processed. The analysis showed a deficiency in CaO due to its evaporation at high temperatures in the melting process. Grains of up to 3 mm were obtained with a high density and first refractory materials were produced. Afterwards, the nonstoichiometric material was adjusted by adding $CaCO_3$. [SCHAFFÖNER 17] Yet, the in situ reaction adjusted the stoichiometry only for the smaller grains, while in the larger grains cubic stabilised zirconium dioxide remained due to longer diffusion paths. The diffusion of CaO and ZrO_2 to $CaZrO_3$ was discussed by Angers et al. [ANGERS 72]

The special reactors using either the conductive crucible or the three electrodes accompanied by the demand of high electrical power, time consumption, and possible evaporation of raw materials lead to refraining from this method for this work.

Molten salt method

To lower the synthesis temperature and obtain fine grade material without additional grinding, the molten salt synthesis (MSS) was used. Thereby, the reactants are partially dissolved in a molten salt medium, which facilitates the mixing and diffusion and subsequently the reaction temperature can be decreased. [HUANG 16]

Yet, the requirement of coarse grained material in a scalable process prevents the choice of this route for the here conducted study.

Li et al. [LI 07] synthesised calcium zirconate with grain size of 0.5 µm to 1.0 µm at 1050 °C for 5 h. As raw materials calcium chloride ($CaCl_2$), sodium carbonate (Na_2CO_3), and zirconia (ZrO_2) powders were used. In Figure 2-4, the process is shown as an overview. The formation of calcium zirconate takes place in a liquid mixture of NaCl and Na_2CO_3. The first is formed by the reaction of $CaCl_2$ with parts of the sodium carbonate at about 700 °C. After washing with hot-distilled water, filtration, and drying, these materials were fired and single-phase $CaZrO_3$ was obtained.

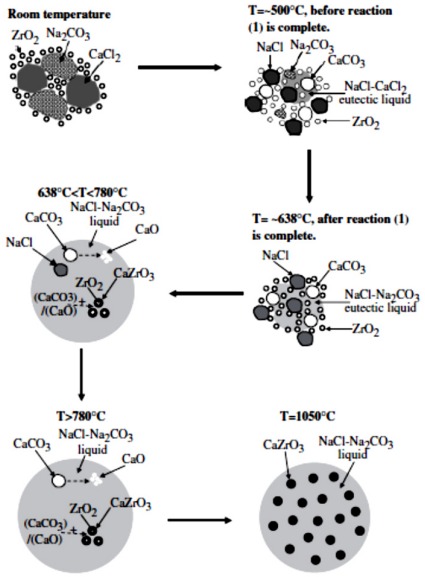

Figure 2-4: Schematic process of the molten salt synthesis. [LI 07]

Fazli and his colleagues [FAZLI 12a, FAZLI 12b, FAZLI 14] investigated this method in more detail. They examined the influence of grain size, salt to oxide ratio, temperature, holding time, and type of used salts. The results showed that a nano- as well as a micro-ZrO_2 sample formed $CaZrO_3$ starting at 700 °C. The most promising salt to oxide ratio was 2:1. Increasing yield was obtained with increasing temperature up to 1000 °C. After washing with hot-distilled water, the samples were heated for 3 h at 800 °C and 1000 °C, whereby single-phase $CaZrO_3$ with 70 to 90 nm and 400 to 450 nm particle size, respectively, was gained. Furthermore, the synthesized particles kept the size and morphology of the zirconia powders, which indicates that a template formation mechanism is dominant for the formation of calcium zirconate with this method. By using a stoichiometric mixture of $CaCl_2$ and LiCl the formation of calcium zirconate started at about 550 °C. Calcium carbonate was used here as raw material. Also, after washing with hot-distilled water, the samples were heated for 3 h at only 650 °C and single-phase $CaZrO_3$ with particle size of 90 nm to 95 nm was obtained. The particle morphology resembled the ZrO_2 powders, too.

Solution combustion method

The solution combustion synthesis (SCS) was developed in the mid-80s of the last century. [VARMA 16] Some reasons leading to this invention were the inhomogeneity of ceramics obtained by the classic solid state route, impurities through repeating grinding and firing cycles, and the urge for finest materials without further crushing and milling. [PATIL 08, p.3–4] Generally, the method bases on self-sustaining reactions of metallic oxide complexes (as oxidant) in aqueous solution and organic fuel without further addition of external energy after reaching the ignition temperature. The oxidant and the fuel are mixed in fixed molar proportions, whereby the several reactions provide a large amount of heat, promoting the overall exothermic redox reaction. During the reaction, a large amount of gaseous by-products is released leading to an expansion of the oxide product as well as a fast decrease of temperature. Consequently the solids obtained are finely dispersed and of nanoscale. [VARMA 16]

Gonenli et al. studied the preparation of pure and gadolinium-doped $CaZrO_3$ powders with this method. Appropriate proportions of calcium chloride dihydrate ($CaCl_2{\cdot}2H_2O$) and zirconium(IV) oxychloride octahydrate ($ZrOCl_2{\cdot}8H_2O$) were dissolved in distilled water. As fuel urea (CH_4N_2O) was used. The mixed solution was placed in an electric furnace at 500 °C. In less than 15 min, the reaction was completed. Doping with a rare earth element was achieved by using an aqueous solution of gadolinium(III) chloride ($GdCl_3$), which was prepared beforehand through the reaction of gadolinium(III) oxide (Gd_2O_3) with hydrochloric acid (HCl). Sample characterization by X-Ray powder diffraction (XRD) showed single-phase $CaZrO_3$. [GONENLI 99]

Ianos et al. compared the classic ceramic route with the solution combustion synthesis for calcium zirconate. A mixture of calcium nitrate ($Ca[NO_3]_2$) and zirconium dioxide was heated at 1000 °C for 1 h for the first method and for the second method $Ca(NO_3)_2$ together with zirconyl nitrate solution ($ZrO[NO_3]_2$) and β-alanine ($C_3H_7NO_2$) were ignited at 300 °C without further heat treatment. In case of the solid-state synthesis, XRD analysis indicated incomplete formation despite the equimolar mixture of the reactants. Thereby, CaO, ZrO_2, and a CaO-stabilised ZrO_2 solid solution were observed. Both, sintering temperature as well as dwell time, did not suffice. The annealed powder was afterwards highly agglomerated and of low specific area (1.4 m^2/g). On the other hand, single-phase $CaZrO_3$ was obtained with the combustion synthesis. Without additional annealing or milling, the $CaZrO_3$ powder thereby showed a surface area of 21.5 m^2/g and an average crystallite size of 23.9 nm. An additional sintering step at 1400 °C for 2 h of the obtained material, which was therefore uniaxially pressed at 200 MPa, resulted in 95 % dense, slightly translucent pellets. [IANOŞ 10]

Limsay et al. reported the preparation of $CaZrO_3$ with a fuel mixture of glycine ($C_2H_5NO_2$) and urea for the solution combustion. The solution was placed into a preheated furnace at 500 °C. The mixture boiled and frothed up after ignition forming a voluminous and foam-like $CaZrO_3$. In less than 10 min the process was completed. XRD analysis showed only single-phase $CaZrO_3$. The average particle size of the synthesized $CaZrO_3$ was 92 nm. [LIMSAY 10]

This synthesis route is very interesting due to the relative low reaction temperature and the nanoscale powder obtained. Yet for larger amounts and larger grains an additional process step would be necessary increasing the amount of work, time, and because of the character of the reactants the costs, too.

Co-precipitation method

In the co-precipitation method, different precursors, for example oxides, alkoxides, inorganic salts or nitrates in solution containing two or more cations, are used to obtain a homogenous material. The product is further processed (for example washing, drying, milling or compacting) before an annealing takes place. [MOURE 15] Commonly this method was used to produce doped calcium zirconate or other perovskites because of the easy, low temperature method with good homogeneity. [KRISHNAN 07]

Among the few researchers objecting undoped $CaZrO_3$ with this route were Hernandez-Sanchez and Tuttle. They prepared calcium zirconate powder through a non-aqueous oxalic acid solution precipitation route. Calcium nitrate ($Ca(NO_3)_2$ and zirconium(IV) n-butoxide ($Zr[C_4H_9O]_4$) were mixed in the presence of oxalic acid ($C_2H_2O_4$), acetylacetone ($C_5H_8O_2$), and n-propanol (C_3H_8O). After a curing time of 1 h, [HERNANDEZ-SANCHEZ 09]

Like in the other solution methods mentioned here, the advantages of good material homogeneity, reactive small crystals, and low processing temperatures are facing the need of a further processing step to obtain calcium zirconate in form of large grain sizes which is essential for this work here.

Hydrothermal method

Hydrothermal synthesis was developed to simulate natural hydrothermal processes occurring in the Earth's crust on the laboratory scale, to better understand geological phenomena. It is a process with phase reactions in aqueous media at elevated temperature and pressure in a closed vessel. In broad terms, hydrothermal synthesis is a technology for crystallizing chemical compounds directly from aqueous solution by controlling the thermodynamic variables. [RIMAN 02]

Kutty et al. studied the preparation of fine calcium zirconate powders by the hydrothermal method. Previously, the used ZrO_2 powder was also prepared by this method using $ZrOCl_2$ or an acid extract of a zircon-frit obtained by fusing

zirconium(IV) silicate ($ZrSiO_4$) and sodium hydroxide (NaOH) at 1000 °C. The mixture of ZrO_2 and a CaO slurry was then heated in the hydrothermal vessel. The preparation parameters were 480 °C and 100 MPa. After washing with distilled water and drying, the product was analysed. The study showed that the reaction temperature for $CaZrO_3$ formation cannot be lower than 450 °C. Without further annealing a particle size of 0.2 to 1 µm was achieved. [KUTTY 90]

Xu et al. prepared $CaZrO_3$ powder from calcium hydroxide ($Ca[OH]_2$) and zirconium(IV) oxychloride ($ZrOCl_2$), and potassium hydroxide (KOH) as the mineralizer. The hydrothermal conditions were temperatures up to 250 °C and time of up to 12 h. Subsequently, these precursors were annealed at temperatures up to 1000 °C. The following analysis showed that $CaZrO_3$ can be obtained under the conditions of n(CaO): n(ZrO_2)=2:1, at 200 °C, for 6 h and firing at a temperature of 900°C. The crystallite size was about 0.5 to 3 µm. [XU 07]

Macedo et al. used a new synthesis route, the so called microwave-assisted hydrothermal (MAH) method, and a subsequently crystallization by annealing. The precursor solution was obtained by adding calcium chloride dihydrate ($CaCl_2 \cdot 2H_2O$), zirconium(IV) oxychloride octahydrate ($ZrOCl_2 \cdot 8H_2O$) and NaOH, as a mineralizing agent, to deionized water. For the MAH process step, a heating rate of 140 ° $K \cdot min^{-1}$ up to 140 °C, synthesis times up to 160 min, and pressures up to 400 kPa were used. After washing, drying and grinding the material was fired at temperatures up to 1200 °C for 1 h. The crystallization process of the calcium zirconate phase started with heating at 800 °C, together with the crystallization of the nonstoichiometric calcium-zirconium oxide. After heat treatment at 1200 °C, the sample consisted of 65% orthorhombic $CaZrO_3$ phase and the nonstoichiometric cubic phase. [MACEDO 18]

The necessary effort to obtain and control these hydrothermal conditions did not suit the tasks striven in this work and this method was therefore not chosen.

Sol-gel method

The sol-gel process starts with a sol (colloidal particles), prepared from the chemical solutions (precursors), followed by gelification, and removal of the solvent. Subsequently, an appropriate heat treatment is necessary. Typical precursors are metal-alkoxides or metal chlorides, which react by hydrolysis and polycondensation, resulting in a colloid (i.e. solid particles dispersed in a solvent). [ROGOJAN 11]

Yu et al. prepared calcium zirconate by the sol–gel wet chemical technology. They wanted to use it as a gate material for metal–oxide–semiconductor field-effect transistor (MOSFET) application. Calcium acetate ($Ca[CH_3COO]_2$) and zirconium acetylacetonate ($Zr[C_5H_7O_2]_4$) were chosen as precursors and diluted in acetic acid $C_2H_4O_2$. Spin-coating technique was used to build up an oxide thin film on $Pt/Ti/SiO_2/Si$ substrates. Thereafter, the deposited films were dried and heated at

temperatures up to 700 °C for 1 h in oxidising atmosphere. The results showed that the film had an amorphous structure with residual calcium carbonate existing when annealed at 550 °C. The carbonate decomposed and thin films crystallized in the perovskite structure when annealed at 600 °C and above. [YU 04]

Dudek and Drożdż-Cieśla reported the synthesis of $CaZrO_3$ powders by adding $CaCO_3$ into a zirconium(IV) nitrate ($ZrO[NO_3]_2$) solution. The solution was then dropped into a saturated solution of ammonium oxalate ($[NH_4]_2C_2O_4$) and ammonia (NH_3). The resulting gel was dried at 100 °C for 12 h. The material was not washed before. The dried $CaZrO_3$ precursor was annealed at temperatures up to 1200 °C within a time up to 2 h. Pure orthorhombic $CaZrO_3$ phase was obtained. [DUDEK 09b , DUDEK 09a]

Rogojan et al. tried two different sets of raw materials. One was conducted by mixing zirconium(IV) chloride ($ZrCl_4$) and calcium nitrate ($Ca[NO_3]_2$) solutions. Then ethanol (C_2H_5OH) was added in small amounts, while stirring at 60° C. The second sol-gel synthesis started from zirconium(IV) propoxide ($Zr[C_3H_7O]_4$) solution and ethanol. In order to stabilize zirconia with 8 wt.-% CaO, calcium isopropoxide ($Ca[C_3H_7O]_2$) was added. The sol viscosity increased at a temperature of 90 °C. For both processes 24 h were set as time for gelification. After that, the obtained materials were dried for 24 h at 100 °C. The powders were thermally treated at 1000 °C, for 2 h. Both routes lead to tetragonal and cubic zirconia [ROGOJAN 11]

Liu et al. fabricated polycrystalline calcium zirconate fibre by the sol–gel method. The starting materials for the spinnable sol of precursors were zirconium acetylacetonate ($Zr[C_5H_7O_2]_4$), calcium nitrate tetrahydrate ($Ca(NO_3)_2{\cdot}3H_2O$ and citric acid ($C_6H_8O_7$). After adding of each starting complex to methanol (CH_3OH) both solutions were mixed together, and then citric acid was added, too. After some curing time, the sol was spinnable. For this, a centrifugal spinning device was used. The obtained fibres were annealed at different temperatures up to 900 °C. After annealing at 700 °C the XRD results showed monophasic $CaZrO_3$. The fibres possessed excellent thermostability, investigated with an oxygen coal gas flame at up to 1800 °C. An impression of these fibre are given in Figure 2-5. [LIU 14]

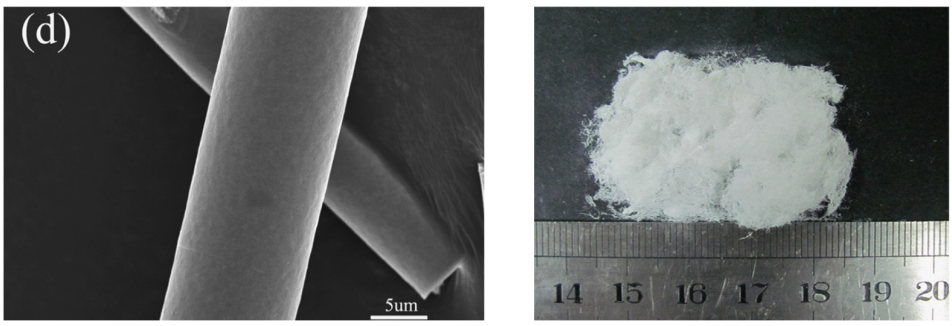

Figure 2-5: SEM image of a fibre annealed at 900 °C (left) and photography of spun fibre after firing at 900 °C (right). [LIU 14]

Gionea et al. obtained calcia stabilised zirconia powder by the sol–gel method, utilizing zirconium(IV) propoxide ($Zr[C_3H_7O]_4$), calcium isopropoxide ($Ca[C_3H_7O]_2$) and 2-metoxiethanol ($C_3H_8O_2$) as precursors. Finally, hot isostatic pressing (HIP) treatment was applied to obtain dense ceramic material. The zirconia powders heat treated at 500 °C for 2 h showed pure cubic phase and after another sintering at 1100 °C for 2 h, too. After the final HIP process at up to 1300 °C for 2 h with a pressure of 150 MPa in argon atmosphere however, the monoclinic phase occurred probably through a too slow cooling rate. [GIONEA 16]

2.1.3 Investigated applications of $CaZrO_3$ ceramics

In the following section the literature review should give an overview of current investigated applications of calcium zirconate materials. Whether it is in fact used there is too much sweeping a statement.

One reason for the investigation of this material is its high melting point and high chemical inertness. [DU 92] Hwang and Choi showed that at low oxygen pressure $CaZrO_3$ is an oxygen ion conductor, whereas at high oxygen pressure it is a mixed ion and electronic conductor. [HWANG 08] Different studies showed the influence on the ion conductivity by either having over-stoichiometric CaO and ZrO_2 or by doping with other oxides for an increase. [WANG 88, RÓG 02] Applications as oxygen sensors for steel melts and in solid oxide galvanic cells were reported. [JANKE 82, RÓG 02] Yajima et al. investigated indium doped $CaZrO_3$, which exhibits proton conductivity and is therefore suitable as hydrogen sensor in aluminium metallurgy. [YAJIMA 95]

The composite material MgO/$CaZrO_3$ was often investigated as a refractory for cement rotary kilns. [KOZUKA 93, KOZUKA 95, RODRÍGUEZ 04, SERENA 04, SERENA 05, RODRÍGUEZ-GALICIA 07, SERENA 09, OBREGÓN 11, LANG 18] First investigations on the behaviour of MgO-CaO-ZrO_2 refractories in cement kilns were presented by Kozuka et al. A post-mortem analysis revealed improved corrosion behaviour and coating adhesion but wear problems due to peeling. [KOZUKA 93, KOZUKA 95] This was followed by investigations on the corroded basic refractories, used until then. [SZCZERBA 10, SZCZERBA 17] Serena et al. investigated the corrosion behaviour of a composite matrix material with 80 wt.-% MgO and 20 wt.-% $CaZrO_3$ by clinker of Portland cement. They observed the formation of a MgO sintered layer inhibiting a further attack of the molten slag on the sample substrates. [SERENA 04] Compared to magnesia aluminate spinel the MgO-$CaZrO_3$ ceramic showed higher resistance to thermal stress and corrosion. [RODRÍGUEZ-GALICIA 07, SERENA 09] MgO and $CaZrO_3$ exhibited no reaction up to a temperature of 2060 °C [SERENA 05] Because of a significant thermal expansion mismatch of MgO and $CaZrO_3$ microcracks are have induced, increasing the work of fracture. [OBREGÓN 11] The $CaZrO_3$/MgO ratio in the matrix decide between either a $CaZrO_3$ or MgO rich layer

formed in contact with the corrosive cement clinker. The MgO rich matrix or layer showed better corrosion resistance, since $CaZrO_3$ exhibited a higher solubility in the cement clinker. [SERENA 09] The solution thereby leads to an increasing viscosity due to the dissolved Zr^{4+}, hindering further liquid phase diffusion. [RODRÍGUEZ-GALICIA 07] For the content of 4 % of MgO, the thermal shock resistance of samples were found as optimal, inhibiting also a grain growth of the $CaZrO_3$. [LANG 18] Some studies aimed at improving the properties of MgO-$CaZrO_3$ based refractories. Contreras et al. investigated the microstructure and properties of $FeAl_2O_4$-MgO-$CaZrO_3$ refractory mixtures. The cold crushing strength (CCS) improved with the addition of the hercynite. A good chemical stability was observed for these phases. [CONTRERAS 05] Rodríguez et al. added spinel ($MgAl_2O_4$) and hercynite ($FeAl_2O_4$) to the matrix improving the thermo-mechanical properties. The SEM analysis revealed their location in the boundaries between the MgO and $CaZrO_3$ particles functioning as a bond linkage. [RODRÍGUEZ 12]

Recently, CaO-ZrO_2 based materials gained attention for melting of titanium and titanium alloys. But this topic is presented in the next section because of the focus on this application in more detail. Yet, the usage of fused $CaZrO_3$ for melting Ti6Al4V showed the dissolution of the cubic phase present due to its production. [SCHAFFÖNER 13, SCHAFFÖNER 15c] In addition the melting of γ-TiAl showed formation of calcium aluminates and showed no satisfactory results. [SCHAFFÖNER 15b] Therefore, the prevention of a secondary phase was the aim in this work. A pure phase $CaZrO_3$ material was assumed as more promising.

Kim et al. investigated different mould materials for casting of a magnesium alloy. They observed for CaZrO3 the best thermal stability, even at an overheating temperature of 600 °C, in contact with the melt. [KIM 01a]

Another application was coal gasification. The cup sample were made of slip casted, sintered $CaZrO_3$ raw materials or fused particles. [LI 13, SCHAFFÖNER 13] Different ashes in oxidizing as well as reducing atmosphere were investigated. The cups based on sintered material showed better resistance against coal ash than samples consisting of fused particles. Yet, thermomechanical properties should be improved, and the corrosion tests were only static. [LI 18]

2.2 About the potential of $CaZrO_3$ as refractory

The following section of this chapter shall provide an overview on topics dealing with the necessities for the development of a refractory material for a certain application. First this is carried out exemplary for melting of titanium and titanium melts. The next issue deals with the studies already published in the literature concerning the corrosion behaviour of compounds in the system CaO-ZrO_2. Finally, the chosen applications targeted in this dissertation are presented.

2.2.1 Case study: Suitable refractory for processing of titanium and titanium alloy melts

As an example, investigations on crucible materials for titanium and its alloys are further regarded in the following section. Because they show how lacking suitability of refractory materials hinder the wider application of promising structural materials. Because of parallelly done examinations of other people, new approaches were chosen for this work. Nevertheless, the following examples show the difficulties and varieties occurring during such a development.

With developing technology, the demand on the properties of metallic materials for a range of applications rose. Often the application temperature limited the qualification of certain metals. Having regards to the price, new, sometimes non-ferrous, alloys, called superalloys, were developed and used. These alloys are more complex to process due to the vacuum necessary during melting. One approach is the vacuum induction melting (VIM). [MITCHELL 92] An induction furnace without core consists of a water cooled copper coil surrounding a refractory crucible placed in a vacuum chamber. Through this coil which turns wrapping up to 80 % of the crucible heights flows an alternating electric current inducing a magnetic field. The induced electromagnetic interaction causes the heating of the metal inside the crucible. [ASM International 08] Another method to produce reactive metals is the arc-melting process in water-cooled copper crucibles using inert atmospheres. Here, electrodes of graphite, tungsten or titanium are used. A modification of this process is the so called 'skull melting', where a layer of the metal is frozen onto the refractory crucible and then acts as protective layer in contact with the molten metal. A rapid heat loss from the molten metal through the solid metal and crucible wall leads to a high power requirement and the amount of molten metal is comparatively small. Another disadvantage of the arc-melting process is the danger which the proximity of the cooling water to the molten metal creates. A leakage would create explosive hydrogen when the water touches the molten metal. The usage of a ceramic crucible, where cooling is not needed, would be more safe and may be energy saving, thus cheaper. [WEBER 57] Same intentions are present for the VIM technology, whereby also water-cooled copper crucibles are used. [SCHIPPEREIT 61]

Titanium and its alloys combine numerous superior properties such as low density, high strength, high corrosion resistance, and a creep resistance up to 550 °C. Also remarkable is their biocompatibility. [LÜTJERING 07, BANERJEE 13] Despite these excellent properties, the broader application of titanium and titanium alloys is inhibited by their high price. A main reason is the complex titanium sponge production. This is still dominantly done by the Kroll process, which contains numerous refining steps, and has been continuously improved over time [KROLL 40, LÜTJERING 07]

Investigations on refractories for titanium and titanium alloys

Li et al. investigated in their study the wetting behaviour of different ceramic oxides against molten TiAl. They observed increasing contact angles between the alloy and the ceramic moulds with increasing chemical stability of these oxides. Y_2O_3 showed the smallest contact angle, followed by different stabilized ZrO_2, CaO, Al_2O_3, zircon ($ZrSiO_4$) and MgO. In addition they showed the different wetting behaviour between contacting under gravity conditions and in an electromagnetic field. [LI 08b]

The thermodynamic stability, also under vacuum atmosphere, and relative cheap raw materials made CaO to a promising refractory material. [KIM 01a , KIM 01b] Disadvantageously, the hydration tendency inhibited a further economical breakthrough but lead to different investigations on their improvement. [NADACHOWSKI 76, KAWANO 91, WONG 95, CHEN 02, CHEN 07a, CHEN 07c, GOMES 08, LI 08a, GHASEMI-KAHRIZSANGI 16] Yet, the hydration is not inhibited completely, and the material is due to the raw material very fine grained.

Y_2O_3 showed dissolution in Ti-46Al-8Nb when used as crucible material. Yttria and oxygen occurred in the solidified metal as well as Y_2O_3 particles. [LAPIN 11] As coating material of alumina crucibles for the melting of γ-TiAl yttria oxide showed improved resistance. An increased oxygen content was remarkable but lower compared to the uncoated Al_2O_3 material. [ZHANG 13a] In another study it was found to be the least contaminating oxide in contact with pure titanium melt at elevate temperatures. [SAHU 97]

Pure ZrO_2, used as shell mould for investment casting of TiAl, showed no severe reaction with the melt, only small modifications on the casted surfaces and only small oxygen pickup. [JIA 04]

Because of the generally low wettability and low price, graphite was also considered for this application. In contact with NiTi alloy, a TiC layer is formed and the carbon content increased. [ZHANG 05] Whereby, the TiC layer decreases further carbon contamination after a second melting process. Also the direct contact of the initial nickel to the crucible was found to be the main factor for the carbon dissolution. [FRENZEL 04] Another studied concluded the contact with titanium as factor for this and suggested the use of a titanium wash melt as initial step before the alloy melting. [NAYAN 07] The melting of TiAl in graphite crucibles led to a carbon contamination too. [KAMYSHNYKOVA 18]

The usage of boron nitride, with addition of some Y_2O_3, as casting shell for molten Ti6Al4V showed small reaction between the refractory surface and the solidifying metal. However, the titanium from the melt reacted with the components from the refractory. Additionally the surface of the casted metal consisted of α-phase combined with an increased microhardness. [LUI 08]

A titanium aluminide based facecoat material for investment casting of TiAl showed severe interaction with a formation of a thick hardened layer. [CHENG 12]

Recent studies investigated $CaZrO_3$ as alternative for melting of titanium and its alloys and gained some attention. Kim et al. compared investment casting moulds made of Al_2O_3, ZrO_2, CaO, and $CaZrO_3$ for casting of commercial pure titanium (cp-Ti), an alloy with 6 wt.-% aluminium and 4 wt.-% vanadium (Ti6Al4V), and a compound with about 50 wt.-% aluminium (γ-TiAl). For the melting of these alloys CaO crucibles were used. Beside the finding, that the corrosion behaviour differs among these titanium materials, calcium zirconate has shown a good performance for cp-Ti and Ti6Al4V showing minimal reaction layer and hardness increase. Similar results showed CaO, hence the processing was more difficult. [KIM 01b] Jia et al. studied the interfacial reaction of a Ti–46Al (at.-%) alloy melt and calcia stabilised zirconia. The results showed a mechanism of interfacial reactions. A dissolution of ZrO_2 occurs at high temperature releasing zirconium and oxygen. First tend to react with the aluminium forming Al_2Zr. The diffusion of the free oxygen led to the formation of TiO and Al_2O_3 on the casted surface. A diffusion of titanium replacing the zirconium in the calcia stabilised cubic ZrO_2 formed the complex cubic compound $Ca_{0.8}Ti_{0.7}Zr_{2.4}O_7$. In contact with TiAl alloy melt; these reactions also led to the transformation of the calcia stabilised ZrO_2 from cubic to tetragonal, and then to monoclinic structure while cooling to room temperature. [JIA 04] Chang and Lin concluded from their study about the interaction of calcia stabilised zirconia in contact with titanium at 1550 °C, that $CaZrO_3$ might be stable in contact with aggressive titanium alloys and has potential as refractory material for the titanium metallurgy. [CHANG 10]

Li et al. tested $CaZrO_3$ refractories with addition of TiO_2 as sintering aid. Melting experiments of crucibles in contact with nickel-titanium alloy (TiNi) and Ti6Al4V were carried out. The corrosion behaviour was very promising, because only small corrosion layers of 30 µm for TiNi and 350 µm for the Ti6AL4V were measured. Within the casted metals neither calcium nor zirconium were found. [LI 10]

In a study of Lu et al. calcium stabilised zirconia (CSZ) was investigated in contact with titanium 1400 °C. In the solid state a considerable diffusion of oxygen and zirconium towards the titanium and only a very little solubility of calcium in the titanium were observed. Additionally, $CaZrO_3$ was found at the interface with the titanium. With increasing CaO content of the CSZ, the observed corrosion decreased. [LU 11]

Other experiments were done by Yang et al. regarding TiFe based alloys. The melting of these materials in $CaZrO_3$ crucibles showed a comparable content of oxygen in contrast to a graphite crucible but without the carbon contamination. [YANG 12]

Schafföner et al. produced melting crucibles based on fused $CaZrO_3$ by cold isostatic pressing (CIP) and evaluated the corrosion behaviour against different

titanium materials: Ti6Al4V, µ-TiAl, and commercially pure titanium. The occurring corrosion mechanism were quite different among the different materials. For Ti6Al4V a dissolution of the cubic calcia stabilised ZrO_2, present trough the manufacturing process of the raw materials, was observed. The $CaZrO_3$, being the main phase, reacted practically inert against the melt. Improved crucibles showed an oxygen contamination of 0.43 wt.-% to 0.58 wt.-% and a zirconium contamination of 0.5 wt.-% to 0.7 wt.-%. For γ-TiAl alloy melts a much higher zirconium contamination was observed whereas the oxygen contaminations increased less high in comparison. An XRD analysis showed different calcium aluminates at the interface between crucible and melt. Here, a combined attack of aluminium and titanium took place. The titanium dissolved the zirconium of $CaZrO_3$, therefore the remaining calcium and oxygen reacted with the aluminium forming calcium aluminates. At the interface with commercially pure titanium melt a heavy evaporation of calcium was observed. Thereby, the highest contamination with oxygen all melting experiments were determined. After vacuum induction melting (VIM) of µ-TiAl a considerable amount of 2.71 wt.-% to 9.96 wt.-% of zirconium from the crucible material was dissolved in the melt. An oxygen contamination of 0.45 wt.-% to 0.81 wt.-% was measured. The formation of different calcium aluminates at the crucible corrosion front was observed. However, this calcium aluminate formation was not found after the same melting procedure with Ti6Al4V. There the zirconium contamination was lower. The corrosion during the melting of cp-Ti showed a heavy evaporation of calcium. After the first formation of a melting pool, the melt infiltrated the crucible. The oxygen and zirconium content of the casted metal samples were among the highest of all melting experiments. Differences in the titanium activity between the investigated titanium materials were held accountable for the different mechanisms and observations. Also, the second, nonstoichiometric phase of cubic zirconium dioxide was found to be more likely to be dissolved by the melts whereby the $CaZrO_3$ was also decomposed by the pure titanium. [SCHAFFÖNER 15a, SCHAFFÖNER 15b, SCHAFFÖNER 15c]

Yuan et al. investigated $CaZrO_3$ materials as facecoat for investment casting moulds for TiAl alloys. The Al2O3, used as the stucco, reacted with $CaZrO_3$ to form (Zr, Ca)O_2 and $CaAl_xO_y$ at temperatures of 1650 °C. For the usage of ZrO_2 no interaction was observed besides some cracks due to the volume expansion of the zirconia during the thermal processing. Oxygen, zirconium, and silicon ions from the tested shell moulds diffused into the TiAl metal to form new phases in the metal/shell interfacial areas. [YUAN 15]

Freitag et al. examined alternate materials for the investment casting of Ti6Al4V based on $CaZrO_3$. They observed improved finishing quality in contrast to silica-based casting shells. [FREITAG 17, FREITAG 18]. In contrast to silica or alumina based materials the $CaZrO_3$ based material showed less dissolution and

therefore a slightly increased oxygen content in addition to a cleaner surface of the casted samples without α-transformation and increased hardness. [KLOTZ 19]

Another new material recently studied is barium zirconate ($BaZrO_3$). Due to its high chemical stability and low thermal expansion it showed good stability against titanium alloys like TiNi, TiFe, and Ti6Al4V and a good thermal shock resistance. [LIU 13, ZHANG 13c, ZHANG 13b, ZHU 14] It was successfully applicated as a coating material for alumina crucibles, too. [LI 15, LI 17] Commercially produced, fused $BaZrO_3$ (showing also a second, nonstoichiometric phase) was isostatically pressed to crucibles with a maximum grain size of 3 mm. The melting of a Ti46Al8Nb alloy showed a low oxygen concentration of 0.078 wt.-%. [CHEN 19]

Summary

The review of studies objected to the special alloy melting and the interaction with ceramic crucibles, moulds, and other showed, that the variety of metal alloys is as big as the utilised refractories. There is currently no material or product satisfying all demands. Yet, it is shown, that the chemical stability is of importance. But processability, thermomechanical properties, and harmlessness are also aspects for the choice of the right material for the respective application, thereby being exposed to the rules of the market.

2.2.2 Corrosion behaviour

In this section investigations on the corrosion behaviour of $CaZrO_3$ or $CaO\text{-}ZrO_2$ based materials are reviewed. Section 2.3.2 on the other hand is dealing with the different corrosion test methods for refractories in general. On the one hand, the corrosion behaviour is limiting the operating time of the used refractory, and on the other hand there is the possibility of a contamination of the contacting material changing its properties or quality.

In Figure 2-6 can be seen, that the Gibbs energy of formation of calcium zirconate is much lower than the sum of the educts calcia and zirconia. This lower Gibbs energy of formation is beneficial for a potential refractory material for titanium melts. [STØLEN 04] Compared to calcia, which was often used before, calcium zirconate has a significant lower linear thermal expansion coefficient and has an observable inertness towards water, giving it advantages in processing. For a temperature range of 20 °C to 900 °C the linear thermal expansion coefficients were determined with 8.5×10^{-6} K^{-1} to 11.8×10^{-6} K^{-1}. [CURTIS 47, NADLER 55, JANKE 82, JONAS 98, GOMES 08] Moreover the vapor pressure of calcium over calcium zirconate at 2000 K was calculated and is significant lower than over calcia. [JACOBSON 89, CAWLEY 90]. That is because of to the low stoichiometric composition range and the low Gibbs energy of formation of $CaZrO_3$ making it

necessary to decompose first to CaO and ZrO_2 before a further reaction of the CaO is possible. [CAWLEY 90]

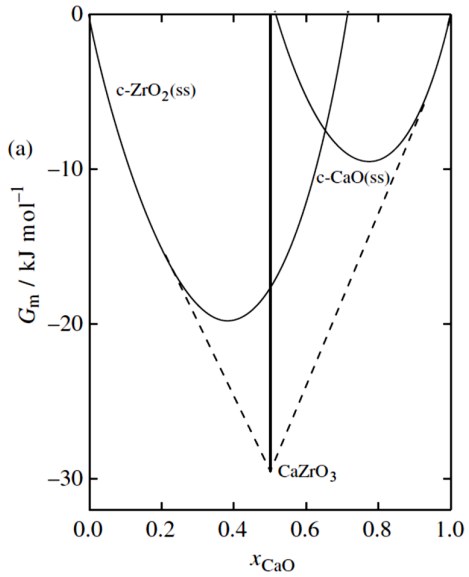

Figure 2-6: Gibbs energy representation of the phases in the system ZrO_2-CaO at 1900 K. [STØLEN 04, p.104]

Pole and Beinlich, Jr. investigated various oxide compositions on their resistance to molten rock phosphate, a sedimentary or igneous rock containing phosphate minerals. Crucibles were die pressed and fired. Inter alia, compositions containing 10 wt.-% to 40 wt.-% CaO with the remainder of ZrO_2 were processed. Samples with 23 wt.-% CaO or less withstood a hydration over time. It is reported, that the crucible with this maximum amount of CaO showed good resistance to the molten rock phosphate. [POLE 43, POLE 46]

Nadler and Fitzsimmons investigated solid state $CaZrO_3$ obtained from equimolar proportions of $CaCO_3$ and ZrO_2 fired at 1450 °C and again at up to 2000 °C. They placed compacted samples of their material on top of common refractory materials and annealed it at 1500 °C. Visual examinations of the interfaces showed no reaction between their $CaZrO_3$ and stabilised ZrO_2, MgO, Al_2O_3, and BeO. Severe reactions were observed with SiC and mullite. [NADLER 55]

Keler and Andreyeva synthesised their material from ZrO_2 and $CaCO_3$ at up to 1600 °C with a yield of up to 97 %. They tested the contact reaction with other oxides at elevated temperatures as well as mixtures of those with their calcium zirconate. Heating of samples of $CaZrO_3$ in contact with specimen of ZrO_2, ThO_2, and Al_2O_3 showed no reactions up to 1450 °C. Yet, SiO_2 and TiO_2 showed reactions starting at 1350 °C. Equimolar mixtures of calcium zirconate and ZrO_2, SiO_2, TiO_2 or Al_2O_3 showed the decomposition of the first-mentioned at 1500 °C. [KELER 61]

Serena et al. produced composites with 80 wt.-% MgO and 20 wt.-% $CaZrO_3$ Substrates made of these fired mixtures were set up with a small probe of pressed Portland cement clinker and heated up to 1500 °C for up to 3 h. A differing microstructure due to different raw materials led to varying corrosion rates. The corrosion was characterized by dissolution processes of the MgO as well as the $CaZrO_3$ while precipitating tricalcium silicate (C_3S). With progressing process, the C_3S is dissolved forming a liquid phase with most oxides except MgO. Thus, for all samples a sintered layer of MgO was found on the substrate. [SERENA 04]

Rodríguez-Galicia et al. investigated the corrosion mechanisms of MgO-$CaZrO_3$–calcium silicate based materials by cement clinker phase. A sample of such material was placed onto the refractory substrate and observed by hot-stage microscopy up to 1600 °C. Afterwards the cross section was analysed with scanning electron microscopy. It was found out that the corrosion mechanism bases on a diffusion of the liquid clinker phase through the grain boundaries and open pores. This liquid phase partially dissolves the $CaZrO_3$ and MgO. In the presence of $CaZrO_3$ a zirconium containing silicate liquid boundary layer is formed, adjacent to the calcium zirconate grains near the interface. The dissolved zirconia increases the viscosity of this liquid phase, hindering further diffusion and therefore enhancing the corrosion resistance of these materials. [RODRÍGUEZ-GALICIA 07]

The investigations of $CaZrO_3$ based materials for melting of different titanium materials was already described in the section before.

2.2.3 Overview of the possible industries for future application

The following sections, describing the different industry branches, are more focused on the variety of applications and their particular requirements than on a historical summary of their development. These business sectors have been chosen because of their current or still present economic and environmental issues, along with their economic importance. But it is not said that other applications could not be considered regarding the plurality of uses of refractory material in all industries.

Steel industry

The steel industry, not only in Germany, suffers currently a lot from cheap mass steel production from China along with high pricing pressure. [NGUYEN 16] Additionally, there are political and environmental obstacles for the business location Germany burden its economic competitiveness. [WAKEFORD 16] At the end, also to secure hundreds of thousands of jobs, the refractory material used in every possible step from the iron ore up to the different kinds and shapes of steel has to be contributing. [SAWANO 98, ROTERING 12]

Up to now every chosen refractory material has passed through extensive researches and practical experiences, too. Nevertheless, the development and urge for

improvement is omnipresent. Even though steel making is only a part in the field of refractory applications, the overview shows that there is no material qualified to fulfil all occurring requirements. Therefore, one cannot expect that the material developed and investigated in this work suits every application but there is enough potential in these applications and the material itself. In general, to stand a chance within the competition as refractory material the here developed product has to comply some common properties, namely: resistance to thermal shocks, volumetrically stability under application conditions, resistance to shape changing under loads at higher temperatures and certain corrosion resistance depending on the application. [SCHULLE 90, p.19] The issue of the corrosion of refractories is thereby treated more detailed in section 2.3.2.

In fact, there are already some studies about the application in the steel industry, mainly as nozzle materials as the following review will show.

Okumura et al. [OKUMURA 91] used CaO-ZrO_2 grains of nonstoichiometric composition (further information on origin or else were not given). They mixed this material with a grain size of up to 0.4 mm with 15 wt.-% graphite and some organic binder. Partly CaO was substituted for the CaO-ZrO_2 grains in their clogging trials. The mixtures were blended, pressed into specimen and cured at 1000 °C in reducing atmosphere. A hydration of the material with excess of the so called non-hydrating CaO as well as a decomposition due to the graphite was not observed or reported during the tests. Yet, due to the increasing CaO amount the anti-clogging behaviour improved in their study.

Ogibayashi [OGIBAYASHI 92] in his review wrote about ZrO_2-CaO-graphite submerged nozzles being used in industrial applications showing stable properties and suppression of build-up for a long casting time. The CaO forms low melting calcium aluminates with the aluminium in the killed steels whereby that liquid phase provides a low energy layer so that subsequent attachment of alumina inclusions is prevented.

Oguri et al. [OGURI 93] proposed in their study, that the anti-clogging mechanism is based on the CaO in the calcium zirconate material which reacts with the alumina inclusions forming liquid calcium aluminates. The calcium aluminates and micro-polycrystalline ZrO_2, left at the nozzle wall, were observed to be pulled into the melt from the steel/refractory interface. The hydration of the CaO has been reported as a problem for higher proportions in the material. An erosion of the refractory material was described for amounts higher than 30% of CaO.

Tsujino et al. [TSUJINO 94] summarised in their introduction, inter alia, some conference articles from 1991 of the annual meeting of The Iron and Steel Institute of Japan, in which materials from the system CaO-ZrO_2-C were presented for the application as nozzle material due to the clogging enhancing behaviour of aluminium killed steel during continuous casting. The actual materials, experiments and findings

are not reported in detail and could not be retraced otherwise. In the study itself, the investigated material consisted of about 20 wt.-% carbon, two nonstoichiometric compositions of CaO-ZrO_2 (one zirconium dioxide rich, the other calcia rich) and SiO_2 as antioxidants (low and high amount). The sample production is not described. They found out, that steel with more alumina inclusions formed more deposits on zirconia-lime-graphite refractories than usual alumina graphite material.

Sahu et al. [SAHU 97] investigated also carbon containing CaO-ZrO_2 compounds with addition of antioxidants (about 20 wt.-% C + 10 wt.-% SiO_2). They used it as layer material within the nozzle. After an industrial trial in a steel plant, with a casting time of 250 min meaning 5 heats in sequence, alumina deposition was almost not given, contrarily to the standard Al_2O_3-SiO_2-C material. Neither spalling of the layer from the base material, nor hydration, nor unusual wear of the layer was commented.

Ohno et al. [OHNO 02] reported that calcium zirconate nozzles can produce zirconia which is washed into the molten steel decreasing the steel quality.

Tuttle et al. [TUTTLE 05, TUTTLE 07] investigated pure phase calcium zirconate powder, isostatically pressed and sintered at about 1600 °C. Static as well as dynamic laboratory tests were conducted. They observed a reaction of the alumina inclusions with the calcium zirconate forming solid calcium aluminates. In contrast to the studies with carbon containing CaO-ZrO_2 materials, no liquid phase was found. The solids were presumed to lead to clogging in the industrial scale application.

In the study of Chen et al. [CHEN 07b] the oxidation behaviour of CaO-ZrO_2-C refractories was shown. Without an antioxidant, in this case SiC, the sample was nearly completely oxidised after heating up to 1300 °C for 10 min. The added SiC did not prevent the complete oxidation but improved it. A disintegration of the oxidised sample or a decomposition of the calcium zirconate phase was not observed.

Gasification

Another interesting field of application is the gasification industry. In the context of environmental worries and the demand for clean energy production, the gasification of coal materials has become an alternative. Thereby, it is also possible to use other carbon containing materials, like waste, sludge or residues for example. The main purpose for this treatment is the production of syngas, a mixture of carbon monoxide and hydrogen. [KRZACK 08] For an extensive description of the gasification of coal and its specialties the book: “Die Veredlung und Umwandlung von Kohle”, by J. Schmaldfeld and P. Arendt is recommended. [SCHMALFELD 08]

There are different types of gasifiers, each featuring specific processes. Therefore, dissimilar conditions are present, and a variety of requirements is derived. This means different temperatures as well as process pressures and atmospheres.

In addition, the choice of feed stock material or rather its quality has an influence on the potential corrosion mechanisms depending on the physical state of the occurring by-products ash and/ or slag and their compositions. [KRZACK 08]

Focus on the refractory lining was given for entrained-flow gasifiers, because of the formation of slag during processing. This liquid form of the ash flows down or is set to flow down the sidewalls and removed at the bottom of the process chamber. About 5 $t \cdot h^{-1}$, depending on the feedstock quality and throughput, can arise. The operating temperature is between 1250 °C and 1550 °C at a pressure of about 3 MPa or more. The purpose of the refractory lining is therefore to protect the outer shell, commonly made of steel, from these temperatures, corrosion, and erosion. On the other hand, the refractory suffers from penetration, reactions through the slag but also the atmosphere. [BENNETT 04] In addition, the burning flame temperature can easily reach 2000 °C. In the areas with the highest strains refractory materials made of chromium oxide proofed longest service life. But these materials are expensive due to the raw material sources, high sintering temperature and processing demands. Furthermore, the formation of toxic chromium(VI) compounds during service is possible, hampering the disposal after product life. In the zones with lower temperatures alumina rich materials are used. [BENNETT 07, GEHRE 13b]

Starting in the 1970s and 80s research and field trials were performed, investigating liner materials. [CROWLEY 75, DIAL 75, KENNEDY 78b, KENNEDY 78a, BONAR 80, BAKKER 84] As a conclusion, only material with a chromia (Cr_2O_3) content of 75% or higher provides acceptable service lifetimes. The reason is the low solubility of chromia in coal slag over a broad area of basicity. [BAKKER 93] Another advantage is the formation of an iron-chromium spinel if the slags contain iron oxides, preventing further penetration through sealing the surface but this leads on the other hand to spalling. [BENNETT 11]

With developing gasification technology over time, the operating temperature was reduced to about 1300 °C. Hence, new economic and ecological friendly chrome free materials were studied. A promising material was spinel ($MgAl_2O_4$), due to their high corrosion resistance against slags in steel ladle lining. [BRAULIO 11] Whereby, the specific compositions of the slags from steel-making are different compared to the slags formed during the gasification process. The major differences are a higher amount of SiO_2, alkalis and Al_2O_3 and a lower content on CaO, Fe_2O_3/FeO, and MgO. [BENNETT 11, CHEN 18]

The addition of phosphate to high chrome oxide refractory decreased the surface expansion, slag penetration, and spalling, therefore the refractory loss was reduced and service time increased. [BENNETT 06]

Gehre et al. investigated different chrome oxide free shaped refractories based on alumina as potential replacement of gasifier lining materials. Generally, the materials sintered under reducing conditions showed a degradation of their mechanical properties but had an improved resistance against thermal shock and alkali-corrosion compared with these materials sintered in an oxidizing atmosphere. A further step was to add brown coal ash to those alumina based castables due to a lower reactivity of the formed phases within the refractory with the phases present in the gasifier slag. Material with a content of 11 wt.-% of brown coal ash, sintered in a reducing atmosphere showed the best results regarding thermomechanical properties and corrosion behaviour at temperatures up to 1400 °C. Later, another approach for chrome oxide free refractories, investigated by them, were cement bonded, spinel comprising castables based on alumina. The addition of 6 wt.-% of a $MgAl_2O_4$ containing cement brought suitable thermomechanical properties and corrosion behaviour. The main factor there was the lowered porosity due to formation of new phases during processing of the ceramic. This spinel was later found to be formed in alumina based refractory when TiO_2 and ZrO_2 were added. Initially, the titania forms $Na_2Al_2Ti_6O_{16}$, with the Na_2O as contamination of the alumina raw materials, improving the thermal shock behaviour significantly. In contact with the slag and the MgO it contains, the spinel is formed building up a protective layer on the interface. This inhibited further penetration and corrosive reactions. [GEHRE 11, GEHRE 12, GEHRE 13a, GEHRE 15]

Recently, Li investigated in his thesis refractories based on $CaZrO_3$ for the application in slagging gasifiers. The refractory material used in this work consisted of about 68 wt.-% $CaZrO_3$ and 32 wt.-% cubic stabilised ZrO_2. Due to a high porosity and a low strength of the binding matrix, the tested samples suffered from heavy infiltration. Neither the $CaZrO_3$ nor the calcia stabilised ZrO_2 phases were found to be stable against different slags (basic, intermediate, acidic) under oxidising or reducing atmospheres. Whereby some reactions were promoted or made possible through earlier reactions of the material with compounds of the respective slag. [LI 18]

2.3 Requirements for refractory materials

In this chapter different factors for the suitability of a material as refractory and its applicability in the industry are explained. The following sections are in general about suiting processing, examination of corrosion behaviour, and thermomechanical properties including their determination and comparability.

2.3.1 Processing and handling

For a successful application as refractory product in the industry, the processing and handling of the material from the raw to a shippable product is crucial.

The costs as well as the obtained properties are affected by the choice of the suiting processing route. For this work, two routes were selected due to their features, which are presented in the following.

Pressing

Uniaxially pressing of samples, for the raw material synthesis as well as the first refractory samples, was selected due to the minimal efforts necessary. A servo hydraulic press with a steel mould of specific dimensions is enough. Sometimes pressing aids are necessary to ease particle packing and as temporary binder. Limiting factors are the simple geometries due to the compaction through only the two punches and the possibility of inhomogeneous density distribution. [SALMANG 07, p.617-621]

Casting

Another processing route suitable to produce refractories is slip casting. Here, not the slip casting in a plaster mould was chosen but vibrocasting in plastic moulds. The details are based on the study Schafföner et al. which processed their fused $CaZrO_3$ to crucibles this way. [SCHAFFÖNER 18] Care was taken towards the additives only to avoid contamination with other oxides. A finished development of a castable based on $CaZrO_3$ for industrial application was assumed to be too time consuming in the schedule of this work. Yet, meaningful results were striven.

In the broadest sense, castables or castable refractories describe a mixture of a heat-resistant ceramic aggregate and a binder, alumina cement for example. For installation, it is blended with water and casted into a form or processed without further shaping. [NISHIKAWA 84, p.582] These so called monolithics are the counterpart of the so called shaped products and are completed by functional parts and insulating materials as the different types of refractory ceramics. [ROUTSCHKA 97, p.1] Usually monolithic refractories are directly installed at the application area and there fired if necessary. This saves energy, time and storage capacity. Additionally, a setup with thinner wall thickness, more complex geometry, or in general without joints is of advantage. [NISHIKAWA 84, p.12]

For this work care should be taken that primarily the casting process for shaping is meant not the monolithic refractories. So, if spoken of castables in the following, the casting slip is intended.

2.3.2 Corrosion and corrosion test methods for refractories

Before explaining the foundations of corrosion test methods or rather of the corrosion mechanisms of ceramics, a short summary of the meaning of refractory ceramics should be provided here. Generally, the corrosion behaviour is no physical quantity. Rather, it is evaluated through comparable experiments. Additionally, there are a lot of factors

affecting the performance of a refractory exposed to corrosive media. [SCHULLE 90, p.151-160]

In general, the corrosion of the refractories during their application is the main factor limiting the service time. There are difficulties for predictions before installation, observation during service, and analysis after the end of their application concerning corrosion behaviour. On point is the variety of changing parameters over a furnace campaign, for example. Inter alia temperature, atmosphere as well as composition and physical state fluctuate, each affecting the interactions. After cooling down for reparation or relining, the material can be investigated, yet the results gained at room temperature are sometimes not representative for processes at higher temperatures which complicates the interpretation. [POIRIER 08]

A corrosive environment regarded here usually contains liquid phases which react with the refractory material forming new phases at elevated, and elevating temperatures. This results in refractory consumption or wear. The attack on refractories by a molten slag for example is a complex process involving many mechanisms and parameters. [LEE 04]

Corrosion mechanisms

There is no single model which can explain all mechanisms of corrosion of a particular refractory in different environments. The corrosion of the refractory in contact with a corrosive liquid phase is usually distinguished in three major categories:

- Wetting and penetration, as described above, the slag or else contacts the refractory and infiltrated present pores causing structural or chemical changes.
- Dissolution, or diffusion, a chemical process in which the refractory material is dissolved into the slag.
- Erosion, which is the abrasion process of the refractory material exposed to the movement of gas and slag. Or spalling due to the stresses induced by the infiltrated slag or its reaction products within the material. [RIGAUD 11, p.399–401]

Wetting and penetration

The corrosion process itself consists of a broad variety of changing reactions and processes. Basically, to start a chemical or physical reaction, the at least two components, as an example refractory surface and molten slag, must get together. This phenomenon is called wetting. If there are different, immiscible or insoluble phases in contact with each other, they tend to an energetic minimum. Thereby, their expansion and alignment changes. Surface tensions occur in between two phases. These are tangential vectors originating from the combined contact point. Regarding a simplified,

refractory case, there is often a solid phase S (refractory material) in contact with a liquid phase L (melt or slag or other) in the presence of a certain gaseous atmosphere V. The solid will not change its expansion and presumed to be flat and smooth. Thus, the two angles between S and V as well as V and L can be neglected. The result is the contact angle ϕ between the solid surface and the liquid. This is illustrated in Figure 2-7 and expressed in the Young's equation (2.1). A high surface tension between a refractory surface and the attacking liquid leads to a high contact angle meaning a non-wetting behaviour. [SCHULLE 90, p.151–157, EUSTATHOPOULOS 99, p.16–24, LEE 99, RIGAUD 11] A poor wetting also results in a slower reaction kinetics between the two components. In general, it is distinguished between reactive and non-reactive wetting. [GERMAN 96, p.235]

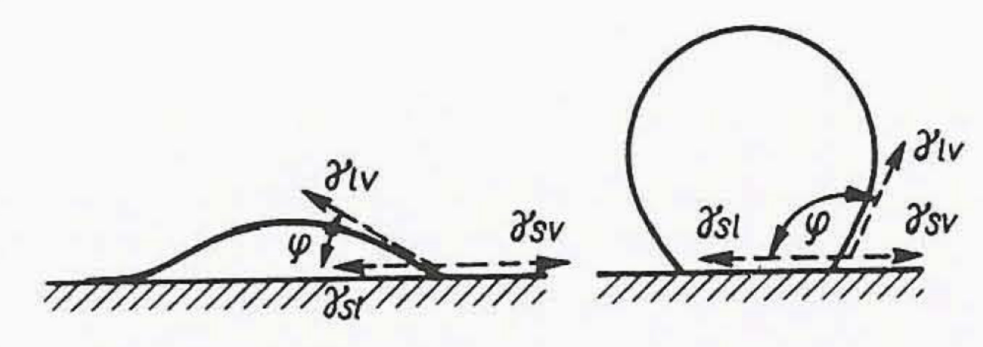

Figure 2-7: Different equilibrium contact angles ϕ, on an ideal smooth surface; with the solid surface tension γ_{SV}, the solid-liquid interface tension γ_{SL}, and the liquid surface tension γ_{LV}, respectively. [SCHULLE 90, p.155]

$$\cos\phi = \frac{\gamma_{SV} - \gamma_{SL}}{\gamma_{LV}} \tag{2-1}$$

Then one must consider two deviations of this simplified model. On the on hand, surfaces or materials are not homogeneous and microscopic smooth and on the other hand, porosity is present, too. Clearly, viewing a material, consisting of several components, there is a difference for each specific constituent regarding the surface tension. Locally, there can be different corrosion mechanisms not only because of the reactivity but the wetting before. Of cause are sharp or rough surfaces having an impact on the adjusting angles as well. [WENZEL 36, EUSTATHOPOULOS 99, p.24–36] If the refractory material contains open porosity the following formulas might be applied:

$$h_{max} = \frac{2\gamma_{LV} \cdot \cos\varphi}{r \cdot \rho_L} \tag{2-2}$$

$$\frac{dl}{dt} = \frac{r\gamma_{LV}\cos\varphi}{4\eta l} \tag{2-3}$$

$$p = \frac{-2\gamma_{LV} \cdot \cos\varphi}{r} \tag{2-4}$$

In this case, h_{max} describes the maximum heights/ depth of penetration/ infiltration depending also on the respective pore radius r and the density ρ_L of the liquid at the certain temperature. Smaller pores tend therefore to favour infiltration and fewer wetting reduces infiltration tendency. [SCHULLE 90, p.157] The rate of penetration in a horizontal pore dl/dt, with a respective pore radius r, is given by the second expression. Thereby is η the viscosity of the penetrating liquid, l the length at time t. Both expressions are valid only at constant temperature, whereas the surface tension and viscosity are influenced by temperature. These equations have often been used to describe the penetration of liquids in refractories. Thereby, it must be distinguished between physical and chemical invasion. However, in the case of a chemical reaction, the dissolution affects the values of γ_{LG} and η, and changes the porosity geometry (l and r). [RIGAUD 11, p.399] The third equation (2-4) shows the pressure p, necessary to penetrate a pore after Washburn. Converted it is the maximum pore size of a material inhibiting a liquid (for example a molten metal) at a certain temperature of penetration in a specific depth of melt bath. [MCCAULEY 95, p.47]

Dissolution

The simplest idea of pure dissolution at the refractory - slag interface is the chemical reaction of the solid with the liquid forming a new liquid phase. This process causes continuously a loss in wall thickness of the refractory linings. The solvation leads to a multicomponent system, that means there is no chemical composition defined by a single concentration nor is a single saturation composition given. For porous refractories, with open porosity having a fine matrix materials, both dissolution and penetration occur. The dissolution of the high reactive fine grained matrix leads to disrupted structure whereby the coarse grained aggregates are carried away by the slag or the newly formed liquid phase. [RIGAUD 11, p.399–401] The chemical composition of the slag in combination with the one of the refractory material has a pivotal influence on the dissolution reactions. Slags, for instances, are basically mixtures of various metal oxides, such as SiO_2, Al_2O_3, Fe_2O_3, CaO, MgO, Na_2O, and K_2O. These components can be allocated in acidic, neutral and basic character. Thereby, the so called slag basicity affects the refractory solubility in the slag. An acidic refractory will resist an acidic slag but will be attacked by (or dissolved in) a basic slag, and conversely. However, a physical measurement of the basicity of a slag cannot be made directly. Furthermore, to express the basicity of a slag the so called V-ratio is often used. Here, the basic oxides are placed on the numerator and the acid oxides on the denominator.

Formulas could be described like this:

$$V = \frac{m(CaO)}{m(SiO_2)} \tag{2-5}$$

$$V = \frac{m(CaO) + m(MgO) + m(FeO) + m(MnO) + \cdots}{m(SiO_2) + m(P_2O_5) + m(Al_2O_{3)} + m(Fe_2O_3) + \cdots} \tag{2-6}$$

A ratio greater than 1 implies a basic slag, and a ratio less than 1 implies an acidic slag, and equal to 1 implies a neutral slag. [BROSNAN 04]

Due to the variety of involved components, the inclusion of ever components reactivity and solubility is difficult. The dissolution reactions and their calculation are often depending on each other and changing the values. The character of the initial reactions also has an influence on further reactions. The slag viscosity for example depends on the reaction product which then have an impact on the further infiltration. Or the formed compounds build up a protective layer on the interface. [SCHULLE 90, p.152–155]

Erosion

In fact, corrosion is determined by the removal of the dissolved material due to its slowness. Promoting factors are rising temperature but mostly convection or other flow mechanisms. [SCHULLE 90, p.157] This convection can be enforced, with stirring of the liquid, rotation of the vessel or occurs with progressing reaction due to density gradients within the liquid as a result of enrichment of corrosion products within. [LEE 99] One specialty occurs, when there is a third, liquid phase, which is dissolving the solid phase. The new formed interfaces have also a specific tension, whereby their sum is unequal to the tension without this phase. Whether it is positive or negative for one side, in this direction the convection will turn. [SCHULLE 90, p.159]

When there is no direct loss of material through slag penetration, the slag encloses partially or completely the volume of refractory and reduces the open porosity. The result during temperature changes is a changed expansion associated with forming of stresses. This will degrade the material strength and stiffness, microcracks appear. These might be totally disruptive cracks in the lining material. This phenomenon is called structural spalling. [RIGAUD 11, p.401]

Corrosion test methods

There are different standardised test methods for the investigation on the corrosion behaviour. They are presented in the following sections. These tests were commonly used to compare different materials or different parameters and show only the results after finishing the experimental procedures and cooled to room temperature.

Sessile drop test (a)

The sessile drop test, which is also known as button test, is shown in Figure 2-8a. Compacted powders are shaped, or larger quantities cut into a small cylinder and placed on the refractory substrate. Then all is heated up to a certain temperature in a controlled atmosphere and held for a defined period. The investigated material will wet and interact with the refractory. This procedure is usually used to regard wetting behaviour and measure contact angles at the interface. This is more complicated when reactions occur. [LEE 04] Typically a hot stage microscope is used. [ANEZIRIS 08, JANKOVSKÝ 18]

Dipping test (b)

In the dipping, immersion or finger test, shown in Figure 2-8b, a cylindrical or prismatic shaped refractory samples are immerged in a liquid like a corrosive slag or molten metal for a certain period. The atmosphere can hereby easily be controlled. The temperature is kept constant during time of contact. To compensate the alteration of the fluid, due to a rapid saturation with reaction products, the volume of the slag should be large enough relative to the size of the samples. Any slag flow in this test arises from the thermal convection in the slag and so is small. [LEE 04]

Cup test (c)

Here a hole of usually 50 mm diameter is drilled in shaped or formed in unshaped refractories and filled with the corrosive material, see Figure 2-8c. Afterwards all is placed in a furnace and heated to a specific temperature for a defined time. Afterwards the cup is cut in half to evaluate the processes. This way, isothermal reactions and penetration behavior are comparable among different materials. [BROSNAN 04, p.75] Post mortem also microstructural and chemical analysis are possible. [GEHRE 12]

Induction furnace test (d)

The induction furnace test is illustrated in Figure 2-8d. For this refractory samples different samples can be set in the shape of a polygonal crucible. Since the contents need to conduct electricity, metal and slag have to be combined in the crucible and melted together by the induction heating. Hereby a temperature gradient can be achieved, and atmosphere as well as temperature can easily be controlled. A rapid and vigorous corrosion is a result of the melt/slag line since the interface tension difference (as described in the Section Erosion above). There is a little motion of the metal induced through the magnetic field and the heating leading to some dynamic aspects. The results are therefore comparable to typical applications in a practical furnace except the uncontrolled flow. [LEE 99]

Rotating finger test (e)

The rotating finger test is shown in Figure 2-8e. In addition to the method (b), the sample is rotated. For cooling an inert gas atmosphere can be used. For post mortem analysis the specimen is cut and studied. The benefit of this method is the defined convection flow around the immersed part of the "finger", reproducing the motion of liquid slag or metal. Through removal of the boundary layer, refractory wear is increased. [BROSNAN 04, p.75]

One possible application is a steel casting simulator in which samples are tested against molten steel in controlled temperature field and atmosphere. [ANEZIRIS 13]

Rotary slag test (f)

The rotary slag test, as shown in Figure 2-8f. For this, refractory bricks are bevelled or casted to form a polygonal crucible within a rotary induction furnace. Metal or slag are melted through induction heating and constantly added. Due to the temperature gradient between the inner and outer surface, the interface can be effectively recreated using this test. This method has some dynamic aspect due to the motion of the slag and fresh material is constantly brought to the contact zone. [BROSNAN 04, p.75]

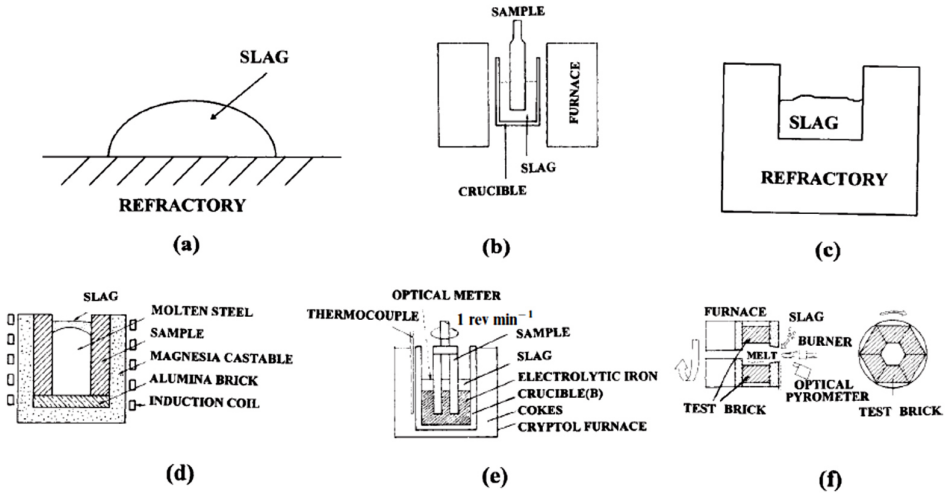

Figure 2-8: Illustration of the general experimental set up of the different corrosion test methods. [LEE 99]

2.3.3 The elasticity of solids

As expressed in the chapters before, refractories are subjected to severe stresses. Therefore, there are different methods to determine their properties and hence their suitability, for example for thermomechanical demands. The following section should thus give an overview of the elastic behaviour of solids and the modulus of elasticity of ceramics in particular.

Solids are named after their dimensional stable condition. However, this does not mean they are rigid. When force is applied, they tend to deform in a certain way, depending on the bonding characteristics. [HARTEN 07, p.95]

Imagine a bar, made of a random solid with the section area A, on which force F is applied (M is the occurring torque). There are five different basic stress types, illustrated in Figure 2-9, showing the possible loading directions (arrows). In the following focus is given to tension and shearing, because compression shows the same relations as tension and torsion for shearing. [BÖGE 11, p.281]

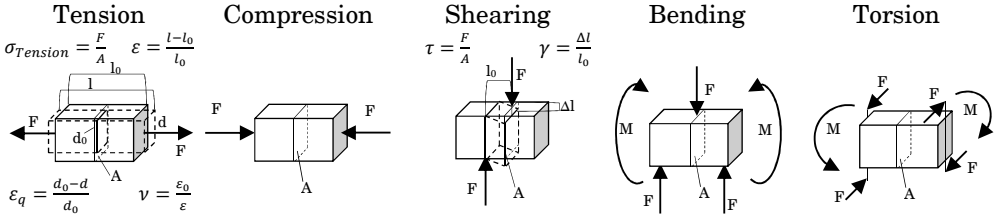

Figure 2-9: Illustration of the five basic stress types regarding the application of force to a rectangular solid.

The deformation under tensile load, called strain ε, is related to the stress σ. Thereby the sample extends from the original length l_0 to the length l. The strain defined the gained length divided by the initial one ($l-l_0=\Delta l$). At the same time the cross-sectional area decreases. The ratio of the differing thickness ($d_o-d=\Delta d$) to the initial thickness d_0 is defined as cross strain ε_q. The ratio from cross strain to strain is the Poisson ratio μ: [BÖGE 11, p.280–281]

$$\mu = \frac{\Delta d/d_0}{\Delta l/l_0} = \frac{\varepsilon_q}{\varepsilon} \tag{2-7}$$

The volume remains constant for plastic flow, viscous flow, and creep, thus: ν = 0.5. For elastic deformations the Poisson's ratio is found to vary between 0.2 and 0.3. [KINGERY 76, p.770]

For a proportional correlation of stress and strain, Hooke's law can be applied:

$$\sigma = E\varepsilon \tag{2-8}$$

In this case E, the modulus of elasticity or Young's modulus, is a constant. Therefore, the object or material shows linear elastic behaviour: after relieving the stress, the object returns to its initial shape. This behaviour merges in a nonlinear elastic range and ends at the elastic limit where it merges to a plastic behaviour. This is characterised by an irreversible deformation. The strain increases disproportionately with the raised stress. In the end, if the stress is further increased, the material will fail - a fracture occurs. [HARTEN 07, p.95–97]

Similar to the tensile load there is a relation for shear load. Hereby, the shear stress τ is the product of modulus of rigidity G and shear strain γ: [KINGERY 76, p.770]

$$\tau = G\gamma \tag{2-9}$$

The Poisson's ratio relates both elastic moduli by the following equation: [KINGERY 76, p.770–771]

$$\mu = \frac{E}{2G} - 1 \tag{2-10}$$

This relationship supposes an isotropic body in which only one value for the elastic constant is independent of direction. Generally, this is not the case for single crystals, yet it is a good approximation for most polycrystalline ceramic materials. [KINGERY 76, p.770–771]

The bulk modulus K completes the elastic moduli. He is defined as the ratio of isostatic pressure and relative volume change. Thereby applies: [KINGERY 76, p.771]

$$K = \frac{E}{3(1-2\mu)} \tag{2-11}$$

In general, the approach on the behaviour of loaded solids is difficult to include every factor. Often the material is not perfect structured, isotropic, and single-phase. In addition, the forces are often higher than for elastic behaviour usual and also the loading velocity is of particular importance. Nevertheless, it is the base for all later considerations. Therefore, the materials were regarded as continuum without further consideration of the atomic structure and the elastic moduli as material constants. This approximation is true due to the relative longer scale of effects in contrast to the medium inter-atomic distance. For a medium distance of 1 Å = 10^{-10} m the effect distance should be 100 Å or longer. Acoustic waves for example with a typical velocity of 10^3 m to 10^4 m result in a maximum frequency with f = v/λ of 10^{11} to 10^{12} Hz. This is the range of sound and ultrasonic waves. Thus, it is a good approximation for the following section, in which the topic of elasticity is deepened for ceramics.

The modulus of elasticity of ceramics

The difficulty for ceramics is their brittleness. They tend to fail through fracture without an actual plastic deformation before. This is due to their polycrystalline structure, the mixture of phases or pores. [KINGERY 76, p.768–773] These factors present the main dependencies on the elastic moduli.

In Table 2-1 the elastic properties of exemplary ceramics are shown. These are theoretical values, which means the impact of defects like impurities, pores, and grain boundaries were not considered.

Table 2-1: Examples for elastic constants of some ceramics. [SOGA 68, MANNING 69, ROSSI 70, SALMANG 07, p.391]

Material	E [GPa]	G [GPa]	K [GPa]	μ
Al_2O_3	410	165	255	0.23
MgO	310	130	155	0.17
ZrO_2	190	75	140	0.27
CaO	184	76	105	0.21
Y_2O_3	171	66	136	0.30
Cr_2O_3	327	130	232	0.26
SiC	480	200	240	0.17

Considering that a material may consist of more than one phase, considering pores as a phase too, there are different approaches for the assessment of the modulus of elasticity. Both consider a homogeneous distribution, equation (2-12) for a parallel alignment towards the applied stress, equation (2-13) respectively for a perpendicular one. [SALMANG 07, p.391]

$$E_g = \sum_{i=1}^{n} \phi_i E_i \tag{2-12}$$

$$\frac{1}{E_g} = \frac{\phi_2}{E_2} - \frac{1-\phi_2}{E_1} \tag{2-13}$$

Thereby, porosity is a topic to whom special interest is dedicated. Different models were developed because of the different pore forms, sizes and total amount within a material. Another factor is the experimental validation due to problems in measurements given by the geometry and high porosity. [RICE 93, BOCCACCINI 97, ROBERTS 00, PABST 07, DAVID 11, WERNER 15, GRABENHORST 19]

Another influence is the temperature. Due to the relation of the elastic properties of ceramics to their structure, a huge impact may be expected. Rising temperature extends atomic distances, therefore the elastic modulus should decrease. [SCHWARTZ 52, WACHTMAN 59, HUGER 02] However, a nonlinear decrease of the Young's modulus decreases at higher temperatures was observed. This was attributed to a grain boundary slip. [WACHTMAN 59]

Measurement of the modulus of elasticity

Basically, there are two different methods to determine the elastic moduli experimentally. The distinction and naming therefore are derived from the applied stress.

Quasi-static

With this method Hooke's law is used, in which the elastic modulus is the slope of the stress-strain curve. Therefore, commonly a three point bending test is made, measuring the strain for increasing stress. For this, force is subjected onto a

rectangular bar which is rests on two supports. At the central load application point, a compression stress is induced while on the other side of the specimen a tensile stress occurs. The stress is defined with:

$$\sigma = \frac{3FL}{2bh^2} \tag{2-14}$$

F is the applied load, L the distance of the bottom supports, b and h are width and heights of the sample. Regarding the area of the specimen and its geometrical moment of inertia, the elastic modulus can be calculated from:

$$E = \frac{FL^3}{4bh^3y} \tag{2-15}$$

Here y represents the deflection of the sample.

Typical standards for determining the Young's modulus from the load-deflection curve of refractory materials are ASTMC469 / C469M, ASTM E111 and DIN EN 843-2.

Dynamic

The so called dynamic methods have the advantage of being a non-destructive way to obtain the elastic moduli. The main concept of the following methods is the propagation of waves in a solid material. They can be divided into the ultrasonic wave velocity method and the resonance frequency method.

Ultrasonic wave velocity method

For this method an ultrasonic wave is channelled through a specimen. Thereby, different waves occur. Two types of them are of special interest. A wave which vibration direction is equal to the propagation direction, called longitudinal wave, while a transverse wave has a perpendicular vibration direction to the propagation. Basically, the time that the longitudinal wave needs to pass through the material is used for the calculation of the modulus of elasticity. However, it has to be taken into account, that there are some the border conditions. An important influence on these equations have the specimen dimensions. Most of the equations and relationships were derived from the model of an infinite long specimen. When the specimen is too short for example, the measured waves could not be right interpreted due to insufficient pulse duration. For appropriate high frequencies of the excitation wave the dimensions become infinite compared to the wavelength. Then the following equation is valid: [RENTSCH 61]

$$E = \rho v_l^2 \frac{(1+\mu)(1-2\mu)}{1-\mu} \tag{2-16}$$

Where ρ is the (bulk) density of the material, v_l is the velocity of the longitudinal wave and μ Poisson's ratio. For the measured velocity of the transverse wave v_t follows the shear modulus G with:

$$G = \rho v_t^2 \tag{2-17}$$

The actual measurement is carried out by either bonding or clamping the sample between a piezoelectric emitter and receiver to measure the transit time of the excited sound waves. From this time the respective velocities are calculated with the length of the specimen.

ASTM E494-15, DIN EN 843-2:2006 and DIN EN 12504-4:2004 are standards describing the actual measurement setup and providing equations for the calculation of elastic constants.

Depending on the measuring setup and used emitter and receiver, there are some specialties to respect. Because of the alternative usage for quality check on concrete components, for example, of some of the equipment, only the pure transit time of the wave is captured. This leads to the following two problems. One is the missing second velocity to determine the Poisson's ratio for further calculation. This is no problem if the material itself is well known and this ratio was determined before, for instance for quality checks during production is this possible, because the time and effort could be kept low. The second problem is more severe. These measurements base therefore on the assumption, that the first recorded wave is the fasted, which is true for the longitudinal wave. But if the specimen is too short, the wave does not have enough time for a preferably complete period duration. Also, the differences between the induced waves are small and then the captured time might not be the one of the longitudinal wave. This leads to wrong calculations. There are no public evidence or studies referring to this very special subject, yet. But the theoretical approach can be retraced from the literature. [RENTSCH 61, RENTSCH 63]

Resonance frequency method

This method is based on the fact that every material has its own resonance frequency. Currently The standards ASTM E 1875-08 and ASTM E 1876-09 are describing setup for the measurements and following calculation of elastic moduli for several specimen shapes. There are two different methods of excitation. This can either be constantly by a piezoelectric transducer where the signal input is induced by a piezoelectric receiver or laser vibrometer, or by a mechanical impulse, where an impulse is manually given, and the result is recorded by a microphone. The name of the method is due to the resonance frequency of the specimen, which is indicated by an increased signal.

In this study the impulse excitation technique (IET) will be used and is described more detailed in the following. The setup is illustrated in Figure 2-10. The

prismatic sample is aligned on the supports. Then an impulse is induced either by a manual striking of the specimen with a suitable implement or automated with a projectile accelerated by an electromagnet. The signal pickup is either a piezoelectric transducer or, like used in this study, a microphone. The respective signal is afterwards conditioned, amplified and analysed. The audio signal in this case is subsequently divided into single waves using the fast Fourier transformation algorithm to obtain a certain frequency spectrum. Often a large variety of frequencies may occur, therefore it is important to stick to the specified support distances and setup. The frequencies obtained can now matched to the flexural or torsional character. The elastic modulus is calculated from:

$$E = 0{,}9465\left(\frac{mf_f^2}{b}\right)\left(\frac{l^3}{t^3}\right)T_1 \tag{2-18}$$

Where m is the mass of the sample, b, l, and t are the sample dimensions, f_f the flexural resonance frequency and T_1 a correcting factor to account the sample dimensions and Poisson's ratio.

For the shear modulus it is:

$$G = \left(\frac{4lf_t^2}{bh}\right)\left(\frac{B}{1+A}\right) \tag{2-19}$$

Where f_t is the frequency of torsion and A and B correcting factors. All correction factors can be calculated from the standard ASTM E 1876.

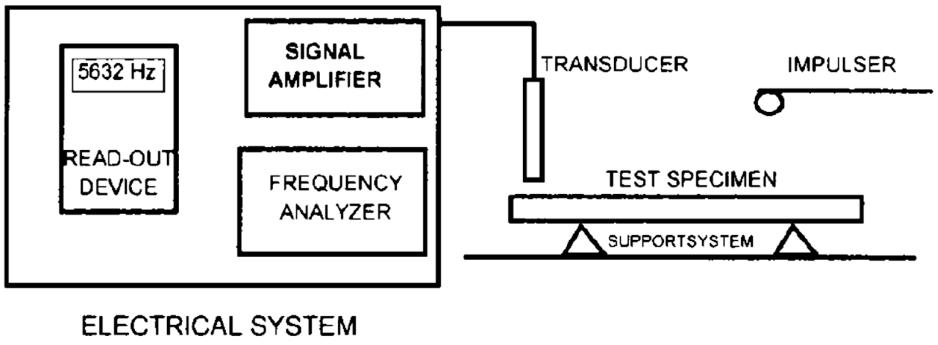

Figure 2-10: General measurement setup for the IET. [ASTM E 1876]

With this method, it is also possible to obtain high temperature elastic modulus measurements for temperatures up to 1600 °C, in case of the application at the Institute of Ceramic, Glass, and Construction Materials at the TU Freiberg, Germany. Therefor the support together with the sample is placed in a dense furnace chamber with electric heating. The excitation is done by a ceramic projectile with electromagnetic impulse acceleration. The audio signal is conducted over an alumina tube to the audio microphone. It is possible to set an oxidational atmosphere or an inter atmosphere with purging. [WERNER 14, WERNER 16a, WERNER 16b, GRABENHORST 19]

2.3.4 Thermal shock parameter

One of the most crucial factors for ceramics, especially for refractories, is the high temperature or rather its rapid change. Due to their usage, refractory materials are exposed several thermal gradients, for example if a molten metal is filled in for transporting or the metal is directly molten within a crucible made of such materials. Unsurprisingly, the resistance of ceramics against these so called thermal shocks is one of the most investigated and reported field of study. In 1955 Kingery was the first to describe several factors affecting the stresses in the material. He introduced thermal shock resistance parameter describing crack initiation within the material due to temperature change. He defined the maximal temperature difference a material can resist, for a very rough thermal shock without heat transfer with:

$$R = \Delta T = \frac{\sigma(1-\mu)}{E\alpha} \tag{2-20}$$

Whereas the stress (σ), the Poisson's ration (μ), the Young's modulus (E) and the thermal expansion (α) are related.

In case of a constant heat transfer the thermal conductivity (λ) was introduced [KINGERY 55]:

$$R' = \frac{\sigma(1-\nu)\lambda}{E\alpha} \tag{2-21}$$

Later, Hasselman expanded the theory regarding not only the maximum stress the material can withstand but also the initiation and propagation of cracks damaging the material. In a wide variety he also includes more conditions for the thermal strains and material properties or characteristic values. Two of the numerous thermal shock damage parameters are:

$$R'''' = \frac{EG_f}{\sigma^2(1-\mu)} \tag{2-22}$$

$$R_{ST} = \sqrt{\frac{G_f}{\alpha^2 E_0}} \tag{2-23}$$

Here the specific fracture energy (G_f) relates to a minimum crack propagation. From that conclusions can be drawn regarding the possible failure or residual strength of a stressed material. And the second one is about the propagation of cracks. [HASSELMAN 69]

Regarding these commonly considered parameters, the role of the modulus of elasticity is quite different. For an increasing R, R', and R_{ST} lower values of E and α are beneficial. Whereas for low crack propagation R"" a high value for E is desired. These are countering considerations, pending on the modelling of the viewed situation. Another fact is that the assumed the elastic constants and other properties as temperature independent, which is not in reality.

2.4 Conclusion

The review on the present researches and the regarded topics of the past chapter shall be concluded here.

There were already several methods investigated to produce materials in the $CaO\text{-}ZrO_2$ phase system. Thereby, an equimolar and a homogeneous mixture is very important. For a complete reaction temperatures of above 1000 °C were reported. Long dwell times or several cycles of forming, sintering and crushing had to be made. Several procedures utilised salts or organometallic complexes or worked in or with alcohol which pose a risk in processing, are hazardous or expensive. The production of dense, coarse grained fraction of single phase calcium zirconate adaptive for mass production was not yet reported. Although the presence of free lime in a sample was not always detectable, it always led to alteration of the samples up to a complete disintegration.

It was shown by some authors, that there are beside the numerous applications as fine ceramic due to its perovskite structure, currently investigations on refractory uses. There are different approaches and results in the tests, yet it was shown that there are problems with polyphase material.

The review on the possible applications and therefore target markets, has shown, that the requirements are very different but also give several chances to challenge currently used materials. There is no material which could cover everything also tacking the costs and production efforts into account. A high Gibbs energy of formation increases the stability against reactive metals, especially in vacuum atmosphere.

The example on the examination of potential refractories for the processing of titanium alloy melts showed the requirements on such materials. Additionally, it showed the potential of calcium zirconate materials for such applications. Yet, the focus was laid on two other applications due to parallel conducted work in the topic of titanium melting. These fields showed the need of new materials due to pricing, improved thermal shock behaviour resulting in longer service time, and fewer hazards during or after service time.

For the selection of the right corrosion tests for an application a variety of factors have to be considered. Besides the actual temperature and atmosphere also their change should be kept in mind during the service time and therefore also for preliminary tests as well as the ratio of corrosive material to refractory and the movement or alteration of the slag.

The impulse excitation technique is a well understood methods for the determination of the elastic constants. Focus is on the modulus of elasticity, which allows conclusions or at least estimations on thermal shock behaviour of a refractory material

All together resulted in the choice of the solid state synthesis as processing route because of the less effort necessary and the simpler upscaling possibility for later industrial realisation. For the fabrication of the refractory samples the uniaxially pressing and slip casting was chosen due their efficient feasibility of producing test specimen in simple and later more complex geometries. Furthermore, the selection of possible applications and their preliminary testing as well as the characterisation of the obtained materials was done accordingly.

3 Part I: Synthesis of calcium zirconate

The first practically section is about the synthesis of the calcium zirconate. Due to their lack of natural deposition it has to be synthesised from the raw materials, as described in section 2.1.2. [GALUSKIN 08] In the following, the used materials, preparation steps and test methods are explained. The main intension is to understand the synthesis reaction and the effects of different parameters. Attention is also given to the requirements of later industrial preparation procedures.

3.1 Experimental

The aspects of a satisfying synthesis are a complete formation of calcium zirconate with no free lime or zirconia, the least maximum temperature of formation, the necessary mixing effort, and the influence of the raw materials. Accordingly, the investigated subjects and testing methods are chosen which are presented beneath.

3.1.1 Raw materials

The formation of calcium zirconate is the reaction of calcium oxide and zirconium dioxide. The chemical equation is:

$$CaO_{(s)} + ZrO_{2\,(s)} \rightarrow CaZrO_{3\,(s)}$$

Hence calcium oxide features a certain tendency of alteration in presence to water and carbon dioxide, other raw materials were investigated. [LI 08a]

A general overview of the used raw materials is given in Table 3-1. A commercial monoclinic zirconium dioxide powder was used. As calcium oxide precursors were three different materials used to examine their reaction behaviour. First, a commercial calcium hydroxide powder, a commercial calcium carbonate powder, and later another calcium hydroxide powder was utilised. The latter was alternatively needed because of possible alteration of the first calcium hydroxide

material concluding from early test results. Pure calcium oxide was not regarded due to its reactivity to water and carbon dioxide. [KAWANO 91]

Table 3-1: Properties of the raw materials.

Chemical compound	Name	Distributor	Properties
ZrO_2	ZirPro CS02	Saint-Gobain	monoclinic d_{50} = 0.8 µm
$Ca(OH)_2$	PreCal 54	Schäfer Kalk GmbH & Co. KG	d_{50} = 0.4 µm
$Ca(OH)_2$	≥96 %, pulv.	Carl Roth GmbH & Co. KG	not determined
$CaCO_3$	PreCarb 400	Schäfer Kalk GmbH & Co. KG	d_{50} = 1.9 µm

3.1.2 Sample preparation

To investigate the synthesis of calcium zirconate with different parameters, a processing route with uniaxial pressing of the dry batches was chosen. This section gives a detailed overview of the specific work steps from the raw materials to the testing samples.

Through varying the mole ratio of ZrO_2 and CaO, the resulting phase composition in the synthesised materials was investigated. The observation of the behaviour of the excess of calcia while and after sintering has also been of interest. The molar ratio ranged from 1.6:1 over 1:1 up to 1:3 (ZrO_2:CaO). Two different mixing methods were used to get an overview of the necessary mixing effort. The reduction of expenses concerning the mixing efforts is a factor for later industrial application of the synthesis. A simple paddle mixer in contrast to a tumbling mixer is less complex, not only because of the fewer utensils used. The possibility of upscaling is of interest as well as the demand of a homogeneous batch.

For the first mixing process, a tumbling mixer (Turbula System Schatz Type T2C, Willy A. Bachofen AG Maschinenfabrik, Muttenz, Switzerland) was used because of the three dimensional oloide mixing motion which unites impulsive rotation, translation and inversion. [PORION 04, FRUHSTORFER 14] For milling and deagglomeration, ball grinding media made of yttrium stabilised zirconia (SiLibeads, Sigmund Lindner GmbH, Warmensteinach, Germany) were used to prevent contamination with further chemical elements. Fruhstorfer et al. figured out that the usage of two different sized grinding balls is most effective and for good homogenisation a mixing time of about 10 min is enough. [FRUHSTORFER 14] Based on their calculations and according to the available qualities of ball sizes, the diameter of the utilized balls was chosen with 2.0 - 2.5 mm and 15.5 mm. Table 3-2 summarizes the properties of the used grinding media balls. Thereby, the relative filling ratio describes the ratio between the volumes of the balls and the container they are filled in.

The raw materials were weighed and filled in a plastic container with a volume of 1000 ml. Then the grinding balls were added. The tumbling mixer is set fix to 30 rpm. Powder and balls were mixed for 10 min, then the distilled water was added, and everything was mixed again for 10 min. Later the powder was separated from the grinding media by screening through a 1.25 mm sieve by hand.

Table 3-2: Properties of the used mixing balls.

Property	Small balls	Large balls
Material	Y_2O_3-stabilizied zirconia	Y_2O_3-stabilizied zirconia
Diameter (mm)	2.0 – 2.5	15.5
Relative filling ratio (%)	63.0	56.6
True density (g·cm^{-3})	6.04	5.98

For the second mixing route a paddle mixer (ToniMIX, Toni Technik Baustoffprüfsysteme GmbH, Berlin, Germany) was used. The powder materials were weighed and mixed for 10 min in the mixing container. Subsequently, water was added and again mixed for 10 min. This alternative route for batch preparation needed less process steps.

In a next step, rectangular bars were pressed (7 x 70 mm^2) at 60 MPa in a die press (ES 270, RUCKS Maschinenbau GmbH, Glauchau, Germany). The mould had a height of 20 mm and was completely filled with material for every sample. The height of the samples therefore depends on the amount of material used. The sample weight was 6 g to 7 g. For each sintering condition, at least ten specimen were prepared of each batch. These bars were later dried for 24 h at 100 °C and then immediately cooled and stored in a desiccator.

For sintering, a Nabertherm furnace (LH 15/14, Nabertherm GmbH, Lilienthal, Germany) was used with a heating rate of 3 K·min^{-1}, a dwell time of 5 h and then free cooling. Different conditions were set regarding the maximum temperature. In the beginning, the firing was carried out at three different temperatures: 1200 °C, 1300 °C and 1400 °C in accordance with Li et al. [LI 13] Additionally, sintering at 1000 °C was investigated to determine the effect of the different temperature of decomposition of the calcia precursors on the formation of calcium zirconate. Higher temperatures of 1500 °C and 1600 °C were also examined to study their influence on the sample properties. Furthermore, the samples were also sintered in a covered kiln furniture at 1200 °C to examine the influence of the possible evaporation of components while firing. For this purpose, another tray of kiln furniture was placed above the one with the samples. At last the influence of heating rate was investigated, which was increased to 10 K·min^{-1}.

Afterwards the specimens were crushed by hand and in a vibratory disc mill for analysing.

3.1.3 Testing methods

In the following section the conducted methods of the characterisation are presented. These are referring to raw materials as well as green and sintered samples. The aim is to understand the processes during the synthesis just like the effects of certain parameters on the resulting properties of the obtained material.

Grain size distribution

The distribution of the particles in the raw materials, besides the later obtained grain classes, is relevant to understand the synthesis process on the one hand, and to calculate the densest packing of the grains in the subsequent refractory material on the other hand. For material above 0.63 mm mesh, the particle size distribution was determined by sieve analysis in accordance with the standard DIN 66165-2:2015 with a vibratory sieve shaker (AS 200 control, RETSCH GmbH, Haan, Germany).

For samples with grain size lower than 0.63 mm, a laser granulometer (Beckman Coulter LS230, Beckman Coulter Inc., Brea CA, USA) according to the standard DIN EN 725-5:2005 was used. Water was used for dispersing.

True density

The density of the material was determined by helium pycnometry (AccuPyc II Tec, Micromeritics Instrument Corp., Norcross GA, USA) according to the standard DIN 66137-2:2004. The samples were therefore ground in a vibratory disc mill to eliminate porosity.

Thermal analysis

To investigate the reaction behaviour of the raw materials as well as the raw material mixtures undergoing a certain heat treatment, thermogravimetry (TG) and differential scanning calorimetry (DSC) curves were investigated (STA 409 PC/PG, NETZSCH-Gerätebau GmbH, Selb, Germany). Therefore, platinum crucibles were heated with a rate of 20 $K \cdot min^{-1}$ up to 1450 °C in air atmosphere. This differential thermal analysis was made according to the standards 51004:1994 to 51007:1994. The samples were already powdered thus, there was no need for further preparation.

Sintering behaviour

After firing, the permanent length change (PLC), apparent density, and mass loss of the samples were determined by comparing the geometrical dimensions and mass before and after sintering.

Phase identification

The mineralogical phases were examined by X-Ray diffraction (XRD) (STOE STADI P, Stoe & Cie GmbH, Darmstadt, Germany). Data evaluation was carried out with the analysis software X'Pert HighScore Plus (Version 2.2.4, 2008, PANalytical B.V., Almeo, The Netherlands). Sample material was dried and ground to a particle size less than 45 µm in a vibratory disc mill.

Surface analysis

The surfaces and the fractured surfaces of the samples were examined using a digital optical microscope (VHX-200 D, KEYENCE Deutschland GmbH, Neu-Isenburg, Germany).

Scanning electron microscopy

The two mixing regimes were compared regarding the homogeneity in the fired samples with scanning electron microscope (SEM) images (SEM/FEI Philips Type XL30, Philips Nederland B.V., Eindhoven, The Netherlands).

The microstructure and the local element distribution from the sintered samples were determined in combination with energy dispersive X-ray spectroscopy (EDX). Therefore, the surface of small pieces of the respective sample was sputter coated with carbon sputter coater (Cressington carbon coater 208carbon, Cressington Scientific Instruments Ltd., Watford, England).

Porosity

The water absorption and resulting porosity values were determined by hydrostatic weighting according to DIN EN 993-1:1998. Soaking medium was always tap water with an adjusted temperature of 24 °C. The measured samples were halves of the test specimens or fragments from larger bricks.

Chemical composition

The chemical composition of liquid solutions of sample material was investigated by inductively coupled plasma optical emission spectrometry (ICP-OES) (Spectroflame Compact S, Spectro Analytical Instruments GmbH, Kleve, Germany).

3.2 Results and discussion

In this section, the results from the aforementioned measurements and analysis are presented and discussed. It is arranged chronologically, starting with the batch making characteristics and ending with the properties of the sintered material. For the sake of completeness, all performed tests are gathered and accessible here. This means that there were also tests made far aside the equimolar ratio and the usual conditions to have a look outside the box.

3.2.1 Creation of the batches

For the first investigations, three different mole ratios (ZrO_2:CaO) were used. Beside the favoured equimolar ratio (1:1), other ratios are regarded: one of the zirconia rich side (1.6:1) and some of the calcia rich side (1:1.5); (1:2); and (1:3). For the calculations, the molar mass of each element was used. Of course, the ratio was adapted to the respective raw calcia precursor. The used molar masses were rounded to two decimal places, whereby the calculated results were rounded to three decimal places. The complete overview of the used and calculated data for this part is given in the Appendix: A. 1 Stoichiometric calculations.

3.2.2 Thermal analysis

The first reason to investigate the thermal behaviour of the batches made of raw materials was to get information about the processes occurring while heating up. Furthermore, the beginning of the reaction of formation of calcium zirconate could be set to a starting temperature resulting in a first parameter for the synthesis striven by this part of work.

At first, calcium hydroxide was investigated as calcia precursor. Figure 3-1 shows the mass loss while heating of batches with a different ratio of zirconium dioxide to calcium oxide. The first mass loss occurred at around 100 °C due to evaporating water. Later, the decomposition of the hydroxide took place at about 450 °C resulting in significant mass loss. Surprisingly these losses did not coincide with the calculated one. For the calcium hydroxide necessary for a ratio of 1.6:1, the theoretical mass loss would have been 6.6 wt.-%, 9.1 wt.-%, and 11.5 wt.-%, respectively for the other two ratios. But a second mass loss was visible at 600 to 700 °C. Investigation on the raw material showed that this was due to the decomposition of calcium carbonate which the calcium hydroxide raw material contained. Comparable observations made Sawada and Ito in there study. [SAWADA 94] The origin of calcium carbonate may have been an alteration during storage.

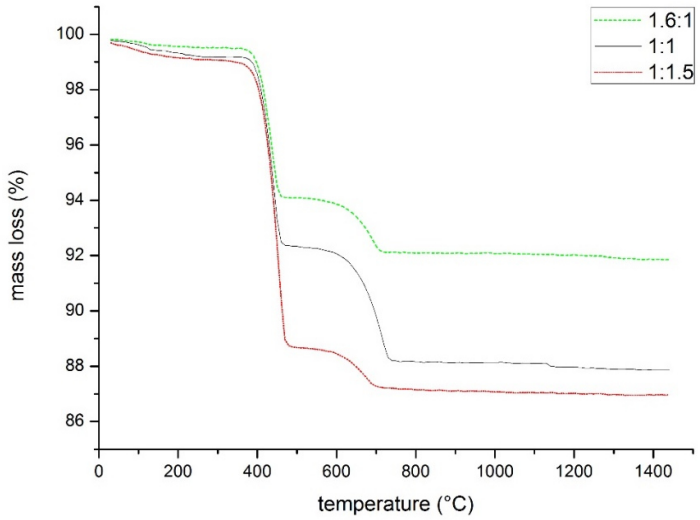

Figure 3-1: Thermal gravimetric measurements of batches made of zirconium dioxide and calcium hydroxide (legend: ratio ZrO_2 : CaO).

Figure 3-2 presents the corresponding calorimetry curves of the three samples. The first endothermic peak recognisable at around 100 °C was due to the evaporating water. The main endothermic peak at around 440 °C corresponded to the decomposition of the hydroxide. It can be seen that the amount of calcium hydroxide within the batches correlated with the depth of the magnitude. An exothermic reaction was remarkable, which began at about 700 °C and ended at about 1200 °C indicating the reaction of calcia with zirconia forming calcium zirconate. Because of the maximum thermal reaction at about 1200 °C, this temperature was chosen as the main sintering temperature for all following investigations. Due to the heating limitation of the used device of 1450 °C during thermal analysis, a possible increasing mass loss of the samples with calcium hydroxide above 1500 °C was not observable.

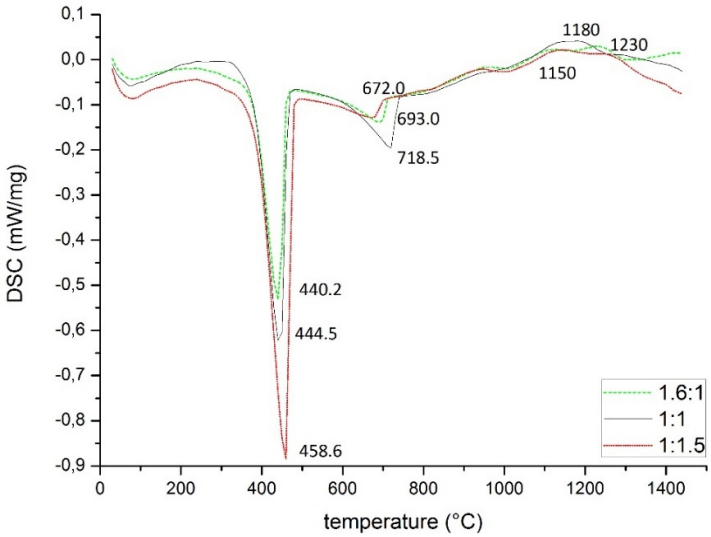

Figure 3-2: DSC curves of batches made of zirconium dioxide and calcium hydroxide (legend: ratio ZrO_2 : CaO).

A DSC/TG investigation on the pure calcia precursor materials confirmed that there was calcium carbonate within the calcium hydroxide. For further investigations, the second $Ca(OH)_2$ was used.

In Figure 3-3 the mass loss of batches with different calcia sources is shown. As assumed, the second drop of the curve was consistent with the decomposition of pure calcium carbonate which the second sample contained. It validates the first assumption that the used calcium hydroxide contained amounts of calcium carbonate.

The curve characteristics of the DSC analysis of the batches with the two different calcia sources (old calcium hydroxide; calcium carbonate) are illustrated in Figure 3-4. The endothermic peak with a minimum at 807.3 °C shows the decomposition of calcium carbonate. In contrast to the sample made with calcium hydroxide with the residual amount, the temperature was higher, but the peak value was overall lower. The temperature was influenced by the particle size and lowered through the initial decomposition of the calcium hydroxide. For the sample made of calcium carbonate there were two local maxima of exothermic peaks and the start of the calcium zirconate formation is shifted compared to the sample made of $Ca(OH)_2$. The comparison of the mass loss of the samples from calcia sources at the same mole ratios in Figure 3-3 shows the different temperatures of decomposition and the different mass loss through this process. It also indicates the early results observed from the raw material investigation, that the calcium hydroxide contained calcium carbonate indicated by the remarkable second decomposition in the same temperature range. Figure 3-4 provides the DSC analysis of these samples with different calcia sources. The individual values of endo- and exothermic effects differed comparing the two samples.

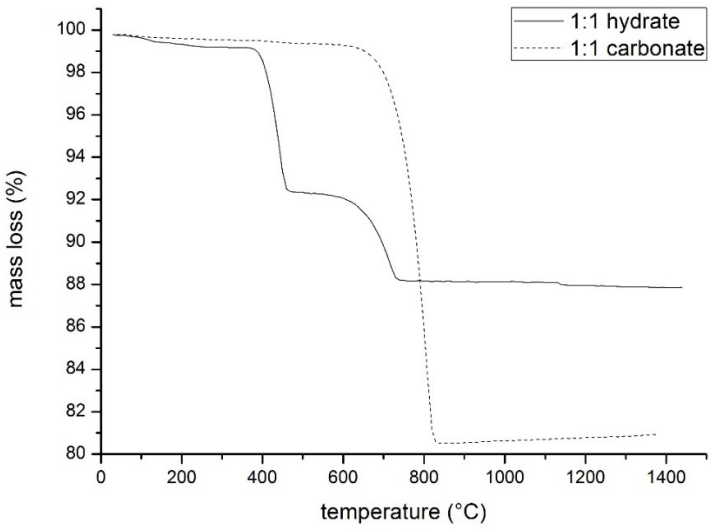

Figure 3-3: Mass loss over rising temperature for the batches made of different calcia precursors. (legend: ratio ZrO_2 : CaO)

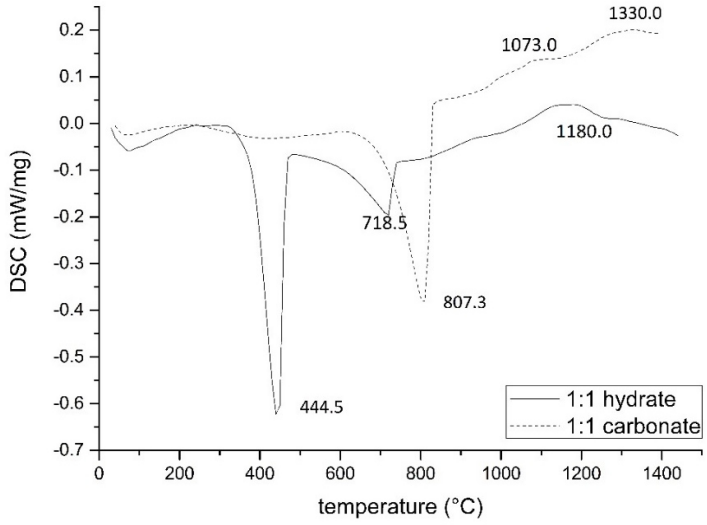

Figure 3-4: Comparison of DSC graphs for equimolar mixtures made from different calcia precursors. (legend: ratio ZrO_2 : CaO)

3.2.3 Properties after sintering

Changes in the length, density, and mass of the fired samples compared to the green samples depending on the used mole ratio and sintering conditions are given in Table 3-3 to Table 3-5. Based on these measurements, the apparent density and total porosity were determined. For each property, five to ten specimen were investigated. Considering first the samples with calcium hydroxide (see Table 3-3), the green density decreased with an increasing amount of calcium hydroxide in the mixture. In general, the density increased with the firing temperature, while the total porosity decreased. But due to a different change of the length of the individual samples there is no direct correlation between density and mole ratio or green density, respectively. Because of the decomposition of calcium hydroxide during firing, the samples expanded and the density decreased from the green to fired state. When the contribution of sintering was sufficient, depending on the temperature and mole ratio, the densification process led to shrinkage and increasing density. This applied for all samples fired at 1400 °C and above, and with increasing amount of calcium hydroxide at lower temperatures. Because of remaining porosity due to the decomposition process, the densification did not reach the theoretical density of 4.60 $g \cdot cm^{-3}$. [YANG 10] Jonas et al. reported a true density of their calcium zirconate samples of 4.95 $g \cdot cm^{-3}$. [JONAS 98] The true density of single phase calcium zirconate in this thesis ranged from 4.62 $g \cdot cm^{-3}$ to 4.67 $g \cdot cm^{-3}$. The differences within the reported studies may have been resulting from undetectable or undetected secondary phases based on ZrO_2. Yang et al. used commercial 98 % pure material whereby Jonas et al. prepared the material on their own. They also reported somewhat shifted XRD patterns. [JONAS 98, YANG 12] The density of ZrO_2 is about 5.68 $g \cdot cm^{-3}$ thus, increasing amounts of secondary ZrO_2 phases will increase the overall

measured density. [MATWEB 19] With increasing amount of calcium hydroxide in the mixture, the porosity did not increase. This was expected, however, due to the higher amount of decomposing material within the respective batch. Thereby, the decreasing true density due to less content of denser zirconium dioxide was taken into account. A higher sinter activity of the surplus calcia at higher temperatures compared to calcium zirconate was considered. On the other hand, the free calcia led to a destruction of all samples with a mole ratio higher than 1:1 due to rehydration combined with a volume expansion. Thus, these samples were not stable enough to determine water absorption, which is why only total porosity is provided. Investigations on the equimolar samples showed that the total porosity consisted of 95 % open porosity. The median pore diameter decreased from 1152 nm to 162 nm comparing the equimolar samples made with calcium hydroxide after sintering at 1200 °C and 1600 °C while total porosity decreased from 66.7 % to 18.1 %.

Table 3-3: Characteristic properties of samples made with calcium hydroxide.

Mole ratio ZrO_2:CaO	Temperature (°C)	Relative PLC (%)	Density ($g \cdot cm^{-3}$)	Porosity (%)	Mass loss (%)	Theoretical mass loss (%)
1.6:1	green		$2.59_{\pm 0.02}$			6.64
	1200	$-5.56_{\pm 0.07}$	$2.01_{\pm 0.01}$	59.6	$8.84_{\pm 0.18}$	
	1300	$-1.73_{\pm 0.12}$	$2.23_{\pm 0.01}$	55.4	$8.63_{\pm 0.12}$	
	1400	$13.73_{\pm 0.08}$	$3.68_{\pm 0.01}$	26.1	$8.49_{\pm 0.16}$	
1:1	green		$2.33_{\pm 0.03}$			9.12
	1200	$-9.62_{\pm 0.06}$	$1.57_{\pm 0.01}$	66.7	$10.71_{\pm 0.10}$	
	1300	$-3.71_{\pm 0.22}$	$1.85_{\pm 0.01}$	60.8	$11.43_{\pm 0.04}$	
	1400	$13.17_{\pm 0.21}$	$3.14_{\pm 0.05}$	21.1	$11.29_{\pm 0.19}$	
1:1.5	green		$2.21_{\pm 0.02}$			11.52
	1200	$-9.80_{\pm 0.03}$	$1.43_{\pm 0.01}$	64.1	$14.37_{\pm 0.00}$	
	1300	$-4.25_{\pm 0.16}$	$1.68_{\pm 0.01}$	57.3	$13.93_{\pm 0.14}$	
	1400	$8.65_{\pm 0.46}$	$2.53_{\pm 0.03}$	36.2	$14.29_{\pm 0.15}$	
1:2	green		$1.98_{\pm 0.01}$			13.26
	1200	$-4.78_{\pm 0.18}$	$1.54_{\pm 0.01}$	56.8	$14.19_{\pm 0.17}$	
	1300	$1.61_{\pm 0.13}$	$1.84_{\pm 0.00}$	48.2	$14.25_{\pm 0.09}$	
	1400	$13.17_{\pm 0.09}$	$2.62_{\pm 0.04}$	26.4	$14.57_{\pm 0.18}$	
1:3	green		$1.80_{\pm 0.01}$			15.63
	1200	$5.76_{\pm 0.06}$	$1.90_{\pm 0.02}$	40.2	$16.68_{\pm 0.05}$	
	1300	$12.40_{\pm 0.00}$	$2.33_{\pm 0.00}$	27.0	$16.59_{\pm 0.11}$	
	1400	$21.52_{\pm 0.08}$	$3.20_{\pm 0.02}$	0.0	$17.30_{\pm 0.11}$	

The mass loss did not change significantly with increasing temperature up to 1400 °C but was higher than the theoretical loss expected from decomposition (see Table 3-3). There were no significant differences at any temperature in mass loss between uncovered and covered samples (see Table 3-4). Therefore, it was not possible to explain the higher loss by evaporation.

Table 3-4: Samples made with calcium hydroxide with different sintering conditions at 1200 °C.

Mole ratio ZrO_2:CaO	Property	Uncovered	Covered
1.6:1	Density (g·cm^{-3})	$2.01_{\pm 0.01}$	$1.95_{\pm 0.01}$
	Mass loss (%)	$8.84_{\pm 0.18}$	$8.89_{\pm 0.02}$
1:1	Density (g·cm^{-3})	$1.57_{\pm 0.01}$	$1.49_{\pm 0.00}$
	Mass loss (%)	$10.71_{\pm 0.10}$	$10.56_{\pm 0.07}$
1:1.5	Density (g·cm^{-3})	$1.44_{\pm 0.01}$	$1.41_{\pm 0.01}$
	Mass loss (%)	$14.37_{\pm 0.00}$	$14.36_{\pm 0.21}$
1:2	Density (g·cm^{-3})	$1.54_{\pm 0.01}$	$1.56_{\pm 0.01}$
	Mass loss (%)	$14.19_{\pm 0.17}$	$13.97_{\pm 0.10}$
1:3	Density (g·cm^{-3})	$1.90_{\pm 0.02}$	$1.87_{\pm 0.02}$
	Mass loss (%)	$16.68_{\pm 0.05}$	$16.68_{\pm 0.06}$

Table 3-5 compares the physical properties before and after sintering of samples made of the different calcia sources. For the samples with calcium carbonate as the raw material, the mass loss during sintering was in the range of the theoretical loss of about 19.7 % and did not change as a function of the sintering temperature. As seen before, the mass loss of the samples with calcium hydroxide was higher than the theoretical value and in addition, it increased by 4 percentage points above 1500 °C sintering temperature. The difference of about 2 percentage points mass loss for each calcia source between 1000 °C and 1200 °C resulted from rehydration of the calcium oxide during cooling and the time till measurement because the formation of calcium zirconate was incomplete.

An increase of the heating rate to 10 K·min^{-1} for sintering at 1200 °C did not result in significant changes of the physical properties after firing.

To investigate the possibilities of increasing the density of the synthesised materials some preliminary investigations were carried out, even though dense calcium zirconate was not primary aim of this study. It is especially possible to use other processing routes. By hot isostatic pressing a denser body is formed in contrast to pressure less sintering. [KINGERY 76, p.501] Nevertheless an investigation of the possibility to obtain dense calcium zirconate through hot isostatic pressing is considered for future work. Also the adding of some sintering additives may increase the density. [GERMAN 96] The focus in this study is on modification of the heat treatment. Thus, the maximum sintering temperature as well as dwell time was increased for the most promising mixture. The relative density was then investigated. Focus was therefore the sintering temperature and dwell time. In Table 3-6 the results are summarised. The extension of the dwell time to 10 h at 1650 °C showed an improvement of total porosity to a value of 8 %. In addition, the increase of the pressure for sample preparation from 50 MPa up to 100 MPa showed no significant changes in water absorption and density.

Table 3-5: Comparison of 1:1 mole ratio mixtures with different calcia sources including the standard deviation.

Temperature	Property	Hydroxide	Carbonate
green	Density (g·cm^{-3})	$2.35_{\pm 0.00}$	$2.07_{\pm 0.02}$
1000 °C	Relative PLC (%)	$-9.82_{\pm 0.15}$	$-10.47_{\pm 0.05}$
	Density (g·cm^{-3})	$1.64_{\pm 0.01}$	$1.30_{\pm 0.01}$
	Mass loss (%)	$8.17_{\pm 0.11}$	$17.74_{\pm 0.30}$
1200 °C	Relative PLC (%)	$-9.62_{\pm 0.06}$	$-10.55_{\pm 0.06}$
	Density (g·cm^{-3})	$1.57_{\pm 0.01}$	$1.24_{\pm 0.03}$
	Mass loss (%)	$10.71_{\pm 0.10}$	$19.81_{\pm 0.23}$
1300 °C	Relative PLC (%)	$-3.71_{\pm 0.22}$	$-4.14_{\pm 0.02}$
	Density (g·cm^{-3})	$1.85_{\pm 0.01}$	$1.42_{\pm 0.00}$
	Mass loss (%)	$11.43_{\pm 0.04}$	$19.81_{\pm 0.05}$
1400 °C	Relative PLC (%)	$13.17_{\pm 0.21}$	$6.02_{\pm 0.12}$
	Density (g·cm^{-3})	$3.14_{\pm 0.05}$	$1.98_{\pm 0.01}$
	Mass loss (%)	$11.29_{\pm 0.18}$	$20.10_{\pm 0.07}$
1500 °C	Relative PLC (%)	$18.47_{\pm 0.19}$	$19.01_{\pm 0.15}$
	Density (g·cm^{-3})	$3.76_{\pm 0.15}$	$3.16_{\pm 0.02}$
	Mass loss (%)	$15.35_{\pm 0.14}$	$20.00_{\pm 0.13}$
1600 °C	Relative PLC (%)	$22.72_{\pm 0.17}$	$27.40_{\pm 0.16}$
	Density (g·cm^{-3})	$3.80_{\pm 0.00}$	$4.32_{\pm 0.05}$
	Mass loss (%)	$15.38_{\pm 0.06}$	$19.99_{\pm 0.11}$

Table 3-6: Investigation how the relative density of 1:1 mole ratio mixture with calcium carbonate depends on increasing firing temperature.

Temperature (°C)	Dwell time (h)	Water absorption (%)	Total porosity (%)
1400	5	$22.33_{\pm 2.24}$	$50.30_{\pm 3.72}$
1500	5	$11.62_{\pm 0.53}$	$35.20_{\pm 1.55}$
1600	5	$3.14_{\pm 0.53}$	$14.35_{\pm 1.35}$
1650	10	$0.99_{\pm 0.28}$	$7.96_{\pm 0.50}$

3.2.4 Phase identification

Figure 3-5 contains representative XRD curves from the different samples. These provide an overview of the different patterns obtained within this study taking the different investigated parameters into account. In the samples with an over-stoichiometric ratio of zirconia was mainly orthorhombic calcium zirconate ($CaZrO_3$) but also cubic calcia stabilized zirconia (CSZ) ($Ca_{0.15}Zr_{0.85}O_{1.85}$), and a small amount of monoclinic zirconia (ZrO_2). Similar results were obtained by Li et al. within their investigations on slip casted samples with the ratio of 1.6:1 using calcium carbonate as the calcia precursor. [LI 13] The equimolar mixtures showed mainly calcium zirconate and a few percent of CSZ. With higher ratios of calcia calcium zirconate and calcium hydroxide was observed. Additionally, with a ratio of 1:2 and above, free lime was remarkable. In contrast to the samples with calcium hydroxide as calcia source, the samples with calcium carbonate only showed a calcium zirconate formation above 1200 °C. After a second firing step at 1200 °C, the 1:1 sample from calcium hydroxide showed 100 % calcium zirconate but no other changes. The samples prepared with the

second mixing route revealed inhomogeneities due to the amount of monoclinic zirconia and calcium hydroxide. The comparison between uncovered and covered samples only revealed differences for the samples with the ratio of 1:1.5. In the covered samples, free lime was determined and in the uncovered ones calcium hydroxide. These results indicate a partially rehydration of the samples probably occurring during cooling in the furnace. At 1400 °C sintering temperature, the samples with 1.6:1 ratio confirmed the absence of residual monoclinic zirconia but more CSZ as well as calcium zirconate. Up to 1600 °C, the equimolar samples exhibited no permanent alteration like decomposition.

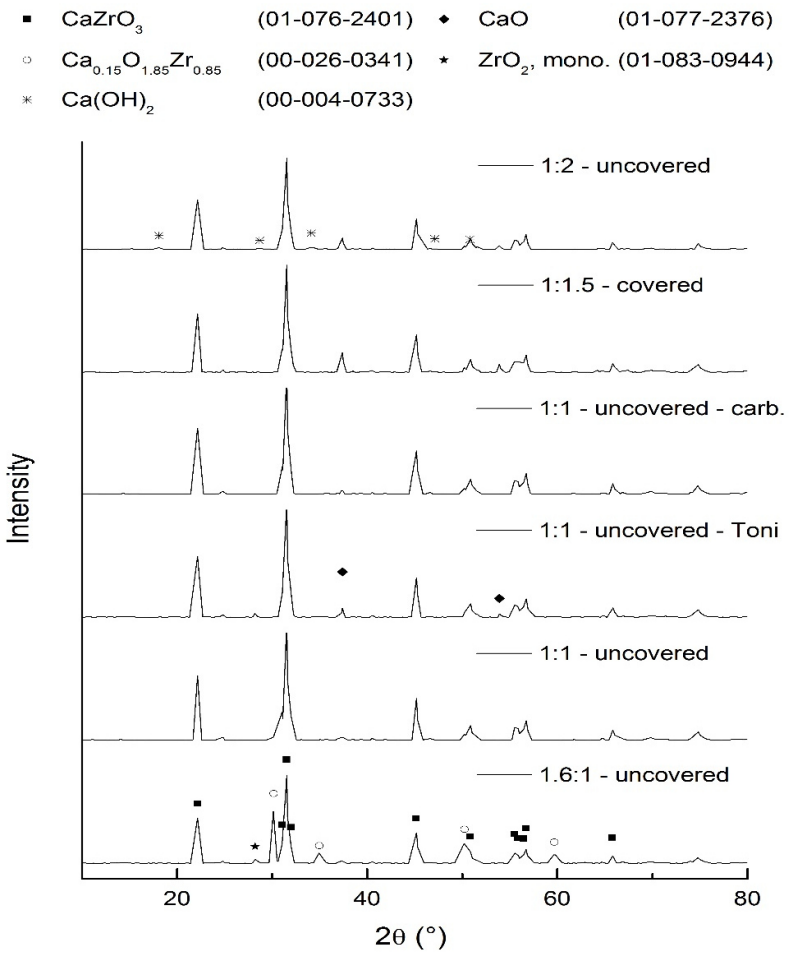

Figure 3-5: XRD patterns of the different samples sintered at 1200 °C. The raw material ratios ZrO_2:CaO, sintering conditions, calcium carbonate instead of calcium hydroxide as calcia precursor ("carb.") and mixing in mortar mixer instead of ball mixing ("Toni") are given. Significant reflexes of the found phases (JCPDS#) are marked.

Figure 3-6 and Figure 3-7 show the investigation on the secondary phase in more detail. Both samples were mixed with calcium hydroxide and fired at 1200 °C. The over-stoichiometric ratio (1.6:1) is sampled in Figure 3-6, while the stoichiometric ratio (1:1) is given in Figure 3-7. SEM images combined with EDX analyses showed,

that the secondary phase was not clearly distinguishable. But the EDX analyses for three areas showed different mole ratios revealing calcium zirconate and calcium stabilised zirconium dioxide. Larger areas of pure zirconium dioxide were not found within this sample. The other image, even if the secondary phase was measured with only about 3 % with XRD, an EDX analyses for three areas displayed clearly a brighter area with a nonstoichiometric mole ratio. Yet the main phase was stoichiometric. A boundary of the secondary phase was therefore not observed. The phases appeared to be mostly distributed within the matrix.

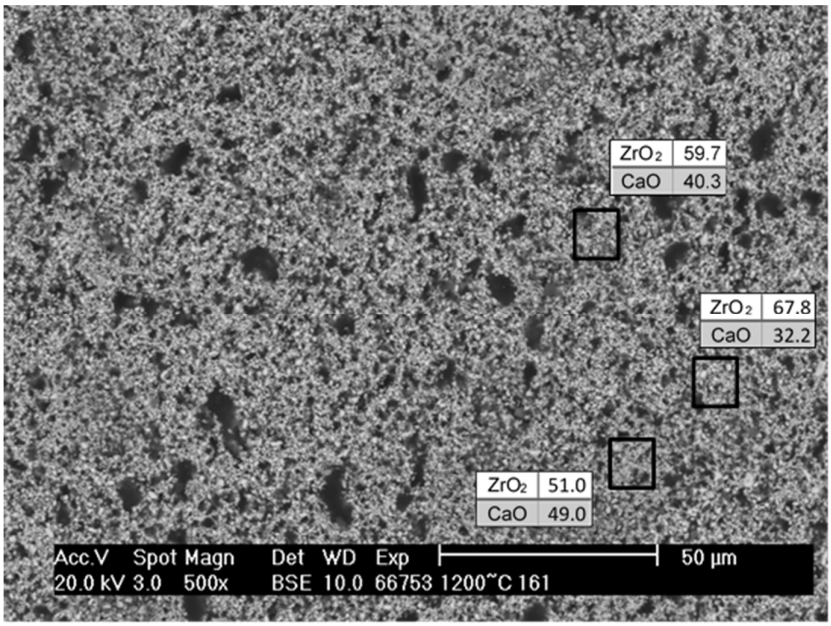

Figure 3-6: SEM image of a sample mixed with an over stoichiometric amount of ZrO_2, sintered at 1200 °C and from calcium hydroxide raw material.

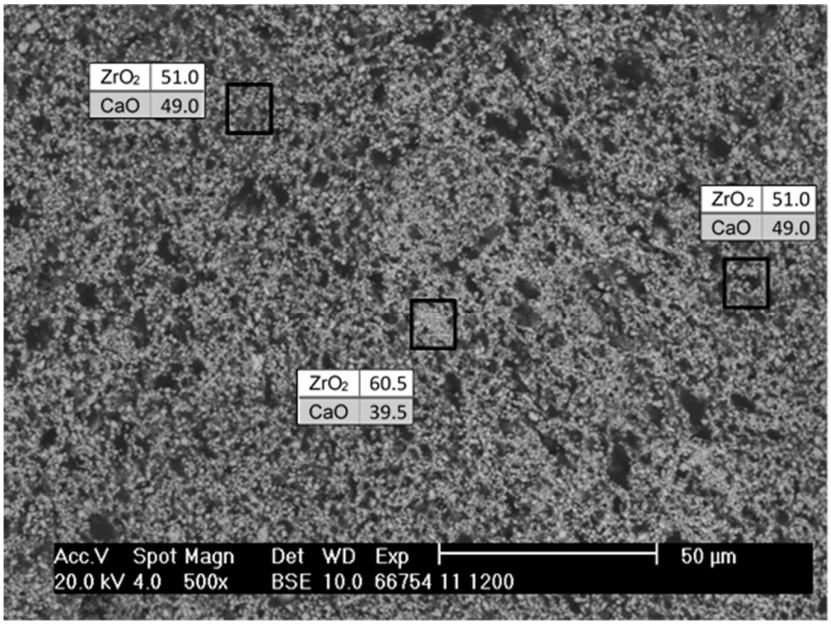

Figure 3-7: SEM image of a sample mixed with a stoichiometric mole ratio, sintered at 1200 °C and from calcium hydroxide raw material.

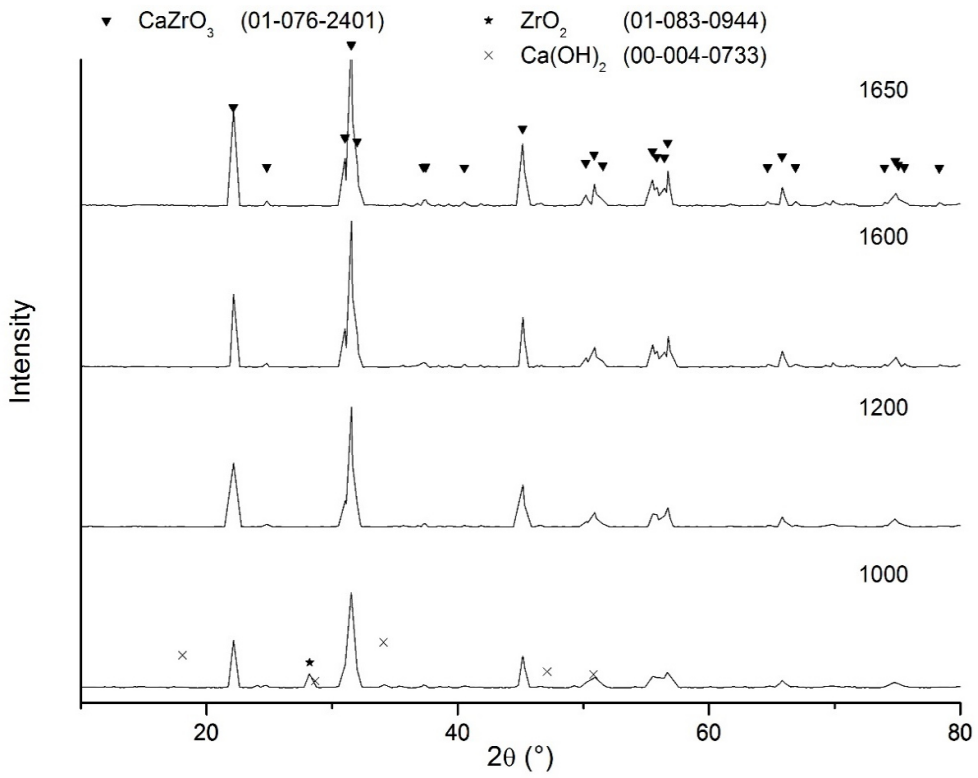

Figure 3-8: XRD curves of stoichiometric samples made of $CaCO_3$ for different sintering temperatures (in °C).

3.2.5 Microstructure

Figure 3-9 summarises the microstructure development of representative samples over different states of sintering. From Figure 3-9(a), it can be seen that the fine grained powders of the raw materials were homogeneously distributed in the green samples. Figure 3-9(b) and (c) display the microstructure of equimolar mixtures from zirconia and calcium hydroxide after firing at 1200 °C and at 1400 °C, respectively. At 1200 °C, the grains were homogeneously distributed and had a size of about 1 µm. Large pores were visible as the result of the decomposition process of calcium hydroxide. After firing at 1400 °C, obviously a higher degree of sintering was observed leading to necked grains, but the high porosity was still perceivable.

Figure 3-10 compares the microstructure of samples after sintering at 1200 °C from the two different calcia precursors. Both micrographs show isometric grains of about 1 µm in size and macroscopic pores. These images demonstrate that there were no differences in the resulting microstructure using different calcia sources.

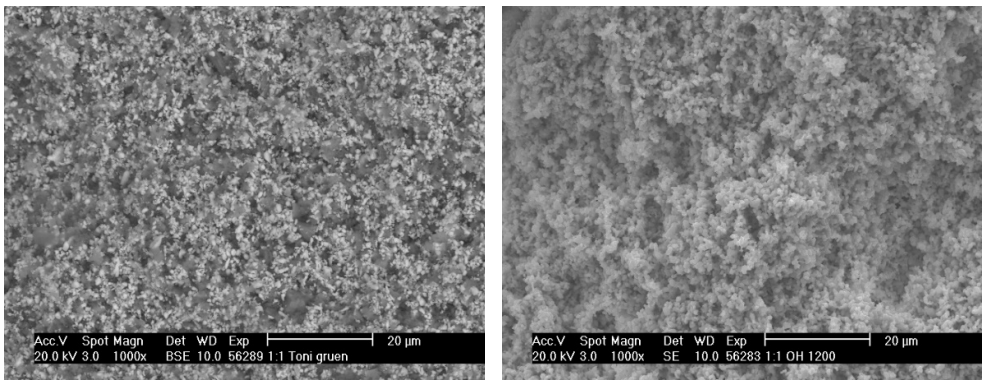

(a) (b)

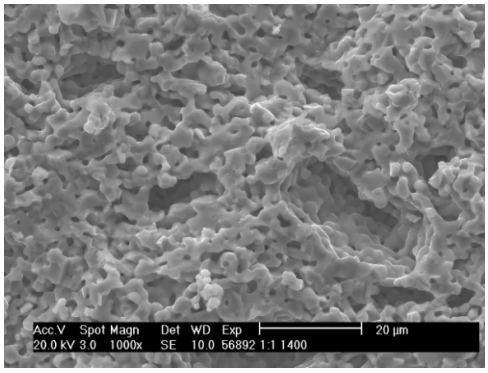

(c)

Figure 3-9: Representative back scattered electron (BSE) and secondary electron (SE) images showing the development of the microstructure of 1:1 samples with calcium hydroxide depending on state of sintering: (a) green, (b) sintered at 1200 °C and (c) sintered at 1400 °C.

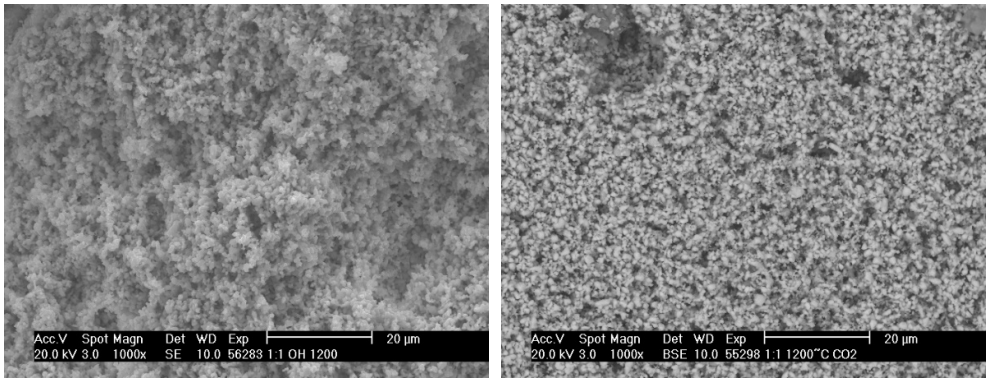

Figure 3-10: Comparison of microstructure of samples based on different calcia precursors at constant ratio of 1:1 sintered at 1200 °C (left) from calcium hydroxide and (right) from calcium carbonate.

Figure 3-11 presents an image of a green sample pressed after the paddle mixing route. Obvious are the inhomogeneous areas. The darker zones contained more calcium hydroxide, the lighter zones contain mainly zirconia. This is also an evidence for the incomplete mixing indicated by XRD analysis of these samples after firing.

For industrial application of paddle mixing, further investigations are necessary to ensure homogeneity.

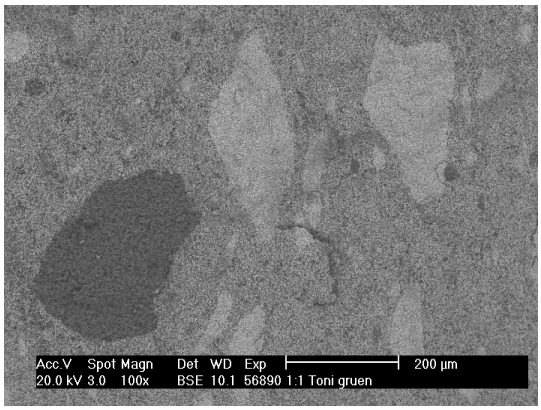

Figure 3-11: SEM image of the green sample mixed with paddle mixing (TONI).

The comparison of the samples fired at 1200 °C but with different heating rates (3 $K \cdot min^{-1}$ and 10 $K \cdot min^{-1}$) exhibited no difference regarding XRD patterns or microstructure. Together with the other results, it can be summarised that there is no influence of the heating rate on the process of decomposition and the reactivity of the calcia, respectively, within the chosen parameters.

3.2.6 Further observations after sintering

This section will give attention to some observations besides the aspired experimental results.

For all samples with over stoichiometric amount of calcia or its precursors, respectively, a severe disintegration of the burnt samples only a few days after cooling were remarkable. Even if there was no free lime or other calcium containing phase detected by XRD. For example, decomposed the samples to a powdery state like indicated in Figure 3-12. The residual CaO, which did not react with the ZrO_2 during firing, reacted intensively with the humidity of the surrounding air. Surprisingly, this undetected amount was, nevertheless, enough for the complete disintegration of the specimens. Comparable results reported Hwang and Choi. [HWANG 05]

Figure 3-12: Representative photography of a sample with a ratio of 1:1.5 with calcium hydroxide as raw material, short after sintering at 1300 °C.

Another remarkable finding was the changed colour of samples sintered at 1600 °C, depending on the used raw material. This brownish colouring of the samples made with calcium carbonate differs from the mostly white ones fired at lower maximum temperature. Furthermore, the colouring does not fulfil the complete samples, it is limited to the top side regarding the placement in the furnace or burning aid, respectively. Yet, it does also extend to the core of the sample. A different phase or contamination were excluded by XRD and SEM/EDX analysis. Fischer et al. described an intensive violet colour of their samples with excess on CaO, burnt at 1800 °C, whereas a disintegration of the samples was not reported. [FISCHER 76] The cause of the colouring could not yet be determined. Some natural doping of the perovskite structure with ions already existent in form of raw material contaminations is possible, too. This could change the crystal structure or lead to lattice defects affecting the optical properties. [PISHCH 98] Thereby, Nadler and Fitzsimmons reported a pink colouring of their $CaZrO_3$ samples fired at 1450 °C, which disappeared after refiring at 1700 °C in a vacuum furnace. Thus, they did not find sufficient contaminations which could have been an explanation. [NADLER 55]

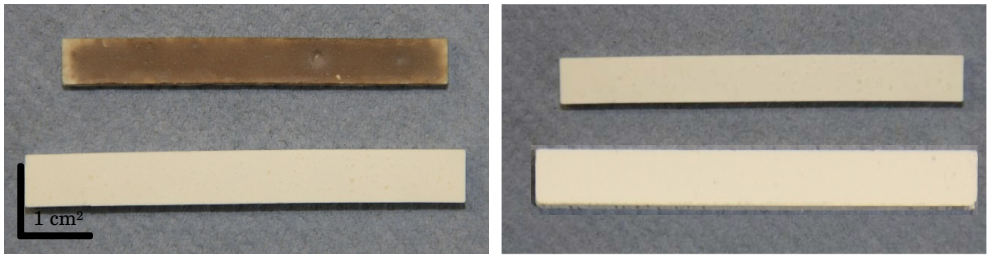

Figure 3-13: Comparison of samples sintered at 1600 °C (top) and green state (bottom) made with $CaCO_3$ (left) or $Ca(OH)_2$ (right).

3.3 Conclusion Part I

The first part of this study investigated the formation of calcium zirconate using zirconium dioxide and two different calcium oxide precursors for a solid state reaction. Therefore, the raw material powders were intensively mixed, whereby only water was added as binder and pressing aid. Samples were uniaxially pressed, dried and sintered under varying conditions. Physical properties as well as microstructural characteristics were investigated. Thereby, the yield on calcium zirconate was the main focus.

For the equimolar mixture of zirconium dioxide and calcium hydroxide, the highest yield of calcium zirconate was found from temperatures above 1200 °C, whereby 100 % conversion was not achieved. A complete formation, however, was obtained in the reference with calcium carbonate at the same temperature.

With an increasing ratio of the calcia source within the mixture, free lime was found after firing leading to disintegration of the samples over time due to hydration

in conjunction with volume expansion. An excess of zirconia led to calcia stabilized zirconia in addition to calcium zirconate and below 1400 °C there was also monoclinic zirconia remaining from the raw material.

All samples fired at lower temperatures showed a high porosity and therefore densities below the true density due to incomplete sintering. An increasing maximum temperature and dwell time showed improved densities. For the further processing to different refractory products, the density of the synthesised material was adjusted by the maximum sintering temperature.

The experiments with paddle mixing where not satisfying regarding the homogeneity, yet. Changes in the parameters for a more homogenous distribution of the raw materials are needed to ensure complete homogenisation.

The heating rate did not affect the behaviour of the raw materials or intermediate compounds regarding the sintering process and properties after firing within the chosen parameters.

4 Part II: Calcium zirconate as refractory material

The second practically section is about the subsequent processing of the synthesised calcium zirconate into materials for refractory usage. The aim of this part will be the evaluation of coarse grain calcium zirconate material for refractory applications. The changes in thermal and mechanical behaviour in relation to the batch composition are investigated. Therefore, the earlier synthesized $CaZrO_3$ material is used to form test specimens. At room temperature, elastic properties, flexural strength, and porosity are determined. A broad characterisation of the present material is striven. As starting point, to observe the refractory properties and the issue with the elastic modulus, die pressing is chosen first. Slip casting is another processing route which is of interest for this work and therefore utilised. But the application of calcium zirconate in a casting slip is considered in detail in chapter 5.

4.1 Experimental

Besides the manner of preparation, this unit deals with the properties of a refractory product. Behaviour at high temperatures as well as remaining properties after thermal shock are of interest. The evolution of the modulus of elasticity over variation of the batch mixture is examined. In the terms of the chosen fields of applications corrosion tests are made. The aim of the investigation is to fully characterize the material developed in this work.

4.1.1 Raw materials

Before the actual refractory product could be realised, it was necessary to make the calcium zirconate available in a certain amount. The sample preparation for the synthesis examination was not sufficient for the amount of material planned for this part of the study. Therefore, another processing route had to be found under the

condition of the same results regarding the mixing homogeneity and phase composition as well as the physical properties.

Production of larger quantities of calcium zirconate

Since the original preparation route was not suitable for bigger lots, adjustments had to be made. For this purpose, an intensive mixer (EL5, Maschinenfabrik Gustav Eirich GmbH & Co KG, Hardheim, Germany) was chosen. It can hold up to 6 kg of batch material and with the opposing movement of container and mixing tool. The speed of rotation was adjustable, too. After weighting the two raw materials $CaCO_3$ (PreCarb 400, SCHAEFER KALK GmbH & Co. KG, Diez, Germany) and ZrO_2 (CS02, Saint-Gobain, Le Pontet Cedex, France) the first mixing took 10 min. After that adhesions on the container and the stirrer were scraped off and then water was added. All together was again blended for 10 min. Subsequently the batch was pressed. For this also a larger mould was necessary. The used uniaxial hydraulic press (PYXT63, VEB Sondermaschinen- und Vorrichtungsbau, Engelsdorf, Germany) has a normal format mould. Preliminary tests showed that the raise of batch humidity to 8 % is suitable for this purpose and no other pressing aids or binders were needed. Occasional laminar cracks within some of the produced stones were harmless because the handling was given. The maximum pressure was about 50 MPa but due to the venerable technology the accuracy of the display was not that high. Yet, within several productions of material there were no special conspicuous features regarding this procedure. These imperfections did not harm at that stage, because the material was crushed anyway after firing as described in the next section.

For firing an electric oven (HT 276/17, Nabertherm GmbH, Lilienthal, Germany) with MgO bricks as lining material was used. The maximum temperature was 1400 °C to ensure completed reaction and to reduce some porosity according to the results in the first part of this dissertation. The thermal treatment was otherwise like the one already described in section 0. Figure 4-1, Figure 4-2, and Figure 4-3 show some impressions of the production.

After cooling the material was crushed in a laboratory jaw crusher (Retsch GmbH, Haan, Germany) and subsequently sieved into different grain size classes (AS 200, Retsch GmbH, Haan, Germany).

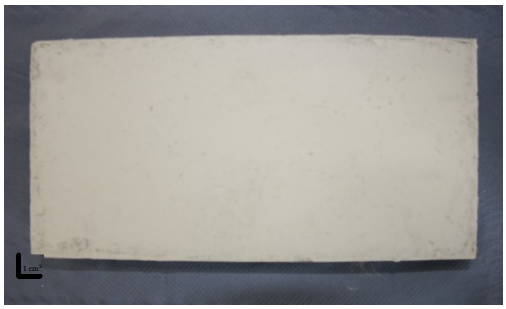

Figure 4-1: Picture of a pressed brick before sintering. The apparent deformation is due to optical illusion.

Figure 4-2: Picture of samples in the furnace after firing. Some broken pieces due to the laminar cracks before and during firing are noticeable.

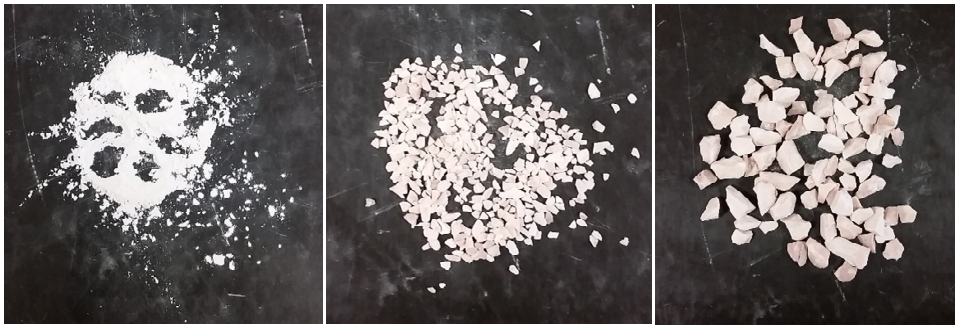

Figure 4-3: Close-up on some grains of different size after crushing and sieving.

Additives

For the preparation route of the final products the polyvinyl alcohol solution Optapix PAF 60 (Zschimmer & Schwarz GmbH & Co. KG, Lahnstein, Germany) was used as temporary binder and pressing aid.

4.1.2 Sample preparation

For batch preparation the synthesised material is weighted in a mixing container used for the mixer (ToniMIX, Toni Technik Baustoffprüfsysteme GmbH, Berlin, Germany). Better results were obtained starting with the finer proportions. After mixing of the dry components, the binder solution was added and again mixed. The mixing time for each step was 5 min. This processing route is in accordance with Schafföner et al. [SCHAFFÖNER 13] and summarised in Figure 4-4. Departing from this, in situ formation of calcium zirconate is promoted by proportional addition of zirconium dioxide and calcium carbonate in some mixtures (see B4-B6). To create the possibility to evaluate the influence of grain size on resulting properties, different maximum grain sizes are used in the mixtures (compare B1-B3). The particle size distribution for the pressing mixtures was adjusted in accordance with the model of Dinger and

Funk [DINGER 92] with the distribution modulus of q = 0.37. For the mixtures which intended in situ formation of calcium zirconate, the smallest grain class was partially replaced with an equimolar mixture of the raw components. Table 4-1 summarizes the composition of the investigated batches, whereby the values after optimisation according to Dinger and Funk are rounded to the nearest tenth. Later, a batch with a coarser particle size distribution, in fact 50 wt.-% over 1 mm, was investigated (B7), too. The beforehand determined particle size distributions can be found in Appendix A. 2.

Table 4-1: Batch compositions for the pressed refractory.

Material	Grain size fraction	B1	B2	B3	B4	B5	B6	B7
$CaZrO_3$	< 0.16 mm	32.00	33.40	27.75	22.00	12.00	2.00	10.00
	0.16 - 0.63 mm	52.00	34.10	26.75	52.00	52.00	52.00	30.90
	0.63 - 1.00 mm	16.00	9.80	7.75	16.00	16.00	16.00	9.10
	1.00 - 2.00 mm	-	15.40	12.00	-	-	-	35.00
	2.00 - 3.15 mm	-	7.30	5.75	-	-	-	15.00
	3.15 - 6.00 mm	-	-	20.00	-	-	-	-
ZrO_2		-	-	-	5.50	11.00	16.50	-
$CaCO_3$		-	-	-	4.50	9.00	13.50	-
Binder		3.50	3.50	3.50	3.50	3.50	3.50	3.50

For the several testing methods, different sample shapes were necessary. Cylinders (50 x 50 mm^2) and rectangular bars (25 x 25 x 150 mm^3) were die pressed at 150 MPa (ES 270, RUCKS Maschinenbau GmbH, Glauchau, Germany). Some standard machine oil was used for lubricating the mould.

Afterwards the samples were dried at 80 °C and 110 °C for 6 h at each temperature. For sintering, electric heated furnaces (HT 276/17 and LH 15/14, Nabertherm GmbH, Lilienthal, Germany), depending on the lot quantity, were used. The heating rate was 2 $K \cdot min^{-1}$ with a dwell time of 2 h at 900 °C and 6 h at 1650 °C. The first dwell time regards the decomposition of calcium carbonate in the batches. Thereby, in situ reaction takes place and a constant thermal treatment for all samples is provided. The second dwell time was at the maximum temperature. The cooling rate was free and again, MgO filling was used to prevent reactions with the kiln furniture or lining.

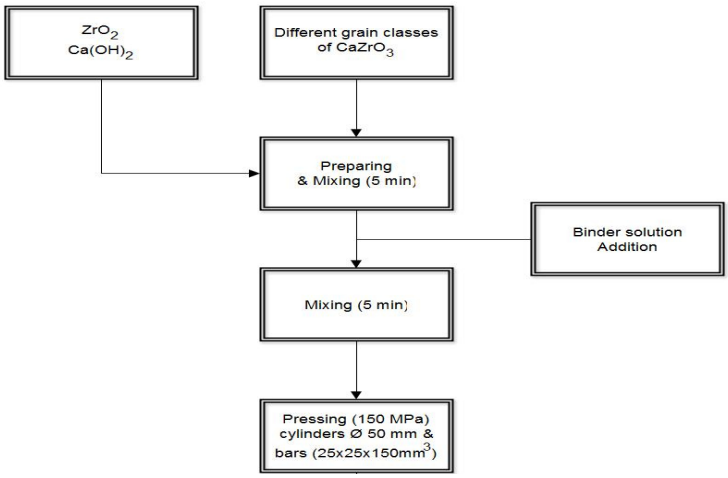

Figure 4-4: Flow chart of the die pressing process route.

4.1.3 Testing methods

The most common characterisation methods used for the samples in this section were also utilised and therefore described in Part I, see chapter 3.1.3. The following implementations of testing deal with the refractory properties of the striven material which are fundamental for the application in any industry. Additionally, these tests shall give the information about any possible limits of the refractory material concerning corrosion and thermal shock. Thereby, the interaction of microstructure and properties are relevant and must be clarified.

Elastic properties

The dynamic Young's modulus was determined at ambient temperature with impulse excitation of vibration before and after one, three, and five thermal shocks according to the standard ASTM E 1876-01 (RFDA-HTVP 1600, IMCE N. V., Genk, Belgium). The analysing software was RFDA MF v. 7.0.2. (IMCE N.V., Genk, Belgium).

Cold modulus of rupture (CMOR)

The modulus of rupture at ambient temperature and the residual strength after certain thermal shock cycles were examined in accordance to the standard DIN EN 993-6:1995 concerning the sintered samples before and such after one, three or five thermal shocks, respectively. For testing, a servo hydraulic universal testing machine (TIRAtest 28100, Tira GmbH, Schalkau, Germany) was used with a support distance of 100 mm and loading velocity of 0.15 N mm^{-2} s^{-1}. Unless otherwise stated, for each series were three to five specimens averaged.

Cold crushing strength (CCS)

The crushing strength at room temperature was determined according to the standard DIN EN 993-5:1998. Cylinders with a diameter of about 50 mm and a height of about 50 mm were used. For testing a servo hydraulic universal testing machine (Zwick/Roell, Toni Technik Baustoffprüfsysteme GmbH, Berlin, Germany) was utilised.

Thermal shock

To investigate the thermal shock behaviour, the rectangular-shaped specimens were tested. All samples were stored at 100 °C in a drying oven before and between the actual processes. Two of the samples were then heated up to 950 °C for 30 min in an oven. After that time, they were placed under an air shower with 1 bar overpressure for 5 min. This cycle was repeated up to 4 times. This testing method was performed in accordance with the standard DIN EN 993-11:2007. Every specimen was oriented so that the pressing direction matches the direction the air was blown on.

Hot modulus of rupture (HMOR)

In addition to the CMOR, the hot modulus of rupture was also determined (HMOR 422 D/3, NETZSCH-Gerätebau GmbH, Selb, Germany) based on the standard DIN EN 993-7:1998. Yet, the temperature was set at 1350 °C, a compromise between the later possible application temperature and the limits of the testing apparatus. For each batch three specimens were measured.

Refractoriness under load (RUL)

The refractoriness under load was measured according to the standard DIN EN ISO 1893:2008 using a hood-type furnace (RUL/CIC 421, NETZSCH-Gerätebau GmbH, Selb, Germany). The load was 0.05 N mm^{-2} at a temperature up to 1650 C with a heating rate of 5 $K \cdot min^{-1}$. The atmosphere was air. For the tests, the cylindrical samples were used.

Linear thermal expansion (LTE)

The same furnace from the RUL was used to determine the thermal expansion of samples according to the standard DIN EN 993-19:2004, from cylindrical specimen too.

Wavelength dispersive X-Ray fluorescence

As another method to determine the composition of certain materials the wavelength dispersive X-Ray fluorescence (WDXRF) (S8 Tiger, Bruker Corporation, Billerica MA, USA) was utilised.

Corrosion tests

The corrosion tests were divided into two parts. The first aimed to investigate corrosion effects of calcium zirconate in contact with hot metals. Therefore, molten steel was chosen regarding future application possibilities. The second test used ash from an entrained-flow gasifier as corrosive material. Previous studies by Gehre investigated refractories based on Al_2O_3 already with this waste material which is obtained directly from the producer. [GEHRE 13b]

For the test with molten steel, a metal casting simulator (SYSTEC Gruppe, Karlstadt, Germany) was used. It consists of a separated inductive melting unit and a tundish system. The latter is also inductive-heated and has two testing nozzles and one security nozzle. The melt flow is controlled by a stopper rod system. The melting crucible is mostly based on zirconia/mullite (Colisit, Großalmerode, Germany). Commercially available steel DIN EN 42CrMo4 (Mat. no. 1.7225, AISI 4142) in cylindrical shape of 72.5 kg is then placed in the melting crucible, heated up to 1650 °C in 90 min under inert atmosphere. The temperature and the oxygen content of the steel melt are measured with an oxygen/temperature-finger sensor-system CELOX (Heraeus Electro-Nite International N.V., Houthalen, Belgium). [ANEZIRIS 13] For the so called 'Finger test' prismatic samples were dipped 60 mm deep into the steel melt by entering the system through a sewer port. After a contact time of 60 s and a rotation of 30 rounds per minute, the sample was removed from the melt and cooled down in a chamber with an argon atmosphere. The melt is cooled down rapidly by switching off the inductor coil. [DUDCZIG 14]

To investigate the suitability of the material as lining refractory in coal gasification plants, corrosion tests with the ash obtained from the gasification process were made. Therefore, cylinders with a drilled hole with a diameter of 20 mm and a depth of 15 mm were filled with the ash. After that, a lid also made of the material covered the cylindrical crucible. All together were placed in a corundum retort filled with petrol coke breeze (Müco Mücher & Enstipp GmbH & Co KG, Essen, Germany) to provide a reducing atmosphere. The thermal treatment took place at 1550 °C for 50 h with heating and cooling rate of 3 $K \cdot min^{-1}$. Then the removed cylinders were cut into half and later smaller pieces for investigation.

Unfortunately, the application in the pilot plant of a slagging gasifier at the Chair of Energy Process Engineering and Thermal Waste Treatment at the TU Freiberg during the study could not be realised due to the tight schedule, the high effort, and cost causation which come along with such industry-oriented trials.

4.2 Results and discussion

The aim of this chapter is to investigate the influences of the batch composition on the properties of the resulting refractory material. Therefore, different maximum grain sizes, distributions and the in situ formation through adding raw material mix was focused on. Subsequently, the most suitable batch was fully characterised. Parallel, the corrosion tests were carried out, which are presented next, and finally some special observations during these investigations are presented.

4.2.1 Influence of the batch composition on physical and thermomechanical properties

In the present section of this work, the composition of a moulding mass was varied regarding the maximum grain size, grain size distribution, and amount of equimolar mixture of m-ZrO_2 and $CaCO_3$. Earlier, Table 4-1 summarised the utilised batches. In general, all pressed specimens were flawless after pressing and after firing, too. No laminar cracks were observed, although the mould pressure of 150 MPa was quite high.

All determined characteristic properties are collated in Table 4-2. To provide a focused overview, the standard deviations were not given also due to the limited space. In general, these deviations were not noteworthy. For example, density and porosity had values between 0.00 and 0.04 and the thermomechanical properties showed no significant outliners, too. The narrow green density deviation among the batches corresponds to the preceding calculations. Noticeably, the batch with almost raw material mix as finest proportion (B6) and the especially coarser designed batch (B7) show lower densification during the pressing process which is in good agreement with the theory of densification during pressing. Furthermore, the increasing maximum grain size led to decreasing density due to the larger steps within the grain size distributions for the calculations leading to more mismatch from the ideal distribution. The density after firing shows the same tendencies, determined with geometrical method as well as calculated from the hydrostatic weighting. In general, a higher compaction leads to higher density after sintering, yet the in situ reaction releases carbon dioxide which forms pores during sintering. Due to the higher sintering temperature and the smaller proportion, the porosity is comparable to the initial synthesis material. In fact, the in situ reaction with proportions over 10 % seems to decrease the total porosity. One reason is the susceptibility of the chosen measurement methods. The geometrical method for example depends on the care taken for determining of the dimension, which also assumes an appropriate shape of the sample, whereby the hydrostatic weighting is depending on the precise removing of the excess water. Of cause a certain number of samples lowers these random errors but some inaccuracy remains. Nevertheless, because of the higher sintering temperature at this

time compared to the sintering temperature for the synthesis, the particles tend to shrink because of thermal induced sintering. The decomposition of the $CaCO_3$ in the batches with intended in situ reaction yields in fine CaO particles, as Barker reported. [BARKER 73] After the reaction with the monoclinic ZrO_2, it forms a very fine particle class within the larger $CaZrO_3$ grains. [HAN 08] It is possible that the newly formed, small $CaZrO_3$ particles fill the present porosity better than the already existing ones from the synthesised material in the batches without intended in situ reaction, due to the different particle size.

Table 4-2: Summary of all measured properties of the initial batches.

Property	Unit	Remark	B1	B2	B3	B4	B5	B6	B7
Green density	$g \cdot cm^{-3}$		2.61	2.57	2.55	2.59	2.59	2.54	2.50
Apparent density	$g \cdot cm^{-3}$		4.47	4.43	4.44	4.48	4.47	4.48	4.40
PLC	cm/m		16.92	19.30	17.31	17.72	18.40	19.54	17.48
Young's modulus	GPa	Before TS	207.20	206.20	142.18	214.19	142.45	148.94	149.26
	GPa	After 1 TS	43.70	47.64	18.22	32.25	22.86	22.47	16.38
CMOR	MPa	Before TS	32.24	16.40	12.21	18.41	15.56	19.06	18.94
	MPa	After 1 TS	3.55	5.25	1.82	1.55	0.82	2.24	3.95
Total porosity	%		4.80	5.40	4.15	4.86	3.76	3.43	4.67

The in situ reaction through added raw material mixture brought a decreasing modulus of elasticity at room temperature, whereby there is no direct relation remarkable. This could also be due to different mechanism. As discussed before, the density does not change, yet the microstructure is different which is indicated by the varying elastic modulus. After the thermal shock treatment, the loss is remarkably higher for the in situ batches. The batch B1 had about a quarter of its initial value residue but the other lost over 80 % of the value. The decreasing porosity led to reduced stress relief. The maximum grain size was also influencing the thermomechanical properties. The use of 3 mm grain size (B2) did not alter the Young's modulus, yet the cold modulus of rupture was initially lower but after the first thermal shock somewhat higher. The porosity did not have an influence on the elastic modulus, yet on the strength. The coarsening of the batch B2, done in batch B7, showed a decreasing modulus of elasticity whereby the CMOR increased but the residual strength after thermal shock again decreased. The changes in the microstructures did therefore not improve the thermal shock resistance. The investigation on the batch with 6 mm maximum grain size (B3) were also done for the sake of completeness. Yet, these results are seen with reservations due to the ratio of sample size to maximum grain size which is theoretically too low to expect reasonable results. The distribution of the grains within the samples may have led to these results. A positive effect was remarkable through the large grains comparing the fractured surfaces of samples with 1 mm maximum grain size and 3 mm, respectively. In Figure 4-5 they are displayed.

The smaller grains of B1 offer lower resistance to an initiated crack, this is called conchoidal fracture. The samples with larger grains, like B2, show more interlocking, an initiated crack is redirected approaching a large grain in the matrix or consumes a large amount of energy splitting it apart. This is a valuable finding for these samples.

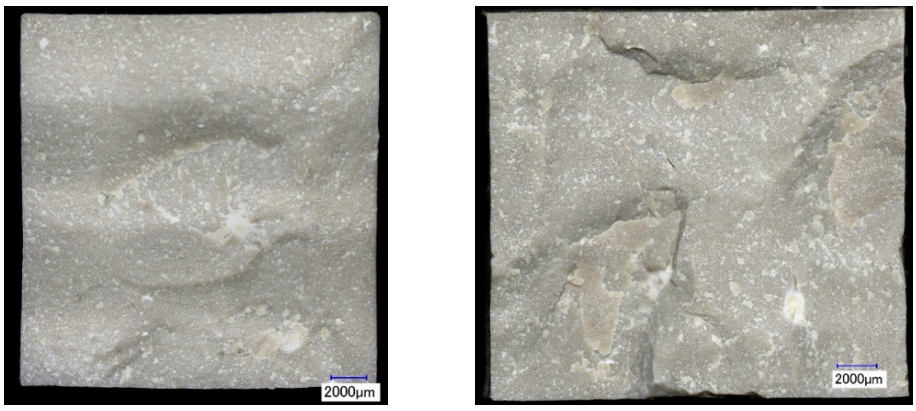

Figure 4-5: Images of representative fracture surfaces of B1 (left) and B2 (right).

In Figure 4-6 are some impressions of the processed samples given. To the colour of the samples attention is paid in section 4.2.5. At this point, it has to be said that this colouring was predominant for every sample produced this way also in the following investigations up to a certain point which is then specifically mentioned. It resembled the colour of the synthesis sample, see section 3.2.6.

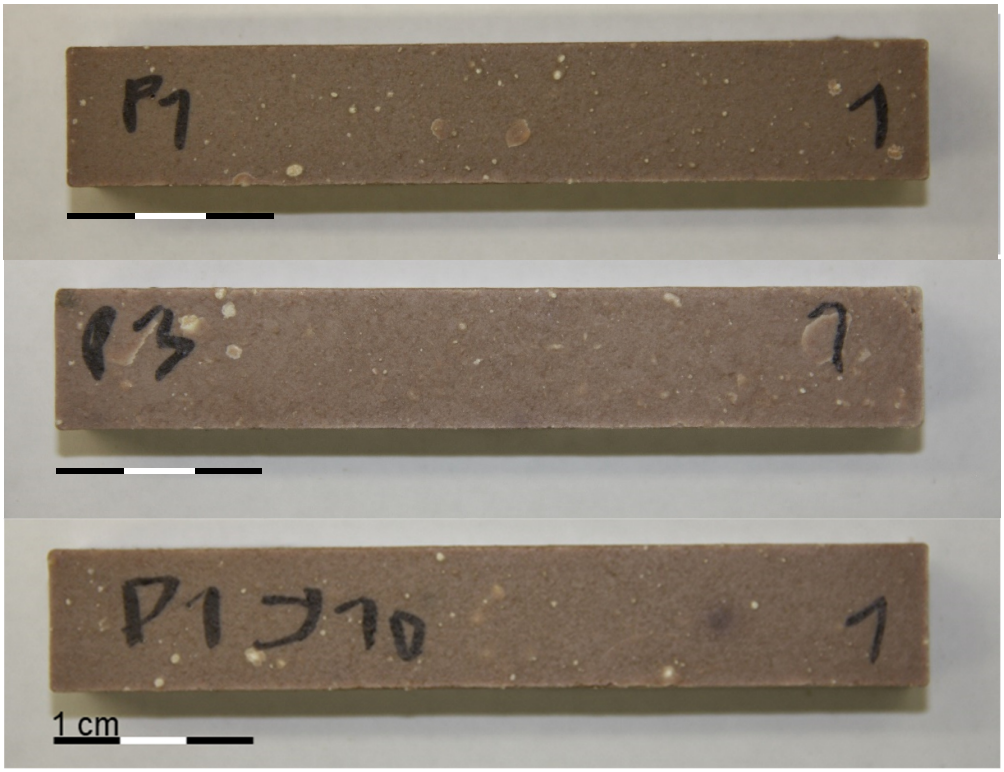

Figure 4-6: Representative photographs of samples of batches B1 (top), B2 (mid), and B4 (bottom) after sintering.

Based on the obtained results, batch B2 was chosen as most promising composition for refractory applications and, thus, investigated in more detail. Yet, the knowledge gained through the batch variation enables the adjustment for other purposes or geometries, where the maximum grain size could be increased or has to be decreased, for the future.

4.2.2 Characteristics of the batch B2

Beside the initial properties determined before, here are some further analyses reported and discussed for batch B2.

Phase analysis

The first measurement was the phase constitution with XRD, due to the aim of a single phase material. Figure 4-7 shows the measured profile of sample B2. Again, the marked phase is the stoichiometric $CaZrO_3$ phase (PDF #01-076-2401). No other phases could be identified or are below the detection limit and are therewith handled as insignificant, which confirms the achieved single phase character.

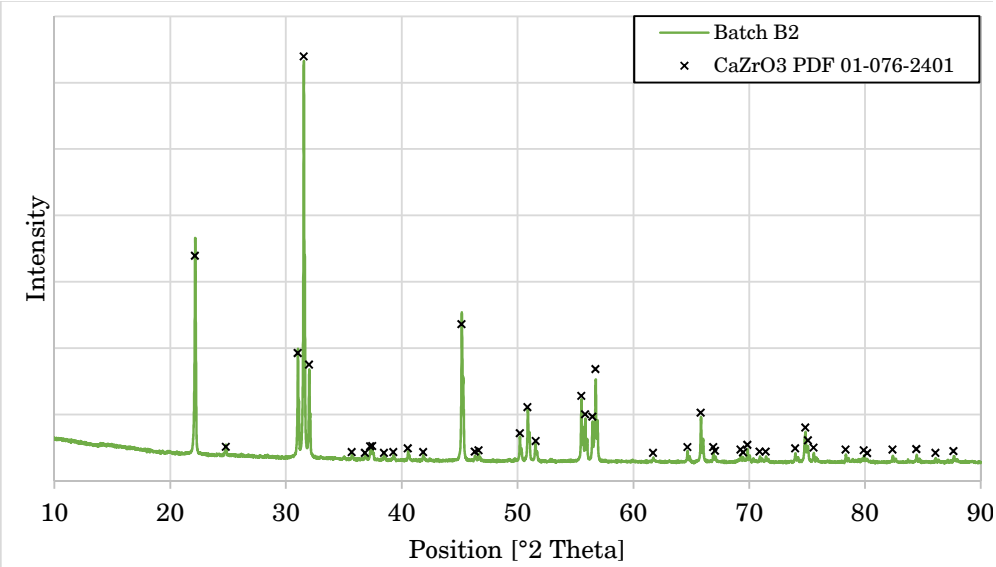

Figure 4-7: XRD profile of batch B2.

Microstructure

In a next step, the microstructure was investigated by SEM. Figure 4-8 presents representative images of samples with different magnitudes. At lower magnitude (see left side) a homogeneous matrix with some small pores is visible. This is also indicated by BSE mode, too. Additionally, this also verifies the findings from XRD. At higher magnitude (see right side) the sintering effect of the higher maximum temperature is remarkable. In comparison to the microstructure of the synthesised material, which

was also fired at 1400 °C, grain boundaries are reduced. The shrinkage (PLC) of about 20 % as seen before is also resulting from that.

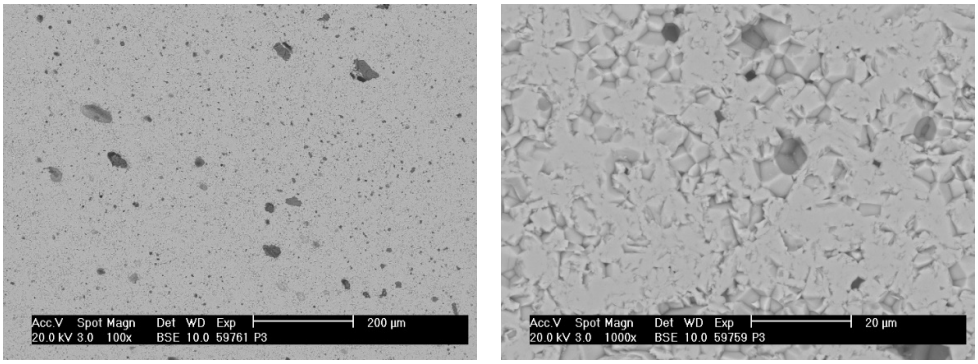

Figure 4-8: SEM images of the microstructure of B2 after sintering at 1650 °C.

Thermomechanical investigations

More samples were prepared to intensify the investigation of the thermomechanical properties. For each measurement of the elastic modulus and the CMOR before, after one, and after five thermal shocks, 30 specimen were prepared.

In Figure 4-9, the box plot diagram shows the values of the Young's modulus after 0, 1, and 5 thermal shock cycles. This type was chosen due to some statistical outliers which are caused by some inhomogeneities within the samples. These resulted from the preparation. Nevertheless, the samples were not corrupted in such a way, that a statistical evaluation would be impossible or false. The majority had a value of 115 to 150 GPa. After the first thermal shock it drops to 25 GPa for half of the samples. From the first up to the fifth thermal shock the drop is lower which means that the initial shock is most destructive for the structure but then the structure is not significantly damaged further that way.

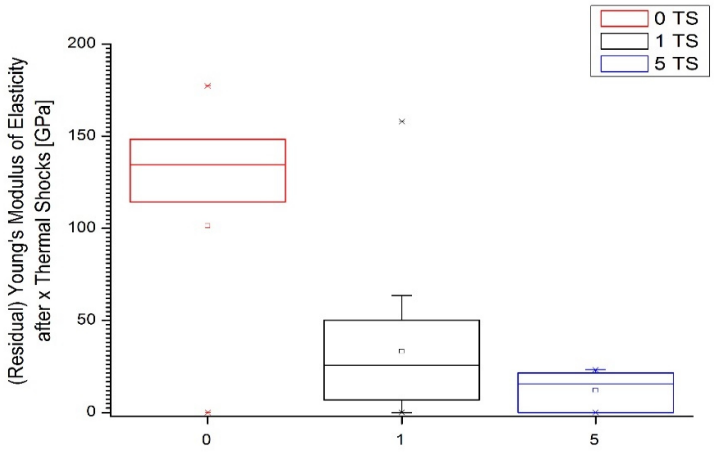

Figure 4-9: Young's modulus of B2 before and after thermal shocks (TS).

The same conclusions apply for the CMOR, given in Figure 4-10. Only about 25 % of the samples reached the initial value of 16 MPa. After the first thermal shock the residual strength decline by 72 % to 3 MPa. Then again, the loss stagnates, and the majority stayed at this value after the fifth thermal shock.

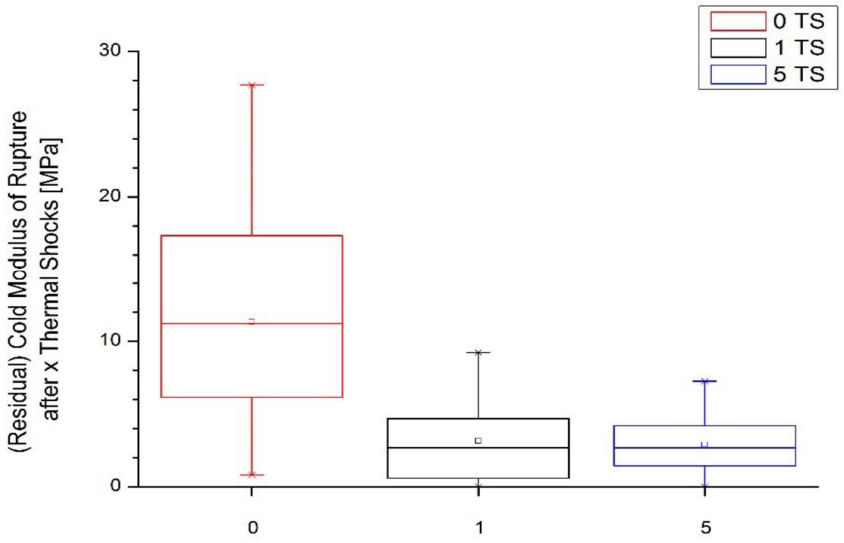

Figure 4-10: CMOR in dependency on the number of thermal shocks (TS).

Due to the sintering effect leading to a severe shrinkage of all samples, it was not possible to obtain specimen suiting the requirements for HMOR and RUL.

4.2.3 Variation of the processing parameter: pressure

Another part of the development of the pressed refractory material based on $CaZrO_3$ was the alteration of processing parameters to observe their influence on the resulting properties. Therefore, the pressure was chosen because of a possible effect on the properties before and after sintering. The density of a uniaxially pressed sample increases with the pressing pressure. [SALMANG 07, p.617–621] Thus, the microstructure and as a result, the properties are influenced. Compared to the initial 150 MPa, the pressure was lowered to 50 MPa and 100 MPa. All measured characteristics are summed up in Table 4-3.

With lower pressure, the material in the die was less compacted, which influenced directly the green density. This resulted also in an increasing density and decreasing porosity with rising pressure in the samples after firing at 1650 °C. The densification between green state and fired state is related to the linear determined permanent length change. Thus, for a batch with the same shrinkage affinity due to its composition, the densification was indirectly affected by the compaction. This can be attributed to lowering of surface energy, the driving force of sintering. A low compacted batch contains more interfaces between material and air and the system strives for minimisation of these. Whereby a more compacted system already contains

a lot of interfaces between material and material, resulting in a lower drive of sintering.

In contrast, however, the investigated samples showed no significant linear or else correlation between pressure and elastic properties. Here, two factors were contributing towards this. On the one hand, there were the values of the density, also related to the porosity and depending on the pressure. On the other hand, there is the shrinkage, determined as PLC. Main driving force for sintering is the lowering of surficial and interfacial energy. These were depending on the used pressure due to the resulting compaction. As a result, the samples pressed at 50 MPa had a higher sintering affinity, leading to a denser connection of adjacent particles with increased strength, yet not all gaps between these particles were closed during the firing. As a result of the higher compaction at 150 MPa, smaller gaps were more easily closed during the sintering process. Possibly, the microstructure is therefore more homogeneous for these samples. The middle course, represented by the samples pressed at 100 MPa, seemed to profit from that regarding the strength. Nevertheless, this was disadvantageously for the thermal shock behaviour, observed by the loss of about 95 % of the initial strength through a single thermal shock from 950 °C to room temperature. The best result regarding the value of the residual strength after TS showed the sample pressed at 50 MPa. Here, a high modulus of elasticity was not impairing the thermal shock behaviour for a on the other hand quite moderate initial strength comparing all samples and with a higher porosity. Maybe the crack propagation was the main factor in this case. Like said in chapter 2.3.4, whether a high or low value of the Young's modulus is beneficial is depending on the prominent reason of failure in a sample impinged by a thermal shock.

Another relation exists between Young's modulus and the CMOR, also for the residual values after one thermal shock. A higher elastic modulus is directly related to the CMOR and not depending on the porosity. The residual values of the modulus of elasticity and CMOR after thermal shock related to their initial values showed also relation in accordance to the proposition of Hasselman (cf. chapter 2.3.4). This leads to the assumption, that the different microstructures reacted equally to the thermal shock. It has to be noted, that, in contrast to the numerous samples from the previous examination for the reference at 150 MPa, only few samples could be prepared with the varied parameter due to the scheduling and availability of material. In this context, the high standard deviations of the thermomechanical properties, which did not occur for the physical properties, must be taken into account regarding their significance.

In conclusion, a lowering of the pressing pressure led to an indifferent downgrading of the properties. The decreasing shrinkage with increasing compaction lowers the possibility of deforming and the formation of sintering cracks. Additionally, a lower pressure in combination with a higher shrinkage led to a moderate strength

with good residual strength after thermal shock (TS). Whereby a higher compaction with increased shrinkage resulted in a high CMOR but showed a tremendous strength loss after 1 TS. To lower the pressure during processing of the material could have increased the service life of the press and the mould due to less abrasion. Nevertheless, the total porosity decreased with rising forming pressure which should be kept in mind regarding the corrosion behaviour.

Table 4-3: Influence of forming pressure on the properties of B2.

Property	Unit	Remark	50 MPa	100 MPa	150 MPa
Green density	$g \cdot cm^{-3}$		$2.30_{\pm 0.01}$	$2.46_{\pm 0.01}$	$2.53_{\pm 0.01}$
Apparent density	$g \cdot cm^{-3}$		$4.35_{\pm 0.01}$	$4.41_{\pm 0.02}$	$4.43_{\pm 0.01}$
PLC	cm/m		$19.35_{\pm 0.06}$	$18.13_{\pm 0.11}$	$17.46_{\pm 0.04}$
Young's modulus	GPa	Before TS	$147.54_{\pm 3.09}$	$159.85_{\pm 7.21}$	$123.57_{\pm 8.33}$
	GPa	After 1 TS	$51.06_{\pm 2.72}$	$15.53_{\pm 5.51}$	$49.44_{\pm 6.27}$
CMOR	MPa	Before TS	$22.44_{\pm 9.15}$	$30.40_{\pm 3.39}$	$11.33_{\pm 6.75}$
	MPa	After 1 TS	$4.21_{\pm 0.82}$	$1.55_{\pm 0.92}$	$3.15_{\pm 2.67}$
Total porosity	%	Water absorption	$6.38_{\pm 0.07}$	$4.48_{\pm 0.10}$	$4.35_{\pm 0.13}$

4.2.4 Corrosion behaviour of the pressed $CaZrO_3$ refractory (B2)

In this section the different corrosion tests, which were performed, are now discussed. The aim was to evaluate the possible usage in the chosen applications.

Evaluation in the steel casting simulator

Figure 4-11 shows a sample of B2 which was immersed into the steel melt, held and rotated for 30 s, put out, and then cooled in inert atmosphere. The hole for mounting the sample in the steel casting simulator can be seen on the left side. Remarkable is the changed surface where the sample was dipped into the melt. There are some cracks and spalling but the sample did survive the thermal shock during the test, which was between 300 °C furnace atmosphere and about 1600 °C melt temperature.

Figure 4-11: Picture of the cooled sample after the dipping in steel melt.

A sample was taken from the reaction zone (cf. exemplary red square in Figure 4-11) and analysed by SEM. Three areas were chosen for a detailed investigation, which are shown in Figure 4-12. Area A (see Figure 4-13) shows a $CaZrO_3$ matrix with

some ZrO_2 crystals. The microstructure seems to be intact, these zirconium dioxide particles may be inhomogeneities resulting from insufficient mixing of the synthesis material. This is also a possible reason for the observed behaviour of some samples in other investigations. In area B (Figure 4-14) a reaction zone is remarkable. The EDX analysis shows some silica which is assumed to come from the steel melt and reacts with CaO from the matrix. The content assumed as Cu can be assumed as falsely assigned and might stand for some other elements from the steel (for example MgO, Al_2O_3 or Fe_2O_3). In area C (Figure 4-15) signs of a liquid phase are viewable, which are from low melting calcium silicates. The matrix is dissolved, and calcium oxide reacted with the silica and other elements from the steel.

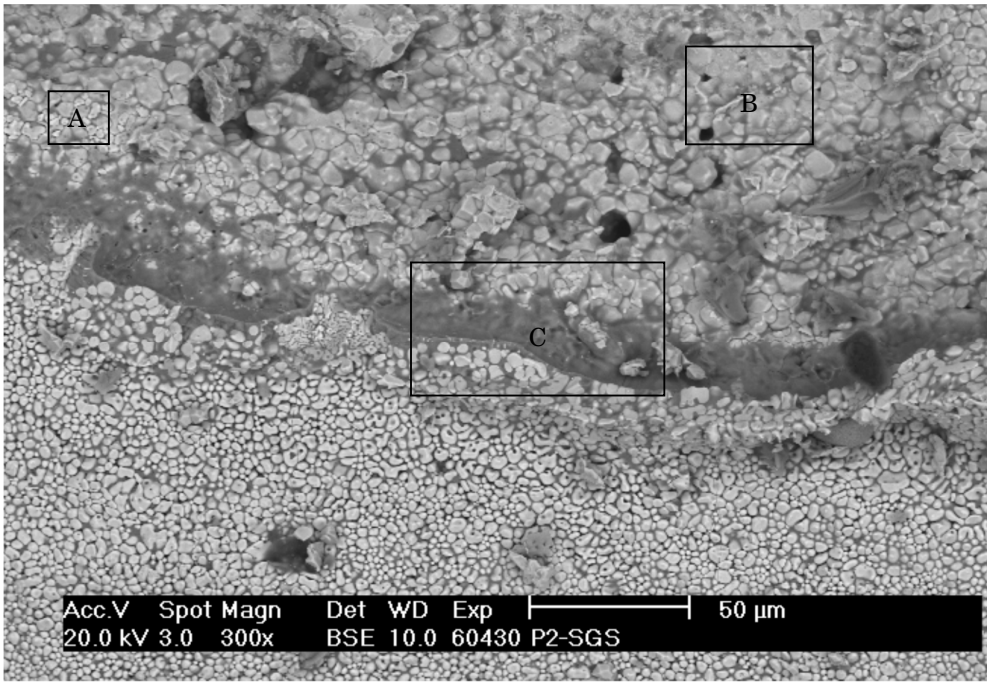

Figure 4-12: SEM image of the sample from the steel corrosion test.

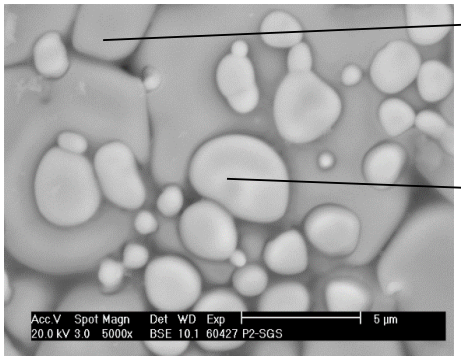

Element	Wt %	At %
O K	20.73	51.86
ZrL	55.39	24.30
CaK	23.87	23.84

Element	Wt %	At %
O K	28.91	67.26
ZrL	63.95	26.10
CaK	07.15	06.64

Figure 4-13: Area A.

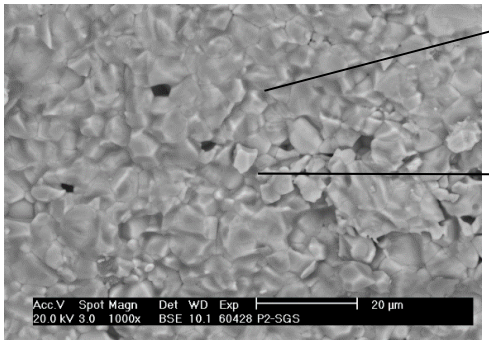

Element	Wt %	At %
O K	28.44	59.16
SiK	02.95	03.49
ZrL	42.14	15.37
CaK	26.47	21.97

Element	Wt %	At %
O K	26.58	57.08
CuL	04.12	02.23
SiK	02.92	03.57
ZrL	41.17	15.51
CaK	25.21	21.62

Figure 4-14: Area B.

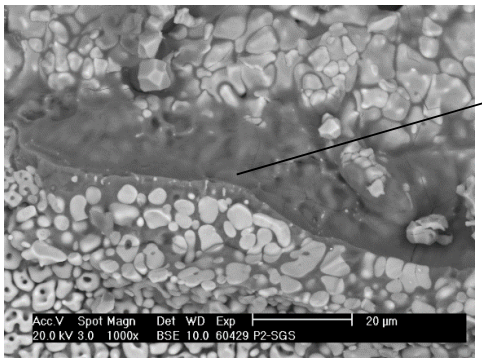

Element	Wt %	At %
O K	48.32	68.57
SiK	15.25	12.32
ZrL	04.30	01.07
CaK	31.03	17.58
MnK	00.46	00.19
FeK	00.65	00.27

Figure 4-15: Area C.

The here obtained results imply that $CaZrO_3$ based materials might be a promising refractory for steel making. Whereby, a comparison of this material with state of the art material in an industrial application should be considered and also the price. The reaction on the surface was not severe and the thermal shock was survived. Attention has to be given to the microstructure and homogeneity of the material. The reaction with silica, whereby no alumina was found, showed the potential of dissolving the material when the matrix is weakened by impurities or residual raw materials. The cracks in the sample might result from thermal shock and could be prevented by a more suitable microstructure and more homogeneous material.

Cup test with gasifier slag

Due to a missing pressing die for cup tests, potential replacements were obtained by drilling into cylinders processed at 150 MPa. The cylinder had only a diameter of 40 mm after sintering, therefore, the hole is smaller as usually. Nevertheless, the experiments are valid because the principle of a slag contacting the refractory surface under atmosphere and temperature were investigated.

The XRF analysis for the utilised gasifier ash (see Table 4-4) showed that mainly SiO_2 and CaO were present. Iron and sulphur are also exiting. However, alkalis might not be a problem for the corrosive attack here. [GEHRE 13b]

After the test at 1550 °C for 50 h in reducing atmosphere, the crucible was taken out and cut in half. An image is shown in Figure 4-16. There are some lamination cracks at the bottom of the crucible which come from the processing of the initial cylinders and did not affect the corrosion test. The pressed prisms did not show those cracks overall investigations. Remarkable is the changed colour from brown to a light grey. This will be discussed in the following sections. There is an infiltrated layer of about 5 mm visible around the hole. For further investigation, different areas where chosen. These areas show from top to bottom: a residual slag mixture, the suspected corrosion layer, a crack within this layer, and apparently unaffected cup material.

Table 4-4: Composition of the used intermediate ash. [GEHRE 13b, p.85]

Component	**Concentration** wt.-%
C	2.40
CO_2	2.20
Na_2O	0.60
MgO	3.80
Al_2O_3	2.44
SiO_2	42.91
P_2O_5	0.07
SO_3	6.45
Cl	0.12
K_2O	0.19
CaO	27.00
TiO_2	0.17
Fe_2O_3	11.05
BaO	0.25
Total	99.65

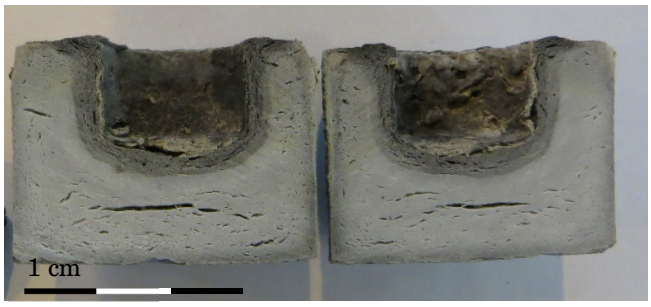

Figure 4-16: Halved cups after gasifier slag test.

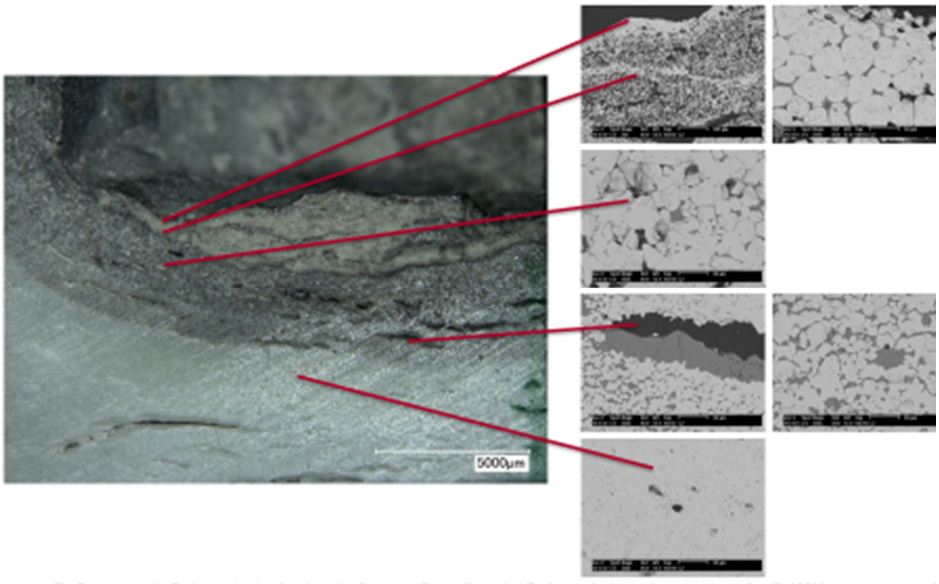

Figure 4-17: Close-up of the investigated zones.

The EDX analysis of the top area, illustrated in Figure 4-18, shows that this is not residual slag from the ash but a zirconium dioxide rich phase beside calcium silicate phase or phases containing also some minor components from the slag. The found element distribution indicates that a reaction took place with the silica and the calcium oxide from ash as well as the calcium oxide from the crucible, resulting in free zirconium dioxide. Which calcium silicates were formed, and whether it is pure zirconium dioxide or a calcium containing phase could not be clarified due to the small amount of material which was not sufficient for an XRD analysis.

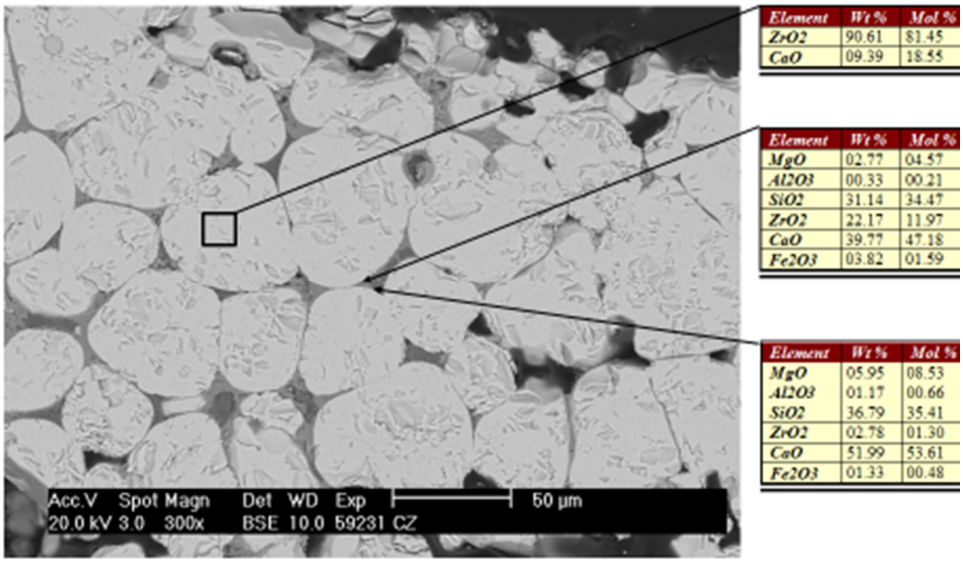

Figure 4-18: Zone with residual material.

The infiltrated zone is illustrated in Figure 4-19. The matrix itself is mainly intact which is quite positive. The pores are filled with mixed phases of CaO-MgO-SiO_2,

dominant components from the ash. The surface of the pores was not severe attacked, and the matrix not dissolved. The crack in the third area showed no further results, as said before, the cracks occurred during the firing of the cylinder itself not through corrosion in the test.

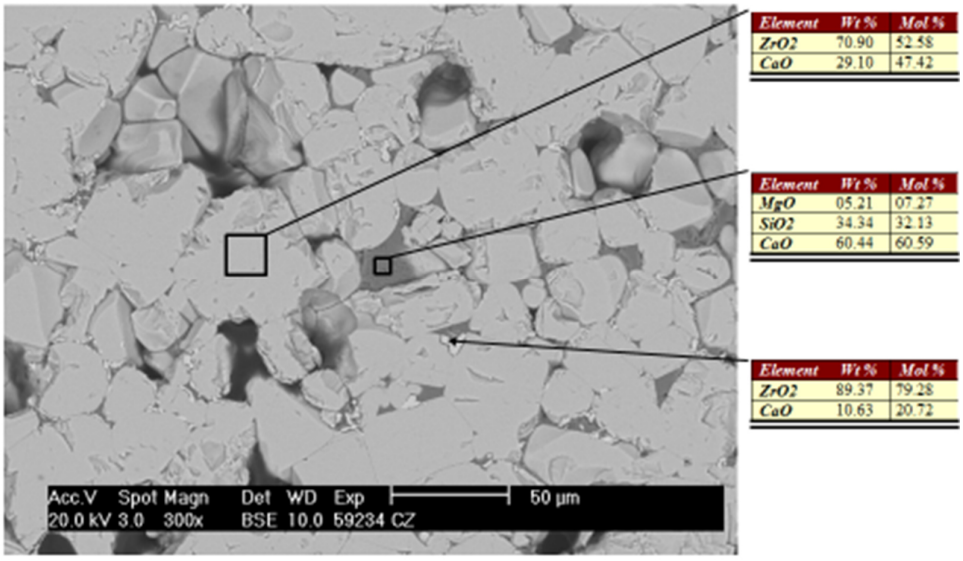

Figure 4-19: Area 2, infiltrated layer.

The base material in Figure 4-20 shows a high density. Additionally, it is observed that the $CaZrO_3$ material itself is stable under these conditions and did not decompose or else.

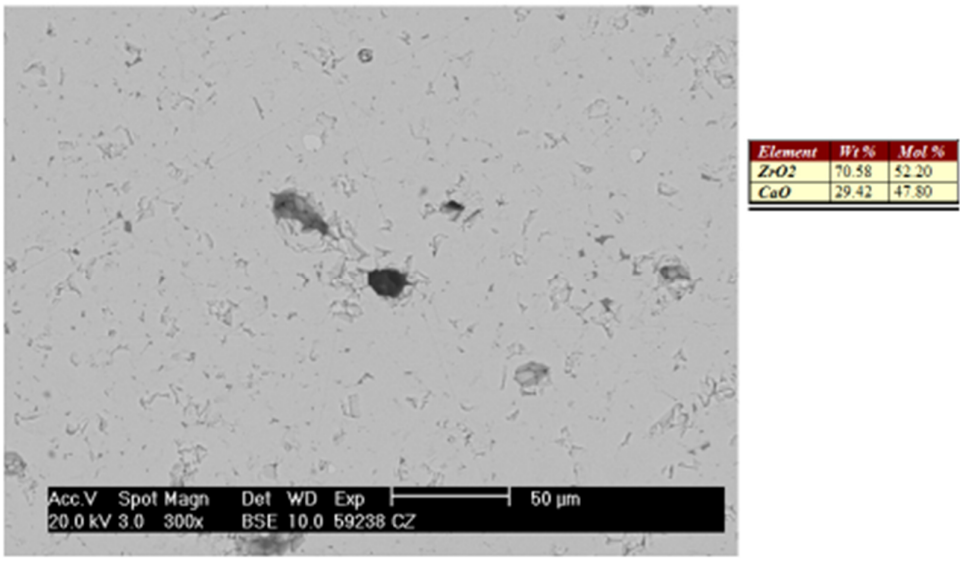

Figure 4-20: Bottom area, base material.

In conclusion, the cup test with intermediate ash from coal gasification for 50 h at 1550 °C in reducing atmosphere showed promising results. There was just a small infiltration layer. The small reactions observed were with calcium oxide which was

dissolved from the base material together with dominantly silicon dioxide from the slag. The matrix itself was stable. Due to the missing movement of the slag and refreshing of the corrosive material, it was not possible to judge about the erosion and stability of the residual and newly formed phases. Therefore, further investigations should regard a near industrial scale.

Recently, Li investigated materials based on CaO and ZrO_2 for gasification applications, too. [LI 18] In contrast to the material investigated here, he used a molar ratio of 1:1.15 ($CaCO_3$ to ZrO_2) for the synthesis of the material. [LI 13] Therefore, also the produced refractory material was no single phase and consisted of about 32 wt.-% cubic stabilised zirconia. Cup tests with, inter alia, the same intermediate ash were performed at 1450 °C for 3 h in air as well as in reducing atmosphere. The results showed only a small reaction layer but no visible infiltration for the test in air atmosphere, yet severe infiltration in reducing atmosphere. The main phases in the corrosion zone for the latter were Baghdadite ($Ca_3ZrSi_2O_9$), Diopside ($CaMgSi_2O_6$), iron-doped Wollastonite ($Ca_{2.87}Fe_{0.13}Si_3O_9$), Åkermanite ($Ca_2MgSi_2O_7$), and ZrO_2. Their components were also found in the analyses done here. From that could be inferred that such phases might also be formed.

Behaviour after annealing in reducing atmosphere

Due to the observation of the changed colour after the corrosion test with the gasifier ash, further investigations were performed concerning the effect of a reducing atmosphere. Due to the earlier mentioned ion conduction, there might be an impact of the partial oxygen pressure on the material. Whereby the mentioned corrosion test showed the stability of calcium zirconate under the thermal and atmospheric conditions there. Sample bars of B2 were taken and bedded in petrol coke within a corundum retort. After 5 h at 1550 °C the samples were removed and a part of it thermal shocked. Latter should recreate an oxidation at elevated temperatures because of the quenching of a heated sample (900 °C) with a cold air stream thereby.

In Figure 4-21 there are representative photographs of the sample for each of the described steps. The initially brown colour changed to a dark grey, almost black subsequent to the heat treatment in the reducing atmosphere. After the thermal shock the colour changed again, here to a light greyish shade. Unlike the original sample (see Figure 4-5) the stain is not inside the sample, only at the surface. Close-up images of fracture surfaces, obtained in the digital light microscope, illustrated in Figure 4-22, show the coked samples with and without thermal shock. As a consequence of the comparable conditions, the sample after heating in reducing atmosphere resembles the crucible material after the gasifier corrosion test. There was also a dark surface remarkable and a light grey core material. This kind of zoning is also visible in the image on the left side in Figure 4-22. A more severe change is remarkable after the

exposure to air at elevated temperature. There, the inner material appears in lighter, yet brown colour again. It must be said that, because of the light setting at the microscope, there are some deviations in the colour rendering. Also, some cracks are visible within the sample. The occurring colours resemble the different visual appearances of iron oxides with different states of oxidation. Therefore, it is assumed that a possible iron contamination during the processing of the synthesis material happened. Additionally, the direct contact with the coke breeze during the test, as well as for the corrosion test, seems to have an impact, too. This would explain the different surface appearance.

Due to another finding during the ongoing experiments a more detailed investigation was striven. This is described in the next section.

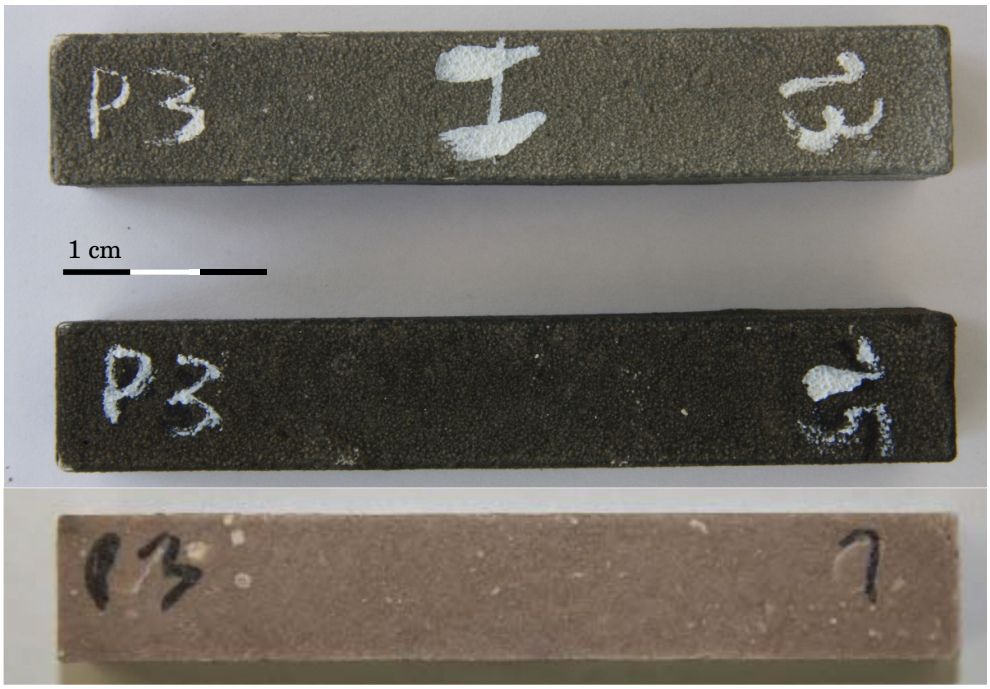

Figure 4-21: Comparison (from bottom to top) sintered sample, aged sample, and aged sample after one thermal shock.

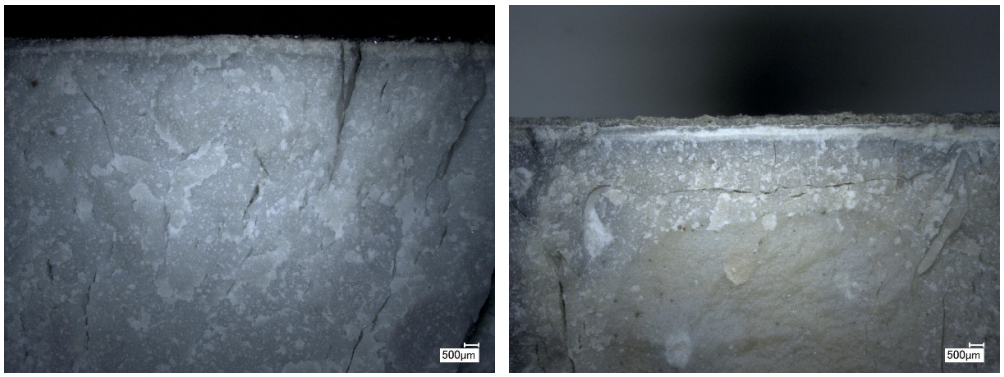

Figure 4-22: Close up of samples after treatment in reducing atmosphere (left) and additional thermal shocking (right).

4.2.5 Further investigations concerning the colouration

Relatively late within the continuing work, new material was needed to produce more samples. As a result of this, the thereby manufactured samples were surprisingly of different colour (see Figure 4-23). The samples are now more yellowish like the fused material or the zirconium dioxide raw material.

First, a contamination with iron oxide was assumed. This could have been entering by the preparation of the grains in the jaw crusher or vibration disc mill. Therefore, magnetic separators were used as well as a commercial processing of the synthesised material, which almost did the same. In addition, small scale tests were made doping the raw material mixture with a small amount of iron (III) oxide (Fe_2O_3), resulting in a similar, yet different brownish colour. A more extensive addition led to an almost black sample colour. In Figure 4-24 these samples are illustrated.

An XRF analysis of different samples showed no increased content on iron in contrast to the raw material or otherwise processed materials. Therefore, also material was synthesised in accordance with the route of Li et al.: [LI 13] An equimolar mixture of $CaCO_3$ and ZrO_2 was processed to a slip, casted in plaster moulds and then sintered like before. Afterwards some of these samples were sintered again at the second firing temperature of 1650 °C (see Figure 4-25). With this route there was not enough material obtained to recreate batch B2.

Figure 4-23: Photography of the newly prepared samples.

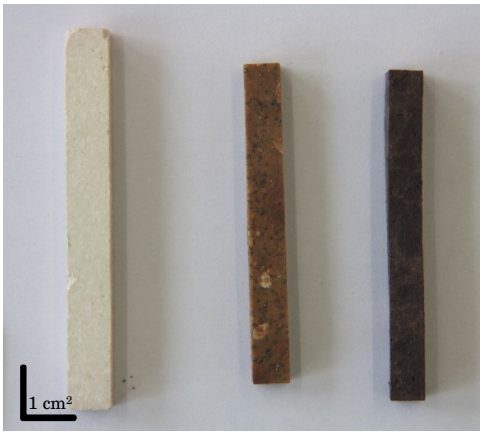

Figure 4-24: Comparison of samples with content of (0, 2.5, and 5) wt.-% Fe_2O_3 after sintering at 1200 °C.

Table 4-5: XFR analyses of the different materials in wt.-%.

Sample ID	Fe_2O_3
Initial raw material mixture	0.03
B2	0.04
B2, new	0.03
Slip casting synthesis	0.03
B2, from external processed material	0.04

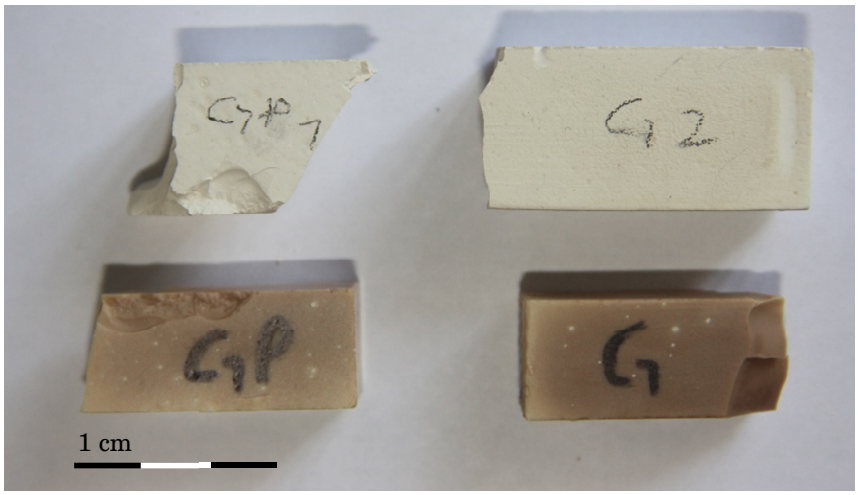

Figure 4-25: Slip casted material, after initial firing at 1400 °C (above) and after a second firing at 1650 °C (below).

It is presumed that there was a problem with the synthesis of the base material. Agglomerated zirconium dioxide was not carefully enough mixed with the calcium carbonate leading to the problems observed during the investigations. Yet, several XRD investigations on the materials did not show any different phase, see also Figure 4-26. Long-time observations then showed a slow but steady decomposition, partly only on the surface, occasionally more severe of some samples. This comes from the residual CaO which is distributed in the samples when zirconia is agglomerated

regarding the batch compositions. It was not enough for a fast disintegration which was observed in Part I, yet it was remarkable. This also reminds on the violet colour Fischer et al. reported. [FISCHER 76] It is also possible, that the small iron oxide content, even if not increased by processing, forms solid solutions at higher temperatures with the calcium zirconate leading to a disordered crystal structure. [GARGORI 12] Yet, it was not remarkable in the XRD. An influence of the different furnaces and their deposits from other firings can also not be ruled out after all.

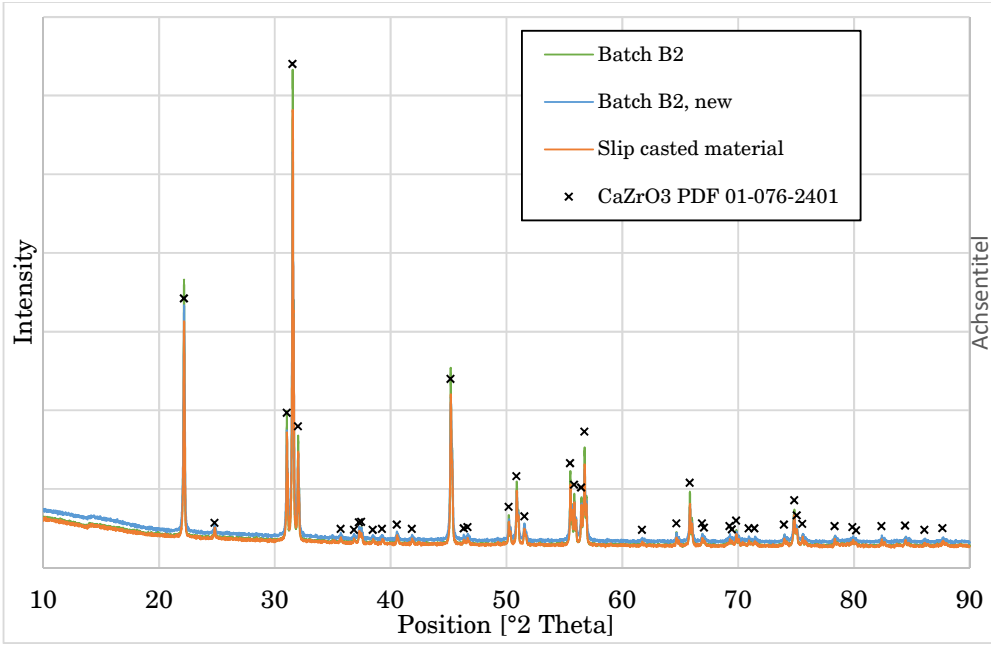

Figure 4-26: Compilation of XRD profiles of the different processed materials.

It is remarkable that the colouring effect occurs only at the second firing or rather the higher sintering temperature but in the case of the newly synthesised material it did not happen. Thus, there were no further investigations done concerning this fact because the phase distribution seemed not interfered, the processing did not contaminate the material, and the mentioned surface reaction over time only occurred for the very first samples, which actual had some deviations in synthesis. Yet, this was resolved successfully. Finally, Figure 4-27 sums up all the conducted findings and investigations during in this part of the work.

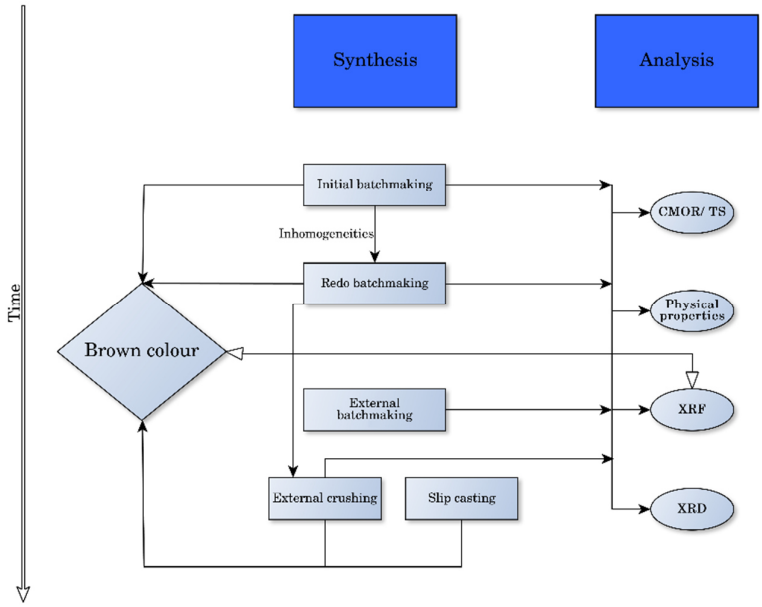

Figure 4-27: Overview over the conducted syntheses and analyses.

4.2.6 Investigation on B2 with new synthesised material

For the sake of completeness, the properties of the new formed samples were determined and are shown in Table 4-6. Improved thermomechanical behaviour is observed, with a residual strength of about 5 MPa after five thermal shocks in contrast to the lower values also of section 4.2.2. There was the possibility to use a larger pressing mould for this material. Thus, it was possible to obtain samples matching the required dimensions for HMOR, RUL, and LTE.

Table 4-6: Characterisation of the pressed material with new base material.

Property	Remark	Measured data
True density		4.69 g·cm^{-3}
Apparent density		4.30 g·cm^{-3}
Total porosity		8.52 $_{\pm 0.51}$ %
Open porosity		7.28 %
Shrinkage/ PLC		13.28 cm·m^{-1}
Young's modulus	Before TS	94.77 $_{\pm 2.27}$ GPa
	After 1 TS	84.19 $_{\pm 8.58}$ GPa
	After 5 TS	30.68 $_{\pm 4.09}$ GPa
CMOR	Before TS	35.54 $_{\pm 2.37}$ MPa
	After 1 TS	not determined
	After 5 TS	4.89 $_{\pm 1.77}$ MPa
CCS		265.37 MPa
HMOR	At 1350 °C	20.47 $_{\pm 5.56}$ MPa
RUL	0.1 % deformation	1547.2 °C
	0.5 % deformation	1593.6 °C
	1 % deformation	1626.5 °C
LTE	25 – 600 °C	8.43 10^{-6} x K^{-1}
	25 – 1000 °C	9.05 10^{-6} x K^{-1}
	25 – 1400 °C	9.52 10^{-6} x K^{-1}

To compare the determined properties with usually used materials in the chosen application, the thermal shock resistance parameter R and R' were calculated. With the formulas, described in section 2.3.4, the following equations were set up:

$$R = \Delta T = \frac{\sigma(1-\mu)}{E\alpha} = \frac{35\ MPa * (1-0{,}234)}{95\ GPa * 9 \cdot 10^{-6}\ K^{-1}} \cong 31{,}4\ K \quad (4\text{-}1)$$

$$R' = \frac{\sigma(1-\nu)\lambda}{E\alpha} = 31{,}4\ K * 2 W m^{-1} K^{-1} \cong 63\ W m^{-1} \quad (4\text{-}2)$$

For the calculations the rounded values were used. The thermal conductivity was not determined within this work, the value of Srirama Murti and Krishnaiah were used. [SRIRAMA MURTI 92] In Table 4-7 there are some values found or rather calculated from the literature for materials currently used in the striven applications. Thereby, it has to be said that those information were not often published in the literature.

However, it should be clarified that the obtained values are not directly comparable. The discrepancy in fabrication, physical and microstructural properties are rather different or unknown. In accordance with the already said in chapter 2.3.4, the role of the microstructure regarding the strength and the modulus of elasticity is important. Nevertheless, the linear thermal extension as well as thermal conductivity are more depending on the actual material than the their microstructure (porosity) which should therefore be considered for the scale of the values comparing such materials. [KRAUSE 00, p.23] Here, the carbon containing materials were different from the compared oxidic materials. Therefore, there is a huge impact on the properties resulting in these tremendous differing values. Thus, comparing those values without the right context and without regarding other properties does not be sufficient.

Table 4-7: Examples of R and R' for some refractory materials [ROUTSCHKA 97, p.85–86, ROUTSCHKA 97, p.161, BENAVIDEZ 15, ALMATH 19]

Material	R [K]	R' [W m^{-1}]
Al_2O_3-C	355	2840
MgO-C	222	4440
Graphite	910	77350
Cr_2O_3 (picro-chromite)	24	72

4.3 Conclusion Part II

The second experimental part of this work dealt with the production and evaluation of pressed refractory materials based on the previously synthesised calcium zirconate. Due to some problems concerning the upscaling of this synthesis, some samples had some agglomerates, yet it was not remarkable in the XRD. Nevertheless, the obtained results, especially concerning the corrosion tests, a declining behaviour is not expected, and the conducted experiments are not worthless.

4 Part II: Calcium zirconate as refractory material

First it should be noted that the synthesis must be done carefully. A good homogenisation has to be assured to obtain satisfying material for the further processing.

An interesting finding was gained during the processing of materials made with the same raw materials and parameters but at different places. A brownish colour of the first samples implied a deviation in the stoichiometry, even though it could not be detected. The origin of the discolouration could not be finally resolved. A contamination with further iron oxide through the processing was not detectable and a nonstoichiometry not seen in the XRD analysis. Due to the ongoing work and the anyway good results, it was not finally clarified. Because later on the samples were of yellowish colour, resembling other calcium zirconate materials from the literature.

Concerning the development of a refractory material the crushed and classified material from the synthesis was used with varying batch compositions. The variation of the batches and processing parameters yielded in a promising batch with a maximum grain size of up to 3 mm for the following experiments.

The variation on the pressure the material is shaped with showed no direct relation to the measured thermomechanical properties but for the physical ones. This could be due to different mechanisms affecting these characteristics. Surprisingly a low pressure (50 MPa) as well as a high pressure (150 MPa) showed promising thermal shock behaviour. This is attributed to different mechanisms during formation of the microstructure during the firing due to the compaction and resulting sinter affinity. As another factor the thermal shock mechanisms were assumed. A comparable high modulus of rupture, determined for the lower pressed samples, showed good residual strength which is contributed to a low crack propagation. The samples pressed at the high pressure had comparable lower values of the modulus of elasticity, yet showed also a high ratio of residual strength which results from a impeded crack initiation concluded from the studies of Hasselman. [HASSELMAN 69]

The corrosion tests showed promising results. The test in the steel casting simulator exposed, that the thermal stability is given for the investigated material. The chemical stability was not perfect due to some inhomogeneities within the samples but the corrosion layer itself was stable and neither erosion nor a material built up was observed. The tests with gasifier ash in reducing atmosphere showed low infiltration over the 50 h of processing. The matrix was still intact after the infiltration which is positive. Some reactions of the compounds of the ash and the contact layer with the sample showed the formation of calcium silicates which indicates the decomposition of the calcium zirconate in the presence of the slag with all its components. Silica showed the severest reaction with the material which should kept in mind for future applications. Unfortunately, the test could not be conducted dynamically. Yet, the stability of the matrix and the low infiltration rate show a potential of calcium

zirconate for the application in coal gasifier. Hereby and in another experiment, it was observed that the calcium zirconate phase is stable in reducing atmosphere at higher temperatures. Yet, industry near tests should be considered as a next step.

The behaviour regarding thermal shock and corrosive media was over all the conducted experiments pretty good. Therefore, the obtained material may also suit for other applications involving high temperatures or corrosive media. Whereby the differences concerning the possible reactions and mechanisms have to be regarded there.

5 Manufacturing of functional products by the example of a castable

The final section of this dissertation regards the idea of refractory products based on calcium zirconate. The example of a casted calcium zirconate is presented here. Melting crucibles were considered as potential target application. In the following, an overview about the necessary steps is given. At this point a detailed investigation and discussion of the used casting slip is set aside due to future work and patent reasons.

5.1 About the casting slip

The initial composition is based on the work of Schafföner et al. [SCHAFFÖNER 18]. Their material is based on fused calcium zirconate and they used a calcium aluminate cement (CAC) as binder. For this work, it has been decided to waive this kind of binder but to use the synthetic single-phase $CaZrO_3$. Consequently, the aim was again to obtain an impurity free material.

While excluding all commercial cement binders, the primary task was to find a new suitable binder for this product. Challenges were, beside the hardening behaviour and a proper workability, to have only calcium zirconate phase after firing. Therefore, binders were used which react to CaO at elevated temperatures. Through addition of monoclinic ZrO_2 the emerging calcia reacts in situ to $CaZrO_3$ when set to the right proportions. Also differing from the original slip composition, the particle size distribution was made after Dinger and Funk [DINGER 92] with the given grain size classes and distributions of the earlier synthesised material. Thereby, the addition of the binder and balancing zirconium dioxide was taken into account regarding the finest particle class. The water content was adjusted to the flowability but in general close to the initial one. The used dispersant and defoamer were not changed in type and proportion.

5.2 Preparation of the casting slip and the crucibles

Before a castable could be realised, some adjustments had to be made. The properties of the originally synthesised grains were not suitable for the application due to the high open porosity. This would have led to a high demand of water for a good workability. Therefore, regarding the results from the first part of this work, the sintering temperature for the synthesis was raised to 1650 °C. Thus, the porosity was low enough, and also the expected shrinkage was lower due to the completed sintering processes up to 1650 °C of the grains. The properties are given in Table 5-1.

Table 5-1: Comparison of the synthesised grain fraction used for refractory preparation.

	Property	Unit	Value
1400 °C	Total porosity	%	44.10
	Apparent density	$g \cdot cm^{-3}$	2.61
1650 °C	Total porosity	%	2.82
	Apparent density	$g \cdot cm^{-3}$	4.53

To produce primordial crucibles, a casting mould made of plastic with silicon throws was available. It consists of four parts: two parts for the outer shell and two parts for the core. The crucible is headfirst situated within the mould which means that the bottom is up and filled in last. The height of the inner volume is 15 cm and the diameter were 13 cm with a wall thickness of about 2 cm for the final product. The volume of the crucible is about 1 l and the volumetric capacity is about 0.77 l. To fill the mould completely with one mixture, 4 kg slip were prepared. For the mixing process a standard concrete mixer (ToniMIX, Toni Technik Baustoffprüfsysteme GmbH, Berlin, Germany) was used. First, the coarse grain fractions were weighed in and blended for 2 min. Afterwards the finer fractions, the dispersant, the binder, and the raw zirconium dioxide was added. All together was again blended for about 5 min. Subsequently the water was added in three parts, with a mixing time of 30 s in between each part and some scraping of the stirrer. With the last water, the defoamer was added and now the complete mixture blended for about 5 min to ensure homogeneity.

Immediately after the mixing procedure, the so prepared castable was filled into the mould which was lubricated with a small amount of standard machine oil. At the same time, the mould was vibrated for the filling time of about 4 min using a vibratory table (JMV 800/1000x800, Jöst GmbH & Co.KG, Dülmen, Germany).

After some time, the core was removed to ensure stressless drying at room temperature. The cured crucibles were then demoulded. Shortly after that, they were heated up to 110 °C in 24 h including a dwell time of 8 h for complete drying.

For firing, several crucibles were placed in an electric oven (HT 276/17, Nabertherm GmbH, Lilienthal, Germany). The heating rate was 2 $K \cdot min^{-1}$ up to 1650 °C with a dwell time of 6 h and an additional dwell time of 2 h at 900 °C.

The cooling was free. To prevent reactions with the oven lining MgO kiln furniture was used.

5.3 Characterisation of slip casted calcium zirconate refractories

For the characterisation of the new refractory material, test specimens were manufactured. The procedure was the same as described above but the mould was a standard cement steel mould 25 x 25 x 150 mm^3 which was covered in plastic foil to prevent adhesion to the walls. Therefore, there was no need for further lubricating with oil. All other treatments remained unaffected. The testing methods were already described and can be found in sections 3.1.3 and 4.1.3.

5.3.1 Mineralogical and microstructural properties

The superordinate task for any further development was to maintain the single-phase character. For investigating the phase composition XRD measurements were carried out. The results are given in Figure 5-1. The marked reflexes were identified while analysing the measured data. It can be seen, that there are no other phases identifiable besides $CaZrO_3$. In conclusion, the aspired in situ reaction in combination with the mixing procedure and the calculated proportions was successful.

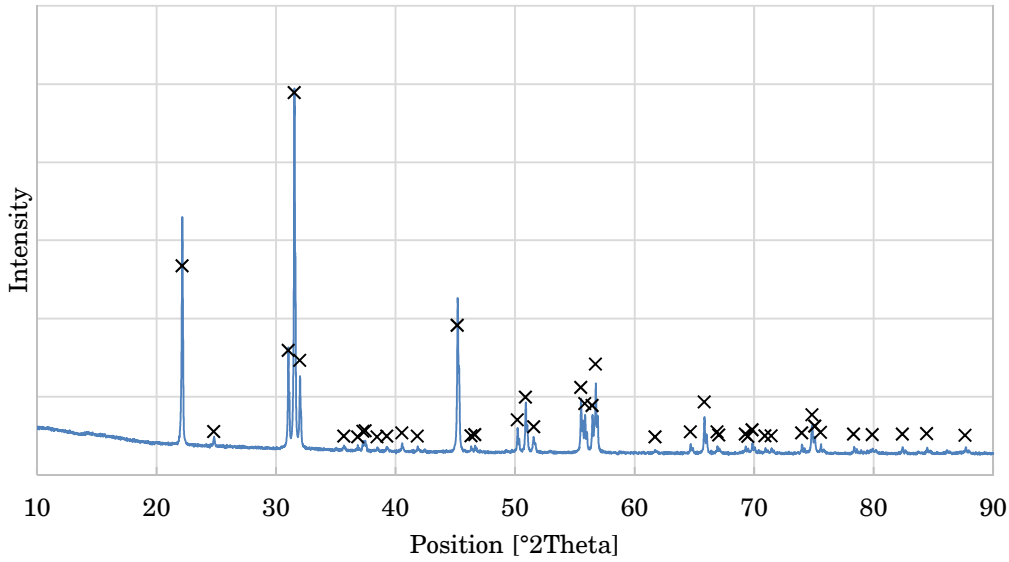

Figure 5-1: XRD profile of the casted crucible material after firing. The matching reflexes of calcium zirconate (PDF 01-076-2401) are assigned.

Figure 5-2 shows an SEM image of the microstructure of a casted crucible after firing. On this fracture surface the dense grains are surrounded by the in situ formed calcium zirconate, recognisable by the pores resulting from the decomposition of the binder. As described in section 4.2.1, the very fine calcium zirconate crystals from the in situ reaction are remarkable, as was assumed before. Due to less compaction of the

set castable in contrast to a pressed moulding mass and because of the different grain size distributions as well as grain porosity, the microstructure differs from each other.

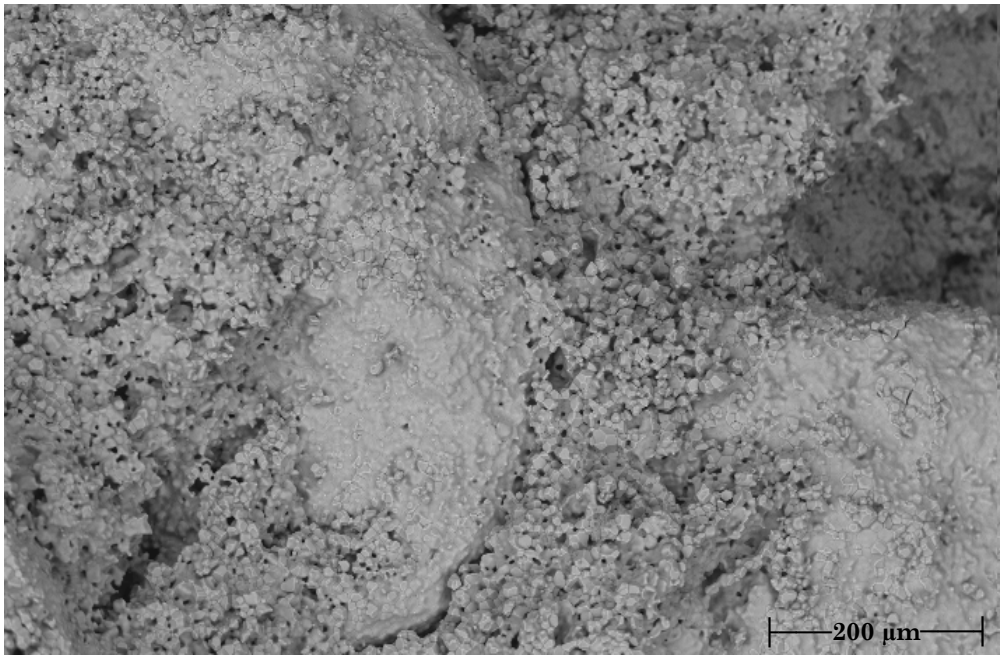

Figure 5-2: Representative SEM/BSE image of the microstructure of the casted crucible, 100x magnification.

5.3.2 Physical and (thermo-)mechanical properties

The measurements and analyses were carried out the way described for the other sections before. All characteristics are summarised in Table 5-2. The porosity differed depending on the chosen method. The water absorption method used bigger samples in contrast to the mercury intrusion method, which was conducted according to the standard DIN 66133:1993. Thus, the measured volume was different as well as the precision of the weighting procedure. For example, the moisture of the cloth removing the excess water before weighting and the manual treatment itself were factors leading to the difference. Remarkable was the small pore size thereby, which is promising for corrosion tests, because the infiltration tendency depends on the pore size due to the surface tension. The shrinkage was quite high for products but there were several factors which might improve this detail. For prefabricated crucibles, for example, this can be compensated through an oversize dimensioned mould. Additionally, the porosity should be decreased, for example by reducing the water content of the castable slip, or different grains size distributions, other or less binder content or adjusting the sintering conditions. But this would also affect the other properties and should therefore be considered, too.

The investigations of the thermal shock behaviour showed a loss of strength of about 66 % after the first thermal shock but the following up to four thermal shock

cycles did not led to further loss in such way. The remaining cold modulus of rupture had a value of about 5 MPa, which is very promising. To depict this fact, after five cycles of heating and quenching each square millimetre of a loaded area withstands a static load of about 500 g.

Regarding the RUL, the results showed a softening at higher temperatures, which has to be taken into account for the future maximum application temperatures. Yet, the used load of 0.05 MPa is comparable to the load on the bottom of a crucible with a height of about 1.3 m. This is regarded without the hydrostatic pressure of the contained melt or else, without the bottom, and not considering any backfilling which is commonly used within the melting units.

The maximum recommended working temperature, defined by $T_{0,5}$, was determined with 1596.0 °C. However, Luz et al. regarded these evaluations critically, because the real application conditions were not taken into account and deformation is only possible if there is enough room, otherwise stress is induced which could relieve with increasing temperature. [LUZ 17] On the other hand, there were reactions with the measurement supports which could not be prohibited and might have had an influence on the values obtained. For applications in VIM furnaces, the heat is directly induced into the metal, which means that there is no temperature field surrounding the crucible. Yet, thermal conductivity from the formed melt to the crucible from the inner to the outer wall will occur. The respective time of a melting process is on the other hand also differing for each application. This would mean, that the maximum temperature of the current material is not directly bound to the maximum temperature of the melt for processing of the metal.

Table 5-2: Characterisation of the castable material.

Property	Remark	Measured data
True density		4.75 g·cm^{-3}
Apparent density		3.87 g·cm^{-3}
Apparent porosity		18.61 $_{\pm 0.27}$ %
Mercury porosimetry, open porosity		13.43 %
Mercury porosimetry, median pore size by volume		4.89 µm
Shrinkage/ PLC		2.67 cm·m^{-1}
Young's modulus	Before TS	60.21 $_{\pm 3.78}$ GPa
	After 1 TS	31.35 $_{\pm 1.67}$ GPa
	After 5 TS	17.54 $_{\pm 0.51}$ GPa
CMOR	Before TS	16.79 $_{\pm 0.75}$ MPa
	After 1 TS	5.77 $_{\pm 0.48}$ MPa
	After 5 TS	4.98 $_{\pm 0.13}$ MPa
CCS		51.83 MPa
HMOR	At 1350 °C	6.71 $_{\pm 0.73}$ MPa
RUL	0.1 % deformation	1557.8 °C
	0.5 % deformation	1596.0 °C
	1 % deformation	1625.6 °C
LTE	25 – 600 °C	8.71 10^{-6} x K^{-1}
	25 – 1000 °C	8.91 10^{-6} x K^{-1}
	25 – 1500 °C	9.07 10^{-6} x K^{-1}

For this material, an assessment of thermal shock parameters will be given. Thereby, it is focused on R and R' because for the others the specific fracture energy has to be known or at least be determined. An estimation of it is considered as not beneficial due to the unsettling values. For the calculations, the rounded values were used. Again, the value of the thermal conductivity was obtained from the literature (cf. chapter 4.2.6). [SRIRAMA MURTI 92] Thus, the following calculations were done:

$$R = \Delta T = \frac{\sigma(1-\mu)}{E\alpha} = \frac{16\ MPa * (1-0{,}2)}{60\ GPa * 9 \cdot 10^{-6}\ K^{-1}} \cong 23{,}7\ K \quad (5\text{-}1)$$

$$R' = \frac{\sigma(1-\nu)\lambda}{E\alpha} = 23{,}7\ K * 2W(mK)^{-1} \cong 47\ Wm^{-1} \quad (5\text{-}2)$$

The critical thermal difference is low with this calculation. Regarding the performed thermal quenching from 950 °C to room temperature without failing, there must be other factors affecting this behaviour or the calculation is containing too much approximations or maybe errors. An improvement of the CMOR would also increase the value proportionally. Also, as mentioned earlier, the values are for room temperature conditions. Another factor is the different processing of each material differing in particle size, densification in green state, and thermal treatment.

Table 5-3: Values of R and R' from the literature. [KINGERY 55, ROUTSCHKA 97, p.111, ZHU 18]

Material	R [K]	R' [W m^{-1}]
Al_2O_3	37	1131
MgO	22	796
ZrO_2 (stabilised)	66	130
Fire clay refractory	38	59
Y_2O_3	140	1830
BN (hot isostatic pressed)	333	6660
$CaZrO_3$, this work, press mass	31	63

5.4 Conclusion

This part of the doctoral thesis did not present any kind of development of a commercial castable product made of calcium zirconate. Yet, there were some adjustments made and the results were very promising.

The experiments carried out showed that it is possible to produce slip casted crucibles based on calcium zirconate with a grain size up to 3 mm. By choosing a suitable binder and through in situ reaction, it was possible to obtain pure phase $CaZrO_3$ after firing. The new refractory material showed auspicious thermo-mechanical properties. Some impressions of the castable process are given in Figures 5-3. It is remarkable, that the fired crucibles tend to show again some discolouring. In contrast to the samples described in section 4, the material was initially presintered at 1650 °C and did subsequently show now remarkable dying.

Additionally, the samples showed, if any, only a changed surface and no complete colour change within the material.

(a) (b) (c)

Figure 5-3: Images of the crucible production: (a) the filled crucible mould, (b) top view from a demoulded crucible, and (c) a fired crucible.

For the future, it is planned to develop functional products based on this castable material for industrial application.

Furthermore, an upscaling to larger crucibles is desired. First semi-industrial trials for melting processes of different metals are in preparation.

6 Summary and outlook

Refractory materials suffer a lot from the environment they are subjected to in their respective applications. These applications are as manifold as their respective parameters. Therefore, there is no single material on the market that prevailed over the other for each of them. With developing technology, the demands towards the refractories raise additionally and foment the research for new materials.

Calcium zirconate, which is very rare in nature, was investigated for a relatively long time, yet the applications were limited to its perovskite structure. Still some research was done regarding its synthesis. Thereby, studies focused not too much on the single phase material without doping and only on fine grained powders. Recently, $CaZrO_3$ showed potential as refractory for titanium and titanium alloy melts for a number of years [KIM 01a , CHANG 10, LI 10, LU 11, FREITAG 17, KLOTZ 19] However, other applications are rarely reported.

The present work had therefore two aims. One was the investigation of the formation of pure phase calcium zirconate, the influence of necessary parameters, and production of different grain size classes. The other one was the development of different products based on the previously synthesised material and their testing regarding potential future applications.

For the evaluation of the calcium zirconate production, the solid state synthesis was chosen as processing route due to the small expenses and the simplicity of a future upscaling. Therefore, monoclinic zirconium(IV) oxide and two different calcia precursors, calcium hydroxide and calcium carbonate, were used. A good homogenisation could be achieved without using of dangerous additives. A few percent of water were enough to obtain stable, crack free and easy to handle specimen. For the first mixtures, a tumbling mixer was used with two sizes of zirconium dioxide mixing balls. The prismatic specimens were die pressed at 60 MPa. After drying and firing at the respective maximum temperature, the samples were analysed. Later, a laboratory intensive mixer was used but led to inhomogeneities within the samples and had to be adjusted for the ongoing work.

The variation of the molar ratio of the raw materials showed that only the perfect equimolar composition of the raw materials led to single phase material. An increase in calcia source within the mixture resulted in free lime after firing, leading to disintegration of the samples over time due to hydration in conjunction with volume expansion. An excess of zirconia led to calcia stabilized zirconia in addition to calcium zirconate and below 1400 °C there was also monoclinic zirconia from the raw material left. A necessary temperatures of 1200 °C was found to obtain fully reacted material with a suitable density. An increasing maximum temperature and dwell time showed improved densities. This might be required for some further processing. A decomposition of the $CaZrO_3$ or a loss of calcium oxide at elevated temperatures was not observed during or after firing.

Calcium carbonate was found to be most suitable as raw material due to the easier handling because of its stability at air and its harmlessness. Additionally, it showed a higher yield on pure phase material at the same temperatures compared to the samples made of $Ca(OH)_2$.

As result of this first experimental part a patent (WO 2019/106052 A1) was registered concerning the fabrication of coarse grained material based on pure phase calcium zirconate and the parameters thereby.

For the manufacturing of refractory products two different processing routes were chosen. The focus laid on the pressing route due to its easier handling, the other processing route was the casting technology.

Beforehand, larger amounts of synthesised material had to be manufactured. Therefore, the findings from the initial part of this work were used. To obtain a higher grain density, the temperature was raised to 1400 °C. Later, for the casting slips, even to 1650 °C. The raw materials were mixed, pressed into larger blocks and then sintered at the mentioned temperatures. Afterwards, the material was crushed and classified into different grain sizes.

For the second experimental part, the production of pressed refractories based on $CaZrO_3$, different batches were created concerning the maximum grain size, the addition of equimolar mixture of the raw materials for an in situ reaction and the grain size distribution. The in situ reaction led to a decreased porosity even if the decomposition of the raw material mix produces CO_2. The rising maximum grain size improved the thermomechanical properties even if the 6 mm grains showed an influence of the sample geometry. As a result, a batch with 3 mm grain size was chosen for a detailed investigation. The variation of the batches and processing parameters yielded in a promising batch with suitable grain size for the following experiments.

Corrosion tests were performed aiming at future industrial applications of the here developed material. The dipping test in a standard steel melt showed in general stability of the material and it withstood the thermal shock. The formation of calcium silicates in the thin corrosion layer indicates a possible decomposition of $CaZrO_3$ in contact with the melt in presence of SiO_2. Yet, the present inhomogeneities are also responsible. An erosion of the layer through the rotation of the sample during test did not happen. The cup tests with gasifier ash were performed in order to investigate the stability against the formed liquid slag in reducing atmosphere. The results are promising, proofing the stability of the calcium zirconate phase in reducing atmosphere at elevated temperatures. The infiltration during the 50 h was smaller than 5 mm. Reactions were observed at the contact surface, yet the infiltrated matrix showed no signs of dissolution. Again, calcium silicates were predominant due to the amount of silica in the ash. However, the stability of the formed reaction layer in a dynamic process, as the gasifier is designed for, could not be resolved. Each of the tests could only consider one set of application parameters.

The obtained material may also suit for other applications involving high temperatures or corrosive media. Yet, both corrosion tests showed preferential reactions with silica out of the respective components of those medias. Future investigations should consider a more detailed investigations on this mechanism regarding atmosphere, temperature, and chemical activity. Because the investigations of Schafföner showed differing reactivities of aluminium as alloying element in titanium alloy melts depending on its proportion. [SCHAFFÖNER 15a] In general, the basicity of a corrosive media might limit the suitability of the here developed refractories. Yet, future work should address this topic in a more extensive way.

Due to some problems concerning the upscaling of this synthesis, some samples were not homogeneous even when it was not remarkable by XRD. Nevertheless, the obtained results, especially concerning the corrosion tests, do not let expect declining behaviour, and the conducted experiments provided still worthy results.

The last part showed the possibility of processing the coarse grained material into casted refractory products. Due to possibly relevant information for a commercial usage, some details had to be left out of the processing aspects. Yet, according to a grain size distribution the fractions of the calcium zirconate were used. These were initially higher sintered to obtain a grain density lower than 10 % to reduce the amount of water for a processable casting slip. At first, the classic rectangular 25 x 25 x 150 mm^3 and later, first crucibles in plaster moulds were casted. Priority had, as before in the other parts, the single phase constitution of the fabricated material. XRD analysis showed that this is true after sintering. The physical and thermomechanical properties showed promising values. Highlighting the good residual strength of about 5 MPa after five

thermal shocks. The produced crucibles showed a good handling even in green state. Yet, the setting time of up to four days was quite long.

Both investigated refractory materials showed the potential for the application in industry. Advantageously, these compositions can easily be adjusted to the size of the future product. Due to the availability of different maximum grain sizes there should be improved thermal shock behaviour compared to the currently used fine grained materials. The pressed calcium zirconate has potential for applications with simple or symmetrical shapes whereas the castable allows the shaping into more complex geometries. Furthermore, there are some other interesting processing routes, like hot or cold isostatic pressing, slip casting in plaster moulds, and spraying.

Future work, which is in fact currently performed, will use this crucibles for applications in VIM melting units to process titanium and titanium alloys for different applications. The interaction with the melt, durability, and melt contamination are focused thereby. Furthermore, the casting slip should be optimised regarding the processability and setting time. This all is made to be the first step of bring refractory products based on single phase calcium zirconate to the market.

In a next step, to commercialise these products, a market and cost analysis is needed. Finding the demanding industrial partners, starting a process chain and knowing what the production costs of such products will be, is another urge developing from the results of this work.

References

[ALMATH 19] Almath crucibles ltd: *Material properties*: https://almathcrucibles.com/materials/graphite/. Accessed 17 September 2019.

[ANEZIRIS 08] C. G. Aneziris and M. Hampel: *Microstructured and Electro-Assisted High-Temperature Wettability of MgO in Contact with a Silicate Slag-Based on Fayalite,* Int. J. Appl. Ceram. Technol., 5(5), pp. 469–479, 2008.

[ANEZIRIS 13] C. G. Aneziris, S. Dudczig, J. Hubálková, M. Emmel, and G. Schmidt: *Alumina coatings on carbon bonded alumina nozzles for active filtration of steel melts,* Ceram. Int., 39(3), pp. 2835–2843, 2013.

[ANGERS 72] R. Angers, R. Tremblay, and A. C. D. Chaklader: *Formation of $CaZrO_3$ by Solid-State Reaction Between CaO and ZrO_2*, J. Am. Ceram. Soc., 55(8), p. 425, 1972.

[ASM International 08] ASM International: *Casting*, Ed. by S. Viswanathan, D. Apelian, R. J. Donahue, B. DasGupta, M. Gywn, J. L. Jorstad, R. W. Monroe, M. Sahoo, T. E. Prucha, and D. Twarog, vol. 15, pp. 116–123, ASM International, 2008.

[BAKKER 84] W. T. Bakker, S. Greenberg, M. Trondt, and U. Gerhardus: *Refractory practice in slagging gasifiers,* Am. Ceram. Soc. Bull., 63(7), pp. 870–876, 1984.

[BAKKER 93] W. T. Bakker: *Refractories for Present and Future Electric Power Plants,* Key Eng. Mater., 88, pp. 41–70, 1993.

[BANERJEE 13] D. Banerjee and J. C. Williams: *Perspectives on Titanium Science and Technology,* Acta Mater., 61(3), pp. 844–879, 2013.

[BARKER 73] R. Barker: *The reversibility of the reaction $CaCO_3 \rightleftarrows CaO+CO_2$*, J. Appl. Chem., 23(10), pp. 733–742, 1973.

[BENAVIDEZ 15] E. R. Benavidez, E. Brandaleze, Y. S. Lagorio, S. E. Gass, and A. G. T. Martinez: *Thermal and mechanical properties of commercial MgO-C bricks,* Matéria (Rio J.), 20(3), pp. 571–579, 2015.

[BENNETT 04] J. P. Bennett and K.-S. Kwong: *Refractory liner materials used in slagging gasifiers,* Refract. Appl. News, 9(5), pp. 20–25, 2004.

[BENNETT 06] J. P. Bennett, K.-S. Kwong, C. P. Powell, A. V. Petty, Jr., H. Thomas, H. D. Prior, and M. Schnake: *Field Trial Results of an Improved Refractory Material for Slagging Gasifiers*, 2006.

[BENNETT 11] J. P. Bennett and K.-S. Kwong: *Failure Mechanisms in High Chrome Oxide Gasifier Refractories,* Metall. Mater. Trans. A, 42(4), pp. 888–904, 2011.

[BENNETT 07] J. P. Bennett, K.-S. Kwong, C. P. Powell, R. Krabbe, H. Thomas, and A. V. Petty, Jr.: *Low chrome/chrome free refractories for slagging gasifiers*: http://www.osti.gov/scitech/servlets/purl/923057.

[BOCCACCINI 97] A. R. Boccaccini and Z. Fan: *A new approach for the Young's modulus-porosity correlation of ceramic materials,* Ceram. Int., 23(3), pp. 239–245, 1997.

[BÖGE 11] A. Böge: *Technische Mechanik - Statik - Dynamik - Fluidmechanik - Festigkeitslehre*, Vieweg+Teubner Verlag / Springer Fachmedien Wiesbaden GmbH, Wiesbaden, 2011.

[BONAR 80] J. A. Bonar, C. R. Kennedy, and R. B. Swaroop: *Coal-ash slag attack and corrosion of refractories,* Am. Ceram. Soc. Bull., 59(4), pp. 473–478, 1980.

[BRAULIO 11] M.A.L. Braulio, M. Rigaud, A. Buhr, C. Parr, and V. C. Pandolfelli: *Spinel-containing alumina-based refractory castables,* Ceram. Int., 37(6), pp. 1705–1724, 2011.

[BROSNAN 04] D. A. Brosnan: *Mechanical engineering*, Vol. 178: *Refractories handbook*, Ed. by C. A. Schacht, pp. 39–77, Marcel Dekker, New York, 2004.

[BROWN 86] R. R. Brown and K. O. Bennington: *Thermodynamic properties of calcium zirconate ($CaZrO_3$),* Thermochim. Acta, 106, pp. 183–190, 1986.

[CAWLEY 90] J. D. Cawley, G. R. St. Pierre, J. D. Calen, J. C. Amante, K. Gourishankar, and K. S. Goto: *Thermodynamic and Diffusivity Measurements in Potential Ultra High Temperature Composite Materials,* Ohio State University, Columbus, Ohio, USA, 1990.

[CHANG 10] Y.-W. Chang and C.-C. Lin: *Compositional Dependence of Phase Formation Mechanisms at the Interface Between Titanium and Calcia-Stabilized Zirconia at 1550°C,* J. Am. Ceram. Soc., 93(11), pp. 3893–3901, 2010.

[CHEN 02] M. Chen and A. Yamaguchi: *Sintering of CaO-ZrO_2 Composite and Its Property of Slaking Resistance,* Nippon Seramikkusu Kyokai Gakujutsu Ronbunshi, 110(1288), pp. 1058–1061, 2002.

[CHEN 07a] M. Chen, C. Lu, and J. Yu: *Improvement in performance of MgO–CaO refractories by addition of nano-sized ZrO_2*, J. Eur. Ceram. Soc., 27(16), pp. 4633–4638, 2007.

[CHEN 07b] M. Chen, N. Wang, J. Yu, and A. Yamaguchi: *Oxidation protection of CaO–ZrO_2–C refractories by addition of SiC,* Ceram. Int., 33(8), pp. 1585–1589, 2007.

[CHEN 07c] M. Chen, N. Wang, J. Yu, and A. Yamaguchi: *Preparation of slaking resistant CaO aggregate from lightweight $CaCO_3$ with oxide addition,* Mater. Lett., 61(1), pp. 45–49, 2007.

[CHEN 18] J. Chen, L. Chen, Y. Wei, N. Li, and S. Zhang: *Corrosion and penetration behaviors of slag/steel on the corroded interfaces of Al_2O_3-C refractories: Role of Ti_3AlC_2*, Corros. Sci., 143, pp. 166–176, 2018.

[CHEN 19] G. Chen, B. Lan, F. Xiong, P. Gao, H. Zhang, X. Lu, and C. Li: *Pilot-scale experimental evaluation of induction melting of Ti-46Al-8Nb alloy in the fused $BaZrO_3$ crucible,* Vacuum, 159, pp. 293–298, 2019.

[CHENG 12] X. Cheng, X. D. Sun, C. Yuan, N. R. Green, and P. A. Withey: *An investigation of a TiAlO based refractory slurry face coat system for the investment casting of Ti–Al alloys,* Intermetallics, 29, pp. 61–69, 2012.

[CONTRERAS 05] J. E. Contreras, G. A. Castillo, E. A. Rodríguez, T. K. Das, and A. M. Guzmán: *Microstructure and properties of hercynite–magnesia–calcium zirconate refractory mixtures,* Mater. Charact., 54(4-5), pp. 354–359, 2005.

[CROWLEY 75] M. S. Crowley: *Refractory Problems in Coal Gasification Reactors,* Am. Ceram. Soc. Bull., 54(12), 1972-1074, 1975.

[CURTIS 47] C. E. Curtis: *Development of Zirconia resistant to thermal shock,* J. Am. Ceram. Soc., 30(6), pp. 180–196, 1947.

[DAVID 11] E. C. David and R. W. Zimmerman: *Elastic moduli of solids containing spheroidal pores,* Int. J. Eng. Sci., 49(7), pp. 544–560, 2011.

[DIAL 75] R. E. Dial: *Refractories for coal gasification and liquefaction,* Am. Ceram. Soc. Bull., 54(7), pp. 640–643, 1975.

[DINGER 92] D. R. Dinger and J. E. Funk: *Particle Packing III,* Interceram, 41(5), pp. 332–334, 1992.

[DU 92] Y. Du, Z. Jin, and P. Huang: *Thermodynamic Calculation of the Zirconia–Calcia System,* J. Am. Ceram. Soc., 75(11), pp. 3040–3048, 1992.

[DUDCZIG 14] S. Dudczig, C. G. Aneziris, M. Emmel, G. Schmidt, J. Hubálková, and H. Berek: *Characterization of carbon-bonded alumina filters with active or reactive coatings in a steel casting simulator,* Ceram. Int., 40(10), pp. 16727–16742, 2014.

[DUDEK 09a] M. Dudek and E. Drożdż-Cieśla: *Some observations on synthesis and electrolytic properties of nonstoichiometric calcium zirconate,* J. Alloys Compd., 475(1-2), pp. 846–854, 2009.

[DUDEK 09b] M. Dudek: *Usefulness of gel-casting method in the fabrication of nonstoichiometric $CaZrO_3$-based electrolytes for high temperature application,* Mater. Res. Bull., 44(9), pp. 1879–1888, 2009.

[DURRANI 06] S. K. Durrani, J. Akhtar, M. Ahmad, and M. A. Hussain: *Synthesis and characterization of low density calcia stabilized zirconia ceramic for high temperature furnace application,* Mater. Chem. Phys., 100(2-3), pp. 324–328, 2006.

[EBERT 33] F. Ebert and E. Cohn: *Beiträge zur Keramik hochfeuerfester Stoffe. VI. Das System ZrO_2-MgO,* Z. Anorg. Allg. Chem., 213(4), pp. 321–332, 1933.

[EUSTATHOPOULOS 99] N. Eustathopoulos, B. Drevet, and M. G. Nicholas: *Wettability at high temperatures*, Pergamon, Amsterdam, New York, 1999.

[FAZLI 12a] R. Fazli, M. Fazli, F. Golestani-Fard, and A. Mirhabibi: *The effects of raw materials particle size and salt type on formation of nano-$CaZrO_3$ from molten salts,* Ceram. Int., 38(7), pp. 5775–5781, 2012.

[FAZLI 12b] R. Fazli, M. Fazli, Y. Safaei-Naeini, F. Golestani-Fard, and A. Mirhabibi: *The effects of temperature, holding time and salt amount on formation of nano $CaZrO_3$ via molten salt method,* Ceram. Int., 38(7), pp. 5363–5368, 2012.

[FAZLI 14] R. Fazli and F. Golestani-Fard: *The effects of processing parameters on molten salt synthesis of $CaZrO_3$ nano-powders using oxide precursors,* Powder Technol., 257, pp. 149–155, 2014.

[FISCHER 76] W. A. Fischer, D. Janke, and M. Schulenburg: *Keramische Eigenschaften von Calciumzirkonat bei Temperaturen bis 1600 °C,* Arch. Eisenhuettenwes., 47(1), pp. 51–56, 1976.

[FREITAG 17] L. Freitag, S. Schafföner, N. Lippert, C. Faßauer, C. G. Aneziris, C. Legner, and U. E. Klotz: *Silica-free investment casting molds based on calcium zirconate,* Ceram. Int., 43(9), pp. 6807–6814, 2017.

[FREITAG 18] L. Freitag, S. Schafföner, C. Faßauer, and C. G. Aneziris: *Functional coatings for titanium casting molds using the replica technique,* J. Eur. Ceram. Soc., 38(13), pp. 4560–4567, 2018.

[FRENZEL 04] J. Frenzel, Z. Zhang, K. Neuking, and G. Eggeler: *High quality vacuum induction melting of small quantities of NiTi shape memory alloys in graphite crucibles,* J. Alloys Compd., 385(1-2), pp. 214–223, 2004.

[FRUHSTORFER 14] J. Fruhstorfer, S. Schafföner, and C. G. Aneziris: *Dry ball mixing and deagglomeration of alumina and zirconia composite fine powders using a bimodal ball size distribution,* Ceram. Int., 40(9), pp. 15293–15302, 2014.

[GALUSKIN 08] E. V. Galuskin, V. M. Gazeev, T. Armbruster, A. E. Zadov, I. O. Galuskina, N. N. Pertsev, P. Dzierzanowski, M. Kadiyski, A. G. Gurbanov, R. Wrzalik, and A. Winiarski: *Lakargiite $CaZrO_3$: A new mineral of the perovskite group from the North Caucasus, Kabardino-Balkaria, Russia,* Am. Mineral., 93(11-12), pp. 1903–1910, 2008.

[GARGORI 12] C. Gargori, S. Cerro, R. Galindo, A. García, M. Llusar, and G. Monrós: *Iron and chromium doped perovskite ($CaMO_3$ M=Ti, Zr) ceramic pigments, effect of mineralizer,* Ceram. Int., 38(6), pp. 4453–4460, 2012.

[GEHRE 11] P. Gehre, C. Wenzel, and C. G. Aneziris: *Investigation of shaped alumina based refractories used in slagging gasifiers,* Ceram. Int., 37(5), pp. 1701–1704, 2011.

[GEHRE 12] P. Gehre and C. G. Aneziris: *Investigation of slag containing refractory materials for gasification processes,* J. Eur. Ceram. Soc., 32(16), pp. 4051–4062, 2012.

[GEHRE 13a] P. Gehre, C. G. Aneziris, D. Veres, C. Parr, H. Fryda, and M. Neuroth: *Improved spinel-containing refractory castables for slagging gasifiers,* J. Eur. Ceram. Soc., 33(6), pp. 1077–1086, 2013.

[GEHRE 13b] P. Gehre: *Korrosions- und thermoschockbeständige Feuerfestfestmaterialien für Flugstromvergasungsanlagen auf Al_2O_3-Basis - Werkstoffentwicklung und Korrosionsuntersuchungen,* TU Bergakademie Freiberg, 2013.

[GEHRE 15] P. Gehre, C. G. Aneziris, M. Klinger, M. Schreiner, and M. Neuroth: *Influence of TiO_2- and ZrO_2-addition on the interaction of alumina castable with molten coal and gasifier slag,* Fuel, 150, pp. 252–260, 2015.

[GERMAN 96] R. M. German: *Sintering Theory and Practice*, Wiley, New York, Toronto, 1996.

[GHASEMI-KAHRIZSANGI 16] S. Ghasemi-Kahrizsangi, A. Nemati, A. Shahraki, and M. Farooghi: *Densification and Properties of Fe_2O_3 Nanoparticles added CaO Refractories,* Ceram. Int., 42(10), pp. 12270–12275, 2016.

[GIONEA 16] A. Gionea, E. Andronescu, G. Voicu, C. Bleotu, and V.-A. Surdu: *Influence of hot isostatic pressing on ZrO_2-CaO dental ceramics properties,* Int. J. Pharm. (Amsterdam, Neth.), 510(2), pp. 439–448, 2016.

[GOLDSCHMIDT 26] V. M. Goldschmidt: *Geochemische Verteilungsgesetze VI-VIII,* Oslo, 1926.

[GOMES 08] F. Gomes, J. J. Barbosa, and C. S. Ribeiro: *Induction melting of γ-TiAl in CaO crucibles,* Intermetallics, 16(11-12), pp. 1292–1297, 2008.

[GONENLI 99] I. E. Gonenli and A. C. Tas: *Chemical Synthesis of Pure and Gd-doped $CaZrO_3$ Powders,* J. Eur. Ceram. Soc., 19(13-14), pp. 2563–2567, 1999.

[GRABENHORST 19] J. Grabenhorst, B. Luchini, J. Fruhstorfer, C. Voigt, J. Hubálková, J. Chen, N. Li, L. Yawei, and C. G. Aneziris: *Influence of the measurement method and sample dimensions on the Young's modulus of open porous alumina foam structures,* Ceram. Int., 45(5), pp. 5987–5995, 2019.

[HAN 08] J. Han, Z. Wen, J. Zhang, Z. Gu, and X. Xu: *Fabrication of dense $CaZr_{0.90}In_{0.10}O_{3-\delta}$ ceramics from the fine powders prepared by an optimized solid-state reaction method,* Solid State Ionics, 179(21-26), pp. 1108–1111, 2008.

[HARTEN 07] U. Harten: *Physik - Einführung für Ingenieure und Naturwissenschaftler*, Springer-Verlag Berlin Heidelberg, Berlin, Heidelberg, 2007.

References

[HASSELMAN 69] D. P. H. Hasselman: *Unified Theory of Thermal Shock Fracture Initiation and Crack Propagation in Brittle Ceramics,* J. Am. Ceram. Soc., 52(11), pp. 600–604, 1969.

[HELLMANN 82] J. R. Hellmann and V. S. Stubican: *The existence and stability of $Ca_6Zr_{19}O_{44}$ compound in the system $ZrO_2 \cdot CaO$,* Mater. Res. Bull., 17(4), pp. 459–465, 1982.

[HERNANDEZ-SANCHEZ 09] B. A. Hernandez-Sanchez and B. A. Tuttle: *Oxalate co-precipitation synthesis of calcium zirconate and calcium titanate powders,* Sandia National Laboratories, Albuquerque, 2009.

[HUANG 16] Z. Huang, F. Li, C. Jiao, J. Liu, J. Huang, L. Lu, H. Zhang, and S. Zhang: *Molten salt synthesis of $La_2Zr_2O_7$ ultrafine powders,* Ceram. Int., 42(5), pp. 6221–6227, 2016.

[HUGER 02] M. Huger, D. Fargeot, and M. C. Gault: *High-temperature measurement of ultrasonic wave velocity in refractory materials,* High Temp. - High Pressures, 34(2), pp. 193–201, 2002.

[HWANG 05] S. C. Hwang and G. M. Choi: *The effect of cation nonstoichiometry on the electrical conductivity of $CaZrO_3$*, J. Eur. Ceram. Soc., 25(12), pp. 2609–2612, 2005.

[HWANG 08] S. C. Hwang and G. M. Choi: *The mixed ionic and electronic conductivity of $CaZrO_3$ with cation nonstoichiometry and oxygen partial pressure,* Solid State Ionics, 179(21-26), pp. 1042–1045, 2008.

[IANOŞ 10] R. Ianoş and P. Barvinschi: *Solution combustion synthesis of calcium zirconate, $CaZrO_3$, powders,* J. Solid State Chem., 183(3), pp. 491–496, 2010.

[JACOB 94] K. T. Jacob and Y. Waseda: *Gibbs energy of formation of orthorhombic $CaZrO_3$*, Thermochim. Acta, 239, pp. 233–241, 1994.

[JACOBSON 89] N. S. Jacobson: *Thermodynamic properties of some metal oxide-zirconia systems,* National Aeronautics and Space Administration, 1989.

[JAHN 18] C. Jahn, S. Schafföner, C. Ode, H. Jansen, and C. G. Aneziris: *Investigation of calcium zirconate formation by sintering zirconium dioxide with calcium hydroxide,* Ceram. Int., 44(10), pp. 11274–11281, 2018.

[JANKE 82] D. Janke: *Oxygen probes based on calcia-doped hafnia or calcium zirconate for use in metallic melts,* Metall. Trans. B, 13(2), pp. 227–235, 1982.

[JANKOVSKÝ 18] O. Jankovský, E. Storti, K. Moritz, B. Luchini, A. Jiříčková, and C. G. Aneziris: *Nano-functionalization of carbon-bonded alumina using graphene oxide and MWCNTs,* J. Eur. Ceram. Soc., 38(14), pp. 4732–4738, 2018.

[JIA 04] Q. Jia, Y. Y. Cui, and R. Yang: *Intensified interfacial reactions between gamma titanium aluminide and CaO stabilised ZrO_2*, Int. J. Cast Met. Res., 17(1), pp. 23–28, 2004.

[JONAS 98] S. Jonas, F. Nadachowski, and D. Szwagierczak: *A new non-silicate refractory of low thermal expansion,* Ceram. Int., 24(3), pp. 211–216, 1998.

[KALINKIN 12] A. M. Kalinkin, K. V. Balyakin, and E. V. Kalinkina: *Kinetic and thermodynamic patterns of $CaZrO_3$ formation at sintering zirconium dioxide with calcium carbonate,* Russ. J. Gen. Chem., 82(11), pp. 1753–1760, 2012.

[KALINKIN 13] A. M. Kalinkin, K. V. Balyakin, and E. V. Kalinkina: *Kinetics of two-stage mechanochemical synthesis of calcium zirconate in $CaCO_3$-ZrO_2 system,* Russ. J. Gen. Chem., 83(8), pp. 1482–1492, 2013.

[KALINKIN 14] A. M. Kalinkin, V. N. Nevedomskii, E. V. Kalinkina, and K. V. Balyakin: *Milling assisted synthesis of calcium zirconate $CaZrO_3$*, Solid State Sci., 34, pp. 91–96, 2014.

[KAMYSHNYKOVA 18] K. Kamyshnykova and J. Lapin: *Vacuum induction melting and solidification of TiAl-based alloy in graphite crucibles,* Vacuum, 154, pp. 218–226, 2018.

[KAWANO 91] F. Kawano, I. Yamoto, J. Nomura, J. Yoshitomi, A. Ikesue, and H. Shikano: *CaO Clinker with Improved Anti-Hydration Property,* Taikabutsu Overseas, 11(3), pp. 29–36, 1991.

[KELER 61] E. K. Keler and A. B. Andreyeva: *Decomposition of calcium zirconate when heated in presence of certain oxides,* Refractories, 2(11-12), pp. 464–469, 1961.

[KENNEDY 78a] C. R. Kennedy and R. B. Poeppel: *Corrosion resistance of refractories exposed to molten acidic coal-ash slags,* Interceram, 27(3), pp. 221–226, 1978.

[KENNEDY 78b] C. R. Kennedy, R. B. Swaroop, D. J. Jones, R. J. Fousek, R. B. Poeppel, and D. Stahl: *Evaluation of ceramic refractories for slagging gasifiers: summary of progress to date,* Argonne National Laboratory, Argonne, Illinois, 1978.

[KIM 01a] S. K. Kim, T. Hong, and Y.-J. Kim: *Evaluation of thermal stability of mold materials for magnesium investment casting,* Mater. Trans., 42(3), pp. 539–542, 2001.

[KIM 01b] S. K. Kim, T. K. Kim, M. G. Kim, T. W. Hong, and Y. J. Kim: *Lightweight Alloys for Aerospace Application*, Ed. by K. Jata, E. W. Lee, W. Frazier, and N. J. Kim, vol. 19, pp. 251–260, John Wiley & Sons, Inc, Hoboken, NJ, USA, 2001.

[KINGERY 55] W. D. Kingery: *Factors Affecting Thermal Stress Resistance of Ceramic Materials,* J. Am. Ceram. Soc., 38(1), pp. 3–15, 1955.

[KINGERY 76] W. D. Kingery, H. K. Bowen, and D. R. Uhlmann: *Introduction to ceramics*, John Wiley, New York, 1976.

[KLOTZ 19] U. E. Klotz, C. Legner, F. Bulling, L. Freitag, C. Faßauer, S. Schafföner, and C. G. Aneziris: *Investment casting of titanium alloys with calcium zirconate moulds and crucibles,* Int. J. Adv. Manuf. Technol., 103(1-4), pp. 343–353, 2019.

[KOZUKA 93] H. Kozuka, Y. Kajita, Y. Tuchiya, T. Honda, and S. Ohta: *Proceedings of Unified International Technical Conference on Refractories*, pp. 1027–1037, Sao Paulo, 1993.

[KOZUKA 95] H. Kozuka, Y. Kajita, K. Tokunaga, K. Sakakibara, and S. Ohta: *UNITECR 95 Proceedings*, Ed. by The Technical Association of Refractories, Japan, pp. 256–263, Kyoto, 1995.

[KRAUSE 00] O. Krause: *Ullmann's Encyclopedia of Industrial Chemistry*, vol. 79, pp. 1–59, Wiley-VCH Verlag GmbH & Co. KGaA, Weinheim, Germany, 2000.

[KRISHNAN 07] V. Krishnan and J. W. Fergus: *Effects of dispersant addition on the synthesis of indium-doped calcium zirconate by co-precipitation techniques,* J. Mater. Sci., 42(15), pp. 6117–6122, 2007.

[KROLL 40] W. Kroll: *Method for manufacturing titanium and alloys thereof* (1940)(US2205854A).

[KRZACK 08] S. Krzack: *Die Veredlung und Umwandlung von Kohle - Technologien und Projekte 1970 bis 2000 in Deutschland*, Ed. by J. Schmalfeld and P. Arendt, pp. 299–304, DGMK, Hamburg, 2008.

[KUTTY 90] T. R. N. Kutty, R. Vivekanandan, and S. Philip: *Precipitation of ultrafine powders of zirconia polymorphs and their conversion to $MZrO_3$ (M = Ba, Sr, Ca) by the hydrothermal method,* J. Mater. Sci., 25(8), pp. 3649–3658, 1990.

[KWON 17] S. Y. Kwon and I.-H. Jung: *Critical evaluation and thermodynamic optimization of the CaO-ZrO_2 and SiO_2-ZrO_2 systems,* J. Eur. Ceram. Soc., 37(3), pp. 1105–1116, 2017.

[LANG 18] J.-F. Lang, J.-G. You, X.-F. Zhang, X.-D. Luo, and S.-Y. Zheng: *Effect of MgO on thermal shock resistance of $CaZrO_3$ ceramic,* Ceram. Int., 44(18), pp. 22176–22180, 2018.

[LAPIN 11] J. Lapin, Z. Gabalcová, and T. Pelachová: *Effect of Y_2O_3 crucible on contamination of directionally solidified intermetallic Ti–46Al–8Nb alloy,* Intermetallics, 19(3), pp. 396–403, 2011.

[LEE 99] W. E. Lee and S. Zhang: *Melt corrosion of oxide and oxide–carbon refractories,* Int. Mater. Rev., 44(3), pp. 77–104, 1999.

[LEE 04] W. E. Lee and S. Zhang: *Direct and indirect slag corrosion of oxide and oxide-c refractories,* The South African Institute of Mining and Metallurgy, 2004.

[LI 07] Z. Li, W. E. Lee, and S. Zhang: *Low-Temperature Synthesis of $CaZrO_3$ Powder from Molten Salts,* J. Am. Ceram. Soc., 90(2), pp. 364–368, 2007.

[LI 08a] Z. Li, S. Zhang, and W. E. Lee: *Improving the hydration resistance of lime-based refractory materials,* Int. Mater. Rev., 53(1), pp. 1–20, 2008.

[LI 08b] B.-S. Li, A.-H. Liu, H. Nan, W.-S. Bi, J.-J. Guo, and H.-Z. Fu: *Wettability of TiAl alloy melt on ceramic moulds in electromagnetic field,* Trans. Nonferrous Met. Soc. China, 18(3), pp. 518–522, 2008.

[LI 10] C. H. Li, Y. H. Gao, X. G. Lu, W. Z. Ding, Z. M. Ren, and K. Deng: *Interaction between the Ceramic $CaZrO_3$ and the Melt of Titanium Alloys,* Adv. Sci. Technol., 70, pp. 136–140, 2010.

[LI 13] M. Li, P. Gehre, and C. G. Aneziris: *Investigation of calcium zirconate ceramic synthesized by slip casting and calcination,* J. Eur. Ceram. Soc., 33(10), pp. 2007–2012, 2013.

[LI 15] C. H. Li, J. He, C. Wei, H. B. Wang, and X. G. Lu: *Solidification and Interface Reaction of Titanium Alloys in the $BaZrO_3$ Shell-Mould,* Mater. Sci. Forum, 828-829, pp. 106–111, 2015.

[LI 17] C. Li, M.-Y. Li, H. Zhang, W. Ali, Z. Qin, H.-B. Wang, and X. Lu: *Fabrication of Y_2O_3 doped $BaZrO_3$ coating on Al_2O_3 applied to solidification of titanium alloy,* Surf. Coat. Technol., 320, pp. 146–152, 2017.

[LI 18] M. Li: *Development of calcium zirconate castables based on slip casted raw material for gasifier,* TU Bergakademie Freiberg, 2018.

[LIMSAY 10] R. H. Limsay, R. A. Tayade, C. B. Talwatkar, S. P. Yawale, S. S. Yawale, and R. S. Bhavsar: *Solution Combustion Synthesis of $CaZrO_3$ using mixed Fuel,* Int. J. Mod. Phys. B, 24(31), pp. 6107–6113, 2010.

[LIU 13] L. J. Liu, G. Y. Chen, Z. Zhang, X. G. Lu, and C. H. Li: *Interface reaction between refractory $BaZrO_3$ and TiM (M= Fe, Ni) Melt,* Hot Work. Technol., 42, pp. 49–54, 2013.

[LIU 14] B. Liu, X. Lin, L. Zhu, X. Wang, and D. Xu: *Fabrication of calcium zirconate fibers by the sol–gel method,* Ceram. Int., 40(8), pp. 12525–12531, 2014.

[LU 11] M. Lu, C. Lin, H. Su, and S. Wei: *Effect of $CaZrO_3$ content on the interfacial phenomenon between titanium and zirconia at 1400°C,* Mater. Sci. Technol. Conf. Exhib., 1, 2011.

References

[LUI 08] H. Lui, B. Shen, M. Zhu, X. Zhou, and X. Mao: *Reaction between Ti and boron nitride based investment shell molds used for casting titanium alloys,* Rare Met., 27(6), pp. 617–622, 2008.

[LÜTJERING 07] G. Lütjering and J. C. Williams: *Titanium*, Springer-Verlag, Berlin, Heidelberg, 2007.

[LUZ 17] A. P. da Luz, D. T. Gomes, and V. C. Pandolfelli: *Maximum working temperature of refractory castables: do we really know how to evaluate it?,* Ceram. Int., 43(12), pp. 9077–9083, 2017.

[MACEDO 18] W. D. Macedo, A. E. Souza, G. T.A. Santos, S. R. Teixeira, and E. Longo: *Microwave-assisted hydrothermal synthesis followed by heat treatment,* Ceram. Int., 44(1), pp. 953–958, 2018.

[MANNING 69] W. R. Manning, O. Hunter, and B. R. Powell: *Elastic Properties of Polycrystalline Yttrium Oxide, Dysprosium Oxide, Holmium Oxide, and Erbium Oxide: Room Temperature Measurements,* J. Am. Ceram. Soc., 52(8), pp. 436–442, 1969.

[MATWEB 19] MatWeb: *Zirconium Oxide* : http://www.matweb.com/search/datasheet.aspx?MatGUID=0742ddaddf80467fb6532e025c694e89&ckck=1. Accessed 17 November 2019.

[MCCAULEY 95] R. A. McCauley: *Corrosion of ceramics*, Dekker, New York, 1995.

[MITCHELL 92] A. Mitchell: *Melting and Refining of Superalloys and Titanium Alloys,* ISIJ Int., 32(5), pp. 557–562, 1992.

[MOURE 15] C. Moure and O. Peña: *Recent advances in perovskites,* Prog. Solid State Chem., 43(4), pp. 123–148, 2015.

[NADACHOWSKI 76] F. Nadachowski: *Refractories based on lime: Development and perspectives,* Ceramurgia Int., 2(2), pp. 55–61, 1976.

[NADLER 55] M. R. Nadler and E. S. Fitzsimmons: *Preparation and Properties of Calcium Zirconate,* J. Am. Ceram. Soc., 38(6), pp. 214–217, 1955.

[NAYAN 07] N. Nayan, Govind, C. N. Saikrishna, K. V. Ramaiah, S. K. Bhaumik, K. S. Nair, and M. C. Mittal: *Vacuum induction melting of NiTi shape memory alloys in graphite crucible,* Mater. Sci. Eng., A, 465(1-2), pp. 44–48, 2007.

[NGUYEN 16] K. Nguyen and M. Wocher: *Billig-Konkurrenz aus China: Stahl-Arbeiter schlagen in Brüssel Alarm*: http://www.handelsblatt.com/unternehmen/industrie/billig-konkurrenz-aus-china-stahl-arbeiter-schlagen-in-bruessel-alarm/12965252-all.html. Accessed 21 March 2016.

[NISHIKAWA 84] A. Nishikawa: *Technology of Monolithic Refractories*, Toppan Printing Company, Ltd., Tokyo, 1984.

[OBREGÓN 11] Á. Obregón, J. L. Rodríguez-Galicia, J. López-Cuevas, P. Pena, and C. Baudín: *MgO–$CaZrO_3$-based refractories for cement kilns,* J. Eur. Ceram. Soc., 31(1-2), pp. 61–74, 2011.

[OGIBAYASHI 92] S. Ogibayashi: *Mechanism and Countermeasure of Alumina Buildup on Submerged Nozzle in Continous Casting,* Taikabutsu Overseas, 15(1), pp. 3–14, 1992.

[OGURI 93] K. Oguri, M. Ando, T. Muroi, and T. Aoki: *Proceedings of Unified International Technical Conference on Refractories*, pp. 1119–1127, Sao Paulo, 1993.

[OHNO 02] F. Ohno, T. Muroi, and K. Oguri: *Development of Anti-Alumina Build-up Materials for Inner Surface of Continuous Caster Submerged Entry Nozzle,* Taikabutsu Overseas, 22(1), pp. 63–66, 2002.

[OKUMURA 91] H. Okumura, N. Toshio, T. Takasu, and T. Aoki: *UNITECR 1991 – Proceedings of Unified International Technical*, pp. 364–367, Stahleisen, Düsseldorf, 1991.

[PABST 07] W. Pabst, E. Gregorová, and G. Tichá: *Effective properties of suspensions, composites and porous materials,* J. Eur. Ceram. Soc., 27(2-3), pp. 479–482, 2007.

[PATIL 08] K. C. Patil, M. S. Hegde, T. Rattan, and S. T. Aruna: *Chemistry of Nanocrystalline Oxide Materials*, WORLD SCIENTIFIC, 2008.

[PISHCH 98] I. V. Pishch and E. V. Radion: *Synthesis of pigments based on perovskite,* Glass Ceram., 55(9-10), pp. 290–291, 1998.

[PIZZINI 72] S. Pizzini and R. Morlotti: *E.m.f. measurements with solid electrolyte galvanic cells on the calcium oxide + zirconia system. Determination of the phase relationships,* J. Chem. Soc., Faraday Trans. 1, 68(0), p. 1601, 1972.

[POIRIER 08] J. Poirier, F. Qafssaoui, J. P. Ildefonse, and M. L. Bouchetou: *Analysis and interpretation of refractory microstructures in studies of corrosion mechanisms by liquid oxides,* J. Eur. Ceram. Soc., 28(8), pp. 1557–1568, 2008.

[POLE 43] G. R. Pole and A. W. Beinlich, Jr.: *New refractory compositions resistant to molten rock phosphate,* J. Am. Ceram. Soc., 26(1), pp. 21–37, 1943.

[POLE 46] G. R. Pole, A. W. Beinlich, Jr., and N. Gilbert: *Physical properties of some high-temperature refractory compositions,* J. Am. Ceram. Soc., 29(8), pp. 208–228, 1946.

[PORION 04] P. Porion, N. Sommier, A.-M. Faugère, and P. Evesque: *Dynamics of size segregation and mixing of granular materials in a 3D-blender by NMR imaging investigation,* Powder Technol., 141(1-2), pp. 55–68, 2004.

[RENTSCH 61] W. Rentsch and G. Krompholz: *Zur Bestimmung elastischer Konstanten durch Schallgeschwindigkeitsmessungen,* Bergakademie, 13(Sonderdruck aus 7-8), pp. 492–504, 1961.

[RENTSCH 63] W. Rentsch and G. Krompholz: *Die Bestimmung der Poissonschen Zahl durch Schallgeschwindigkeitsmessungen,* Wiss. Z. Hochsch. Bauw., Leipzig, Sonderdruck, pp. 177–181, 1963.

[RICE 93] R. W. Rice: *Evaluating Porosity Parameters for Porosity – Property Relations,* J. Am. Ceram. Soc., 76(7), pp. 1801–1808, 1993.

[RIGAUD 11] M. Rigaud: *Electrochemical Society series*: *Uhlig's corrosion handbook*, Ed. by H. H. Uhlig and R. W. Revie, pp. 387–398, Wiley, Hoboken, N.J, 2011.

[RIMAN 02] R. Riman, W. L. Suchanek, and M. M. Lencka: *Cristallisation hydrothermale de ceramiques,* Ann. Chim. Sci. Mat., 27(6), pp. 15–36, 2002.

[ROBERTS 00] A. P. Roberts and E. J. Garboczi: *Elastic Properties of Model Porous Ceramics,* J. Am. Ceram. Soc., 83(12), pp. 3041–3048, 2000.

[RODRÍGUEZ 12] E. Rodríguez, G.-A. Castillo, J. Contreras, R. Puente-Ornelas, J. A. Aguilar-Martínez, L. García, and C. Gómez: *Hercynite and magnesium aluminate spinels acting as a ceramic bonding in an electrofused MgO–$CaZrO_3$ refractory brick for the cement industry,* Ceram. Int., 38(8), pp. 6769–6775, 2012.

[RODRÍGUEZ 04] J. L. Rodríguez, C. Baudín, and P. Pena: *Relationships between phase constitution and mechanical behaviour in MgO–$CaZrO_3$–calcium silicate materials,* J. Eur. Ceram. Soc., 24(4), pp. 669–679, 2004.

[RODRÍGUEZ-GALICIA 07] J. L. Rodríguez-Galicia, A. H. de Aza, J. C. Rendón-Angeles, and P. Pena: *The Mechanism of corrosion of MgO-$CaZrO_3$–calcium silicate materials by cement clinker,* J. Eur. Ceram. Soc., 27(1), pp. 79–89, 2007.

[RÓG 02] G. Róg, M. Dudek, A. Kozłowska-Róg, and M. Bućko: *Calcium zirconate: preparation, properties and application to the solid oxide galvanic cells,* Electrochim. Acta, 47(28), pp. 4523–4529, 2002.

[ROGOJAN 11] R. Rogojan, E. Andronescu, I. Iliescu, R. Truşcă, and B. S. Vasile: *Synthesis and characterization of calcia stabilized zirconia nano-powder, obtained by sol - gel method,* Rom. J. Mater., 43(3), pp. 240–247, 2011.

[ROSSI 70] L. R. Rossi and W. G. Lawrence: *Elastic Properties of Oxide Solid Solutions: The System Al_2O_3-Cr_2O_3*, J. Am. Ceram. Soc., 53(11), pp. 604–608, 1970.

[ROTERING 12] J. Rotering, P. von Hochberg, N. Naujok, and T. Schmidt-Brockhoff: *Die Stahlindustrie in Deutschland „Rückgrat des Industriestandorts Deutschland“,* Booz & Company, 2012.

[ROUTSCHKA 97] G. Routschka: *Taschenbuch Feuerfeste Werkstoffe*, Vulkan-Verl., Essen, 1997.

[RUFF 13] O. Ruff: *Arbeiten im Gebiet hoher Temperaturen I. Über das Schmelzen und Verdampfen unserer feuerbeständigsten Oxyde im elektrischen Vakuumofen,* Z. Anorg. Allg. Chem., 82(1), pp. 373–400, 1913.

[RUFF 14a] O. Ruff, H. Seiferheld, and O. Bruschke: *Arbeiten im Gebiet hoher Temperaturen II. Über die Herstellung feuerfester Gegenstände aus Zirkondioxyd,* Z. Anorg. Allg. Chem., 86(1), pp. 389–400, 1914.

[RUFF 14b] O. Ruff and G. Lauschke: *Arbeiten im Gebiet hoher Temperaturen IV,* Z. Anorg. Allg. Chem., 87(1), pp. 198–208, 1914.

[RUFF 16] O. Ruff and G. Lauschke: *Arbeiten im Gebiet hoher Temperaturen IX. Über die Herstellung von Zirkongegenständen,* Z. Anorg. Allg. Chem., 97(1), pp. 73–112, 1916.

[RUFF 29a] O. Ruff, F. Ebert, and E. Stephan: *Beiträge zur Keramik hochfeuerfester Stoffe II. Das System ZrO_2-CaO,* Z. Anorg. Allg. Chem., 180(1), pp. 215–224, 1929.

[RUFF 29b] O. Ruff and F. Ebert: *Beiträge zur Keramik hochfeuerfester Stoffe l: Die Formen des Zirkondioxyds,* Z. Anorg. Allg. Chem., 180(1), pp. 19–41, 1929.

[RUFF 32] O. Ruff, F. Ebert, and W. Loerpabel: *Beitrge zur Keramik hochfeuerfester Stoffe. V. Die ternren Systeme: ZrO_2-ThO_2-CaO, ZrO_2-ThO_2-MgO, ZrO_2-BeO-CaO, ZrO_2-BeO-CeO_2,* Z. Anorg. Allg. Chem., 207(3), pp. 308–312, 1932.

[SAHU 97] J. K. Sahu, S. K. Chaudhuri, and B. Prasad: *Proceedings of Unified International Technical Conference on Refractories*, Ed. by M. A. Stett, pp. 1435–1440, 1997.

[SALMANG 07] H. Salmang and H. Scholze: *Keramik*, Springer Verlag, Berlin, 2007.

[SAWADA 94] Y. Sawada and Y. Ito: *Thermal decomposition of calcium hydroxide deposited on the substrate,* Thermochim. Acta, 232(1), pp. 47–54, 1994.

[SAWANO 98] K. Sawano: *Refractories handbook*, Ed. by H. Shikano, pp. 341–422, Technical Association of Refractories, Japan, Tokyo, 1998.

[SCHAFFÖNER 13] S. Schafföner, C. G. Aneziris, H. Berek, J. Hubálková, and A. Priese: *Fused calcium zirconate for refractory applications,* J. Eur. Ceram. Soc., 33(15-16), pp. 3411–3418, 2013.

[SCHAFFÖNER 15a] S. Schafföner: *Calcium zirconate as a refractory material for titanium and titanium alloy melts,* TU Bergakademie Freiberg, 2015.

[SCHAFFÖNER 15b] S. Schafföner, C. G. Aneziris, H. Berek, J. Hubálková, B. Rotmann, and B. Friedrich: *Corrosion behavior of calcium zirconate refractories in contact with titanium aluminide melts,* J. Eur. Ceram. Soc., 35(3), pp. 1097–1106, 2015.

[SCHAFFÖNER 15c] S. Schafföner, C. G. Aneziris, H. Berek, B. Rotmann, and B. Friedrich: *Investigating the corrosion resistance of calcium zirconate in contact with titanium alloy melts,* J. Eur. Ceram. Soc., 35(1), pp. 259–266, 2015.

[SCHAFFÖNER 17] S. Schafföner, J. Fruhstorfer, C. Faßauer, L. Freitag, C. Jahn, and C. G. Aneziris: *Influence of in situ phase formation on properties of calcium zirconate refractories,* J. Eur. Ceram. Soc., 37(1), pp. 305–313, 2017.

[SCHAFFÖNER 18] S. Schafföner, T. Qin, J. Fruhstorfer, C. Jahn, G. Schmidt, H. Jansen, and C. G. Aneziris: *Refractory castables for titanium metallurgy based on calcium zirconate,* Mater. Des., 148, pp. 78–86, 2018.

[SCHIPPEREIT 61] G. H. Schippereit, A. F. Leatherman, and D. Evers: *Cold-Crucible Induction Melting of Reactive Metals,* JOM, 13(2), pp. 140–143, 1961.

[SCHMALFELD 08] J. Schmalfeld and P. Arendt: *Die Veredlung und Umwandlung von Kohle - Technologien und Projekte 1970 bis 2000 in Deutschland*, J. Schmalfeld and P. Arendt, DGMK, Hamburg, 2008.

[SCHULLE 90] W. Schulle: *Feuerfeste Werkstoffe - Feuerfestkeramik, Eigenschaften, prüftechnische Beurteilung, Werkstofftypen ; mit 143 Tabellen*, Dt. Verl. für Grundstoffindustrie, Leipzig, 1990.

[SCHWARTZ 52] B. Schwartz: *Thermal Stress Failure of Pure Refractory Oxides,* J. Am. Ceram. Soc., 35(12), pp. 325–333, 1952.

[SERENA 04] S. Serena, M. A. Sainz, and A. Caballero: *Corrosion behavior of $MgO/CaZrO_3$ refractory matrix by clinker,* J. Eur. Ceram. Soc., 24(8), pp. 2399–2406, 2004.

References

[SERENA 05] S. Serena, M. A. Sainz, S. de Aza, and A. Caballero: *Thermodynamic assessment of the system ZrO_2–CaO–MgO using new experimental results,* J. Eur. Ceram. Soc., 25(5), pp. 681–693, 2005.

[SERENA 09] S. Serena, M. A. Sainz, and A. Caballero: *The system Clinker–MgO–$CaZrO_3$ and its application to the corrosion behavior of $CaZrO_3$/MgO refractory matrix by clinker,* J. Eur. Ceram. Soc., 29(11), pp. 2199–2209, 2009.

[ŚNIEŻEK 15] E. Śnieżek, J. Szczerba, and I. Jastrzębska: *Preparation of porous ceramic materials based on $CaZrO_3$*, Mater. Tehnol., 49(4), pp. 573–577, 2015.

[SOGA 68] N. Soga: *Elastic properties of CaO under pressure and temperature,* J. Geophys. Res., 73(16), pp. 5385–5390, 1968.

[SRINIVASAN 91] R. Srinivasan, R. J. de Angelis, G. Ice, and B. H. Davis: *Identification of tetragonal and cubic structures of zirconia using synchrotron x-radiation source,* J. Mater. Res., 6(6), pp. 1287–1292, 1991.

[SRIRAMA MURTI 92] P. Srirama Murti and M. V. Krishnaiah: *Investigation of the thermal conductivity of calcium cerate and calcium zirconate,* Mater. Chem. Phys., 31(4), pp. 347–350, 1992.

[STOCH 12] P. Stoch, J. Szczerba, J. Lis, D. Madej, and Z. Pędzich: *Crystal structure and ab initio calculations of $CaZrO_3$*, J. Eur. Ceram. Soc., 32(3), pp. 665–670, 2012.

[STØLEN 04] S. Stølen, T. Grande, and N. L. Allan: *Chemical thermodynamics of materials - Macroscopic and microscopic aspects*, Wiley, Hoboken, NJ, 2004.

[SZCZERBA 10] J. Szczerba: *Chemical corrosion of basic refractories by cement kiln materials,* Ceram. Int., 36(6), pp. 1877–1885, 2010.

[SZCZERBA 17] J. Szczerba, E. Śnieżek, and V. Antonovič: *Evolution of Refractory Materials for Rotary Cement Kiln Sintering Zone,* Refract. Ind. Ceram., 58(4), pp. 426–433, 2017.

[TSUJINO 94] R. Tsujino, A. Tanaka, A. Imamura, D. Takahashi, and S. Mizoguchi: *Mechanism of Deposition of Inclusion and Metal in ZrO_2-CaO-C Immersion Nozzle of Continuous Casting,* ISIJ Int., 34(11), pp. 853–858, 1994.

References

[TUTTLE 05] R. B. Tuttle, J. D. Smith, and K. D. Peaslee: *Interaction of alumina inclusions in steel with calcium-containing materials,* Metall. Mater. Trans. B, 36(6), pp. 885–892, 2005.

[TUTTLE 07] R. B. Tuttle, J. D. Smith, and K. D. Peaslee: *Casting Simulation of Calcium Titanate and Calcium Zirconate Nozzles for Continuous Casting of Aluminum-Killed Steels,* Metall. Mater. Trans. B, 38(1), pp. 101–108, 2007.

[VARMA 16] A. Varma, A. S. Mukasyan, A. S. Rogachev, and K. V. Manukyan: *Solution Combustion Synthesis of Nanoscale Materials,* Chem. Rev., 116(23), pp. 14493–14586, 2016.

[WACHTMAN 59] J. B. Wachtman and D. G. Lam: *Young's Modulus of Various Refractory Materials as a Function of Temperature,* J. Am. Ceram. Soc., 42(5), pp. 254–260, 1959.

[WAKEFORD 16] S. Wakeford: *Can the steel industry pass through carbon costs without losing market shares?,* Paris, 2016.

[WANG 88] C. Wang, X. Xu, H. Yu, Y. Wen, and K. Zhao: *A study of the solid electrolyte Y_2O_3-doped $CaZrO_3$*, Solid State Ionics, 28-30, pp. 542–545, 1988.

[WARTENBERG 32] H. von Wartenberg and E. Prophet: *Schmelzdiagramme höchstfeuerfester Oxyde. V. Systeme mit MgO,* Z. Anorg. Allg. Chem., 208(4), pp. 369–379, 1932.

[WARTENBERG 37] H. von Wartenberg, H. J. Reusch, and E. Saran: *Schmelzpunktsdiagramme höchstfeuerfester Oxyde. VII. Systeme mit CaO und BeO,* Z. Anorg. Allg. Chem., 230(3), pp. 257–276, 1937.

[WEBER 57] B. C. Weber, W. M. Thompson, H. O. Bielstein, and M. A. Schwartz: *Ceramic Crucible for Melting Titanium,* J. Am. Ceram. Soc., 40(11), pp. 363–373, 1957.

[WENZEL 36] R. N. Wenzel: *Resistance of solid surfaces to wetting by water,* Ind. Eng. Chem., 28(8), pp. 988–994, 1936.

[WERNER 14] J. Werner, C. G. Aneziris, and S. Schafföner: *Influence of porosity on Young's modulus of carbon-bonded alumina from room temperature up to 1450°C,* Ceram. Int., 40(9), pp. 14439–14445, 2014.

[WERNER 15] J. Werner: *The influence of composition, processing and temperature on the Young's modulus of elasticity of carbon-bonded refractories,* TU Bergakademie Freiberg, 2015.

[WERNER 16a] J. Werner, J. Fruhstorfer, A. Mertke, C. Ode, and C. G. Aneziris: *The influence of nano scaled additions on the Young's modulus of carbon-bonded alumina at temperatures up to 1450 °C,* Ceram. Int., 42(14), pp. 15718–15724, 2016.

[WERNER 16b] J. Werner and C. G. Aneziris: *The influence of pyrolysis temperature on Young's modulus of carbon-bonded alumina at temperatures up to 1450 °C,* Ceram. Int., 42(2), pp. 3460–3464, 2016.

[WONG 95] L. L. Wong and R. C. Bradt: *Lime Refractories with Limestone and Synthetic Calcium Hydroxide Additions,* J. Am. Ceram. Soc., 78(6), pp. 1611–1616, 1995.

[XU 07] F.-Q. Xu, F. Xiong, Q.-F. Zhang, X.-A. Zhang, and G.-B. Yang: *On Preparation of $CaZrO_3$ Powder by Hydrothermal Synthesis Method,* Wuji Cailiao Xuebao, 22(1), pp. 163–166, 2007.

[YAJIMA 95] T. Yajima, K. Koide, H. Takai, N. Fukatsu, and H. Iwahara: *Application of hydrogen sensor using proton conductive ceramics as a solid electrolyte to aluminum casting industries,* Solid State Ionics, 79, pp. 333–337, 1995.

[YANG 10] H. Yang, Y. Ohishi, K. Kurosaki, H. Muta, and S. Yamanaka: *Thermomechanical properties of calcium series perovskite-type oxides,* J. Alloys Compd., 504(1), pp. 201–204, 2010.

[YANG 12] B. Yang, K.-L. Zhu, X. Lu, Z.-L. Li, Z. Wu, G. Wu, and C. Li: *Preparation of TiFe based alloy melted by $CaZrO_3$ crucible and its hydrogen storage properties,* Guocheng Gongcheng Xuebao/ J. Process Eng., 12(5), pp. 849–856, 2012.

[YE 07] G. Ye and T. Troczynski: *Mechanochemical Activation-Assisted Low-Temperature Synthesis of $CaZrO_3$*, J. Am. Ceram. Soc., 90(1), pp. 287–290, 2007.

[YU 04] T. Yu, C. H. Chen, X. F. Chen, W. Zhu, and R. G. Krishnan: *Fabrication and characterization of perovskite $CaZrO_3$ oxide thin films,* Ceram. Int., 30(7), pp. 1279–1282, 2004.

[YUAN 15] C. Yuan, X. Cheng, and P. A. Withey: *Investigation into the use of $CaZrO_3$ as a facecoat material in the investment casting of TiAl alloys,* Mater. Chem. Phys., 155, pp. 205–210, 2015.

References

[ZHANG 05] Z. Zhang, J. Frenzel, K. Neuking, and G. Eggeler: *On the reaction between NiTi melts and crucible graphite during vacuum induction melting of NiTi shape memory alloys,* Acta Mater., 53(14), pp. 3971–3985, 2005.

[ZHANG 13a] H. Zhang, X. Tang, C. Zhou, and S. Zhang: *Comparison of directional solidification of γ-TiAl alloys in conventional Al_2O_3 and novel Y_2O_3-coated Al_2O_3 crucibles,* J. Eur. Ceram. Soc., 33(5), pp. 925–934, 2013.

[ZHANG 13b] Z. Zhang, K. Zhu, L. Liu, X. Lu, G. Wu, and G. Chen: *Preparation of $BaZrO_3$ Crucible and Its Interfacial Reaction with Molten Titanium Alloys,* Guisuanyan Xuebao, 41, 2013.

[ZHANG 13c] Z. Zhang, F. Y. Xing, M. Zhu, K. L. Zhu, X. G. Lu, G. X. Wu, and C. H. Li: *Vacuum Induction Melting of TiNi Alloys Using $BaZrO_3$ Crucibles,* Mater. Sci. Forum, 765, pp. 316–320, 2013.

[ZHU 14] W. Zhu, J. He, E. Wei, H. Wang, and C. Li: *Preparation of $BaZrO_3$-based mould shell for titanium alloy,* Tezhong Zhuzao Ji Youse Hejin, 34, 2014.

[ZHU 18] L.-L. Zhu, Y.-J. Park, L. Gan, H.-N. Kim, J.-W. Ko, and H.-D. Kim: *Fabrication of transparent Y_2O_3 ceramics with record-high thermal shock resistance,* J. Eur. Ceram. Soc., 38(11), pp. 4050–4056, 2018.

Appendix

A. 1 Stoichiometric calculations

Raw material	**M [g*mol^{-1}]**
ZrO_2	123.22
CaO	56.08
$Ca(OH)_2$	74.10
$CaCO_3$	100.09

Mole ratio ZrO_2:CaO		1.6 : 1	1 : 1	1 : 1.5
Mass of raw material, according to the ratio [g]	ZrO_2	197.15	123.22	123.22
	CaO	56.08	56.08	84.12
	$Ca(OH)_2$	74.10	74.10	111.15
	$CaCO_3$	100.09	100.09	150.14
Mass fraction ZrO_2 [g/g]	CaO	0.779	0.687	0.594
Mass fraction CaO precursor [g/g]	$Ca(OH)_2$	0.293	0.413	0.536
	$CaCO_3$	0.395	0.558	0.724

Mass fractions ZrO_2/X for 100 % 1.6:1	ZrO_2	
	0.727	0.663
	$Ca(OH)_2$	$CaCO_3$
	0.273	0.337

Mass fractions ZrO_2/X for 100 % 1:1	ZrO_2	
	0.624	0.552
	$Ca(OH)_2$	$CaCO_3$
	0.376	0.448

Mass fractions ZrO_2/X for 100 % 1:1.5	ZrO_2	
	0.526	0.451
	$Ca(OH)_2$	$CaCO_3$
	0.474	0.549

A. 2 Particle size distributions for the moulding mass calculations

Grain size class	d [µm]														Density
[mm]	**4**	**10**	**40**	**90**	**150**	**315**	**630**	**1000**	**1250**	**2000**	**2500**	**3150**	**4000**	**5000**	**Σ**	**ρ [g/cm³]**
0 - 0.16	0	1.46	19.11	79.43	0	0	0	0	0	0	0	0	0	0	100	4.70
0.16 - 0.63	0	0	0	6.72	30.29	62.99	0	0	0	0	0	0	0	0	100	4.70
0.63 - 1.0	0	0	0	0	0	0	100	0	0	0	0	0	0	0	100	4.70
1.0 - 2.0	0	0	0	0	0	0	3.71	7.5	88.79	0	0	0	0	0	100	4.70
2.0 - 3.15	0	0	0	0	0	0	0	0	0	100	0	0	0	0	100	4.70
3.15 - 4.0	0	0	0	0	0	0	0	0	0	0	0	100	0	0	100	4.70
4.0 - 5.0	0	0	0	0	0	0	0	0	0	0	0	0	100	0	100	4.70
5.0 - 6.0	0	0	0	0	0	0	0	0	0	0	0	0	0	100	100	4.70